UNIVERSIDADE DE BRASÍLIA – UnB

INSTITUTO DE GEOCIÊNCIAS – IGD

CARACTERIZAÇÃO E METALOGÊNESE DO DEPÓSITO DE ELEMENTOS DO GRUPO DA PLATINA DO COMPLEXO LUANGA, PROVÍNCIA MINERAL DO CARAJÁS

Eduardo Teixeira Mansur

Dissertação de Mestrado nº 388

Brasília - DF

2017

UNIVERSIDADE DE BRASÍLIA – UnB

INSTITUTO DE GEOCIÊNCIAS – IGD

CARACTERIZAÇÃO E METALOGÊNESE DO DEPÓSITO DE ELEMENTOS DO GRUPO DA PLATINA DO COMPLEXO LUANGA, PROVÍNCIA MINERAL DO CARAJÁS

DISSERTAÇÃO DE MESTRADO

Autor: Eduardo Teixeira Mansur

Orientador: Prof. Dr. Cesar Fonseca Ferreira Filho

Brasília – DF

2017

UNIVERSIDADE DE BRASÍLIA – UnB

INSTITUTO DE GEOCIÊNCIAS – IGD

Caracterização e metalogênese do depósito de elementos do grupo da platina do Complexo Luanga, Província Mineral do Carajás

Autor: Eduardo Teixeira Mansur

Examinadores:

Prof. Dr. Cesar Fonseca Ferreira Filho (UnB)

Prof. Dr. Claudinei Gouveia de Oliveira (UnB)

Profa. Dra. Juliana Charão Marques (UFRGS)

Brasília, 23 de fevereiro de 2017

RESUMO

Os primeiros trabalhos de pesquisa mineral no Complexo Luanga datam de 1983 e desde então, ao longo de mais de 20 anos de pesquisa mineral, a área foi estuda por diversas empresas, com foco exploratório em diferentes bens minerais. Em 2001, a VALE S.A. deu início a um projeto de exploração com foco em Elementos do Grupo da Platina (EGP) na região da Serra Leste, Carajás. Este trabalho apresenta a primeira descrição sistemática do Complexo Luanga e seu depósito de EGP, desenvolvida com o auxílio das extensiva base de dados gerada pela VALE.

Neste cenário, esta dissertação objetiva entender a gênese e evolução geológica do Complexo Luanga e seus diferentes estilos de mineralização de EGP. Para isso foram realizados trabalhos de campo, mapeamento geológico, descrição e amostragem de testemunhos de sondagem, interpretação de seção de sondagem, interpretação de dados de geoquímica, petrografia óptica, química de minério, química mineral, imageamento em microscópio eletrônico de varredura (MEV) e análises químicas isotópicas de isótopos de Sm, Nd e S.

O Complexo Luanga é parte da suíte magmática Serra Leste, localizada na porção nordeste da Província Mineral de Carajás. O Complexo Luanga é uma intrusão de médio porte, que pode ser dividida em três zonas principais: i. Zona Ultramáfica, localizada na porção inferior da intrusão, composta por cumulados ultramáficos (peridotitos), ii. Zona de Transição, localizada na porção central da intrusão, composta por uma intercalação de cumulados ultramáficos e máficos (harzburgito, piroxenito, norito) e iii. Zona Máfica, localizada na porção superior da intrusão, composta por uma sequência monótona de cumulados máficos (noritos) com intercalações pontuais de ortopiroxenito. A Zona Ultramáfica sobrepõe a Zona de Transição, que sobrepõe a Zona Máfica, sugerindo assim que o complexo está tectonicamente invertido. A mineralogia primária dos cumulados citados é frequentemente substituída em resposta a uma transformação metamórfica heterogênea sobreposta. Apesar da recristalização mineralógica, a transformação metamórfica preserva as texturas e domínios composicionais das rochas magmáticas.

Diferentes estilos de mineralização de EGP ocorrem ao longo do Complexo Luanga, com o destaque para ocorrências associadas a sulfetos disseminados e ocorrências sem associação clara com sulfetos e/ou cromititos. O primeiro caso é ilustrado por um horizonte de 10-50 metros de espessura, localizado na passagem entre

as Zonas Ultramáfica e de Transição, com uma disseminação de sulfetos (i.e. 3% vol.) denominado *Sulfide Zone*. A mineralogia dos sulfetos é tipicamente pentlandita > pirrotita >>> calcopirita, o que resulta em um elevado *tenor* de Ni (i.e. 16-18%) e alta razão Ni/Cu (i.e. 10-12). A *Sulfide Zone* hospeda a maior parte dos recursos de EGP do depósito de Luanga (i.e. 142 Mt@ 1.24g/t EGP+Au e 0.11% Ni). O segundo estilo de mineralização é definido por horizontes de 2-10 metros de espessura, estratigraficamente acima da *Sulfide Zone,* que apresentam concentrações anômalas de EGP, denominados *silicate-related PGE*. As rochas observadas nestes horizontes não possuem nenhuma característica textural ou mineralógica que as distinga dos cumulados supracitados. Os dois estilos citados apresentam características geoquímicas distintas, quanto às concentrações de EGP. A *Sulfide Zone* possui razões Pt/Pd de aproximadamente 0.5 e um padrão de EGP, normalizados ao manto primitivo, típico de depósitos de sulfetos magmáticos hospedados em intrusões máfica-ultramáficas. O *silicate-related PGE* possui razões Pt/Pd de aproximadamente 1.2-1.3 e forte depleção em Ir e Os. Outra característica importante é a ocorrência de cristais de olivina com até 7500 ppm de Ni em alguns harzburgitos que hospedam a mineralização do tipo *silicate-related PGE.* Tais características sugerem que os dois estilos são formados por processos geológicos distintos.

Cromititos estratiformes, com textura variada e espessura de até 60 centímetros, ocorrem ao longo do Complexo Luanga, hospedados no topo da Zona de Transição e base da Zona Máfica. Em função do extensivo processo de metamorfismo que afeta as rochas do Complexo Luanga, as composições dos cristais de cromita são modificadas. A alteração da composição primária é marcada em cristais zonados, com Mg# ($Mg/Mg+Fe^{2+}$) progressivamente menor do núcleo para a borda. Estas alterações na composição primária de cristais de cromita comprometem sua aplicabilidade em estudos petrogenéticos. Nossos resultados sugerem que estas feições são comuns em cromititos hospedados em rochas alteradas em outros locais no mundo.

A composição do magma parental do Complexo Luanga não pode ser obtida por métodos diretos, aplicados a intrusões bem expostas e preservadas (i.e. diques correlatos, margens de resfriamento, equivalentes extrusivos). Desta forma, a composição do magma responsável pela geração de olivinas extremamente ricas em Ni e horizontes ricos em EGP na intrusão estudada, não é óbvia. De fato, diferentes modelos podem explicar a origem de magmas ricos em Ni e a existência ou não de magmas férteis para a geração de depósitos de EGP. Os resultados apresentados

suportam a geração de um magma rico em Ni que dá origem ao Complexo Luanga e a existência de uma suíte magmática fértil para a geração de depósitos de EGP na porção leste da Província Mineral de Carajás.

Palavras-chave: Intrusão máfica-ultramáfica; EGP; Níquel; Cromitito; Depósito de sulfeto magmático; Carajás.

ABSTRACT

Since 1983 the area of the Luanga Complex has been studied by different mining companies, aiming different commodities. In 2001, Vale S.A. started an exploration program for PGE in the Serra Leste region. This project resulted in a great volume of geological data upon the layered intrusions and related mineralizations of the region. This study provides the first systematic study of the Luanga Complex and its PGE mineralization supported by the extensive database provided by VALE.

Based on this scenario, the present dissertation aims the genesis and geological evolution of the Luanga Complex and its associated PGE mineralization. To achieve this objective we performed field work, geological mapping and sampling, drill core description and sampling, reinterpretation of geological sections, detailed petrography, mineral chemistry, interpretation of lithogeochemical data, scanning electron microscope images (SEM) and isotopic analyses for Sm-Nd and S systematics.

The Luanga Complex is part of the Serra Leste Magmatic Suite, located in the northeastern portion of the Carajás Mineral Province. The Luanga Complex is a medium-sized layered intrusion consisting of three main zones: i. the lower Ultramafic Zone, comprising ultramafic cumulates (peridotite), ii. the Transition Zone comprising interlayered ultramafic and mafic cumulates (harzburgite, orthopyroxenite and norite) and iii. the upper Mafic Zone comprising a monotonous sequence of mafic cumulates (norite) with minor orthopyroxenite layers. The Ultramafic Zone overlies the Transition Zone, which overlies the Mafic Zone, suggesting thus that the layered sequence is tectonically overturned. Metamorphic assemblages commonly replace primary igneous minerals of the Luanga Complex. This metamorphic alteration is heterogeneous and characterized by an extensive hydration that largely preserves primary textures, bulk rock compositions and the compositional domains of igneous minerals.

Different styles of PGE mineralization occur along the Luanga Complex, with occurrences associated with disseminated sulfides and occurrences with no clear association with sulfides and/or chromites. The first, ascribed as Sulfide Zone, consists of a 10 – 50 m thick interval with disseminated sulfides located along the contact of the Ultramafic and Transition Zones of the intrusion. The mineralogy of the Sulfide Zone consists of base metal sulfides with pentlandite > pyrrhotite > >> chalcopyrite, resulting in high Ni tenors (i.e. 16-18) and high Ni/Cu ratios (i.e. 10-12). The Sulfide Zone hosts

the bulk of PGE resources of the Luanga Complex (i.e., 142 Mt at 1.24 ppm Pt+Pd+Au and 0.11% Ni). The other PGE mineralization, ascribed as silicate-related PGE, consists of 2-10 m thick stratabound zones across the Transition Zone. These sulfide- and chromite-free rocks, mainly harzburgite and orthopyroxenite, do not show any distinctive texture or change in modal composition that characterize the PGE enrichment. The Sulfide Zone and silicate-related PGE show differences in geochemistry behavior of PGE. The Sulfide Zone has Pt/Pd ratios of 0.5 and mantle-normalized PGE patterns typical of magmatic sulfide deposits hosted in layered intrusions. The silicate-related PGE has Pt/Pd ratios of 1.2-1.3 and a strong depletion in Ir and Os. A remarkable feature is the occurrence of anomalously Ni-rich olivines (up to 7400 ppm Ni) in harzburgites closely associated with silicate-related PGE mineralization. The geochemical and textural differences between these mineralization styles suggest that they were formed by distinct geological processes.

Several variable textured stratiform chromitites, up to 60 centimeters thick, occur in the upper portion of the Transition Zone and the lower portion of the Mafic Zone. Due to the extensive metamorphic transformation overprinted over the Luanga Complex, the primary compositions of chromite crystal are extensively modified. Alteration of primary magmatic composition is indicated by zoned crystals with progressively lower Mg# ($Mg/Mg+Fe^{2+}$) from core to rim. Significant changes on primary compositions of chromite identified in the Luanga Complex compromise their application for petrogenetic studies. Our results suggest that these features should be common in chromitites hosted in altered rocks worldwide.

The composition of the parental magma of the Luanga Complex cannot be constrained by common approaches used to define their composition in well-exposed and well-preserved intrusions (e.g., chilled margin, bulk composition, extrusive equivalents, related dykes). Hence, the composition of the parental magma that leads the formation of Ni-rich olivines and PGE-rich horizons is not straightforward. Actually, different models have been proposed to explain the origin of Ni-rich magmas and the existence or not of PGE-fertile suites. The results of this study support the generation of a Ni-rich magma that originates the Luanga Complex and the existence of a PGE-fertile suite at the eastern portion of the Carajás Mineral Province.

Keywords: Mafic-ultramafic intrusion; PGE; Nickel; Chromitite; Magmatic sulfide deposit; Carajás.

Lista de Figuras

Lista de Tabelas

Sumário

CAPÍTULO 2

CAPÍTULO 3

INTRODUÇÃO

A maior parte dos recursos de Elementos do Grupo da Platina (EGP) está concentrada em um pequeno número de intrusões (Cawthorn et al., 2005). Estes depósitos podem ser divididos em dois grupos principais, baseados na associação destes EGP: i. depósitos de EGP associados a sulfetos e ii. depósitos de EGP associados a cromititos. Estes dois grupos podem ser ilustrados pelos depósitos de sulfetos Merensky reef, e cromititos do UG2, ambos localizados no Complexo de Bushveld, África do Sul (e.g., Barnes & Maier, 2002; Cawthorn et al., 2002 e 2005; Naldrett, 2004).

Alguns fatores podem justificar a concentração de recursos de EGP em poucas intrusões. Destacam-se a elevada eficiência dos processos que concentram EGP e a possibilidade da existência de determinadas províncias magmáticas férteis em EGP. Ao que diz respeito aos processos de concentração de EGP, estudos indicam processos geológicos com uma eficiência de ordens de 10^5 (Finnigan et al., 2008; Mungal & Naldrett, 2008). Por outro lado, ao que condiz a existência ou não de uma província magmática fértil para a geração de depósitos de EGP, tem-se um extenso debate. Alguns estudos propõem a existência de províncias que geram magmas de composições distintas, que originam depósitos de Ni-Cu-PGE (e.g., Maier & Groves, 2011; Griffin et al., 2013). Por outro lado, alguns autores afirmam que os dados obtidos em intrusões estudadas ao redor do mundo não suportam a existência destas suítes férteis (e.g., Fiorentini et al., 2010; Barnes et al., 2015).

O Complexo Luanga faz parte da suíte magmática Serra Leste (Ferreira Filho et al., 2007), localizada na porção nordeste da Província Mineral de Carajás. Esta suíte foi definida com base em concentrações anômalas de EGP. Desta forma, o estudo sistemático e entendimento da evolução magmática do Complexo Luanga, assim como de outros complexos da região (Teixeira et al., 2015) permitem entender quais os principais fatores que atuam na formação de depósitos de EGP.

Esta dissertação apresenta uma descrição sistemática do Complexo Luanga e mineralizações associadas e visa contribuir com o entendimento de processos que levam à concentração de EGP. Adicionalmente, o trabalho faz uma caracterização sistemática de cromititos que ocorrem ao longo do complexo e uma análise crítica do efeito de processos de alteração pós-magmática e metamórfica na composição de cristais de cromita. Tal análise crítica pode ser extrapolada para o estudo de rochas ricas em cromita de outros complexos ultramáfico-máficos. Por fim, o trabalho destaca a

importância de processos de concentração de EGP sem uma associação típica a sulfetos magmáticos e/ou cromititos. Os resultado obtidos são comparados a dados da região de Carajás e outros complexos máfico-ultramáficos do mundo, desta forma, o Complexo Luanga é posicionado em um cenário global.

OBJETIVO, PERGUNTAS E HIPÓTESES

Este trabalho tem por objetivo principal entender a gênese e evolução geológica do Complexo Luanga e seu depósito de Elementos do Grupo da Platina.

Este objetivo visa responder as seguintes perguntas elaboradas dois anos atrás e durante o desenvolvimento da dissertação:

i. Qual a evolução magmática do Complexo Luanga? E qual a estrutura magmática deste Complexo?
ii. Como se deu a formação dos diferentes estilos de mineralizações de EGP do Complexo Luanga?
iii. Qual o impacto de processos pós-magmáticos e metamórficos nos estudo petrológicos do Complexo Luanga? Como estes processos podem ser extrapolados para diferentes complexos?
iv. Como os resultados obtidos para o Complexo Luanga se comparam com os diferentes complexos ultramáfico-máficos da Província Mineral de Carajás? e com os principais complexos do mundo?

Para responder estas perguntas testamos as seguintes hipóteses:

i. O Complexo Luanga apresenta a estrutura típica de intrusões máfica-ultramáficas acamadas geradas por sucessivos pulsos magmáticos,
ii. Os diferentes estilos de mineralizações de EGP são originados por processos magmáticos distintos durante a evolução do Complexo Luanga.
iii. A composição da cromita nas várias camadas de cromititos resulta em grande parte de processos pós-magmáticos.
iv. Os teores muito elevados de Ni das olivinas do Complexo Luanga resultam da sua cristalização à partir de magmas anômalos para Ni,

v. A abundância de intervalos estratigráficos com diferentes estilos de mineralização de EGP é resultado de um magma parental originalmente enriquecido em EGP.

ESTRUTURA DA TESE

Esta dissertação de mestrado está organizada em três capítulos redigidos na forma de artigos científicos direcionados para publicação em periódicos científicos de ampla circulação especializados nos temas abordados.

Os detalhamentos de cada tema que esta dissertação propõe responder, com seus objetivos, resultados, métodos e conclusões, estão especificados em cada um dos seguintes capítulos.

CAPÍTULO 1

Este capítulo apresenta o artigo intitulado "Magmatic structure and geochemistry of the Luanga Mafic-Ultramafic Complex: further constraints for the PGE-mineralized magmatism in Carajás, Brazil", publicado no periódico "Lithos" em setembro de 2016 [Mansur, E.T., Ferreira Filho, C.F., 2016, Magmatic structure and geochemistry of the Luanga Mafic-Ultramafic Complex: further constraints for the PGE-mineralized magmatism in Carajás, Brazil. Lithos, v. 266-267, p. 28-43]. O artigo foi reformatado em um capítulo para atender os padrões de diagramação de dissertação da Universidade de Brasília.

Este artigo apresenta uma caracterização sistemática das litologias, estrutura magmática e evolução geológica do Complexo Luanga. O artigo também discute dados de química mineral de olivina, com conteúdos anômalos de Ni, e suas implicações para a evolução da intrusão e formação do depósito de EGP.

CAPÍTULO 2

Este capítulo apresenta o artigo intitulado "Chromitites from the Luanga Complex, Carajás, Brazil: stratigraphic distribution and clues to processes leading to post-magmatic alteration" e foi submetido ao periódico "Ore Geology Reviews" em

julho de 2016. O manuscrito foi aceito com revisões moderadas pelo editor da revista. A versão revisada foi encaminhada ao editor em novembro de 2016..

Neste trabalho são sistematicamente caracterizadas as ocorrências de cromititos ao longo do Complexo Luanga. O trabalho conta com um vasto banco de dados de química mineral de cromita (~700 análises pontuais, realizadas ao longo de seções transversais), que permite uma avaliação criteriosa dos processos que modificam a composição primária destes cristais. Os resultados são integrados com as demais análises de química mineral para melhor entendimento da evolução geológica da intrusão.

CAPÍTULO 3

Este capítulo é intitulado "The Luanga deposit, Carajás Mineral Province, Brazil: different styles of PGE mineralization hosted in a medium-size layered intrusion". O artigo foi estruturado para submissão ao periódico "Economic Geology".

Neste capítulo é apresentada a primeira caracterização sistemática do depósito de EGP de Luanga, incluindo uma discussão genética dos diferentes estilos de mineralização. O posicionamento estratigráfico e a gênese dos intervalos mineralizados está inserido no arcabouço geológico e petrológico definido nos. capítulos anteriores.

REFERÊNCIAS

Barnes, S-J., and Maier, W.D., 2002. Platinum-group element distributions in the Rustenberg Layered Suite of the Bushveld Complex, South Africa, in, Cabri, L.J., ed., The Geology, Geochemistry, Mineralogy and Mineral Beneficiation of Platinum-Group Elements, Canadian Institute of Mining, Metallurgy and Petroleum, Special Volume 54, 431-458.

Barnes, S.J., Mungall, J.E., Maier, W.D., 2015. Platinum group elements in mantle melts and mantle samples. Lithos 232, 395–417.

Cawthorn, R.G., Merkle, R.K.W., and Viljoen, M.J., 2002, Platinum-group element deposits in the Bushveld Complex, South Africa, in, Cabri, L.J., ed., The Geology,

Geochemistry, Mineralogy and Mineral Beneficiation of Platinum-Group Elements, Canadian Institute of Mining, Metallurgy and Petroleum, Special Volume 54, 389-430.

Cawthorn, R.G., Barnes, S.J., Ballhaus, C., and Malich, K.N., 2005, Platinum group element, chromium and vanadium deposits in mafic and ultramafic rocks: Economic Geology 100th Anniversary Volume, 215-249.

Finnigan, C.S., Brenan, J.M., Mungall, J.E., and McDonough, W.F., 2008. Experiments and models bearing on the role of chromite as a collector of platinum group minerals by local reduction: Journal of Petrology 49, 1647-1665.

Fiorentini, M.L., Barnes, S.J., Lesher, C.M., Heggie, G.J., Keays, R.R., Burnham, O.M., 2010. Platinum-group element geochemistry of mineralized and non-mineralized komatiites and basalts. Economic Geology 105, 795–823.

Ferreira Filho, C.F., Cançado, F., Correa, C., Macambira, E.M.B., Siepierski, L., Brod, T.C.J., 2007. Mineralizações estratiformes de EGP-Ni associadas a complexos acamadados em Carajás: os exemplos de Luanga e Serra da Onça. In: Publitec Gráfica & Editora, Contribuições à Geologia da Amazônia, vol. 5, pp. 01-14.

Griffin, W., O'Reilly, S.Y., Begg, G.C., 2013. Continental-root control on the genesis of magmatic ore deposits. Nature Geoscience 6, 905–910.

Maier, W.D., Groves, D.I., 2011. Temporal and spatial controls on the formation of magmatic PGE and Ni-Cu deposits. Mineralium Deposita 46, 841-857.

Mungall, J.E., and Naldrett, A.J., 2008. Ore deposits of the platinum-group elements: Elements, 4, 253-258.

Naldrett, A.J., 2004, Magmatic sulphide deposits: Geology, geochemistry and exploration: Berlin, Springer-Verlag, 728 p.

Teixeira, A.S., Ferreira Filho, C.F., Giustina, M.E.S.D., Araujo, S.M., Silva, H.H.A.B., 2015. Geology, petrology and geochronology of the Lago Grande layered complex: Evidence for a PGE-mineralized magmatic suíte in the Carajás mineral province, Brazil. Journal of South American Earth Sciences 64, 116-138.

CAPÍTULO 1

Magmatic structure and geochemistry of the Luanga Mafic-Ultramafic Complex: further constraints for the PGE-mineralized magmatism in Carajás, Brazil

Magmatic structure and geochemistry of the Luanga Mafic-Ultramafic Complex: further constraints for the PGE-mineralized magmatism in Carajás, Brazil

Eduardo Teixeira Mansur[1] and Cesar Fonseca Ferreira Filho[1]

[1] Instituto de Geociências, Universidade de Brasília, Brasília-DF, 70910-900, Brazil.

Abstract

The Luanga Complex is part of the Serra Leste Magmatic Suite, a cluster of PGE-mineralized mafic-ultramafic intrusions located in the northeastern portion of the Carajás Mineral Province. The Luanga Complex is a medium-sized layered intrusion consisting of three main zones: i. the lower Ultramafic Zone, comprising ultramafic adcumulates (peridotite), ii. the Transition Zone comprising interlayered ultramafic and mafic cumulates (harzburgite, orthopyroxenite and norite) and iii. the upper Mafic Zone comprising a monotonous sequence of mafic cumulates (norite) with minor orthopyroxenite layers. Several PGE-mineralized zones occur in the Transition Zone but the bulk of the PGE resources are hosted within a 10 – 50 meters thick interval of disseminated sulfides at the contact of the Ultramafic and Transition zones. The compositional range of cumulus olivine ($Fo_{78.9-86.4}$) is comparable to those reported for layered intrusions originated from moderate primitive parental magmas. Mantle normalized alteration-resistant trace element profiles of noritic rocks are fractionated, as indicated by relative enrichment in LREE and Th, with negative Nb and Ta anomalies, suggesting assimilation of older continental crust. Ni contents in olivine in the Luanga Complex (up to 7,500 ppm) stand among the highest values reported in layered intrusions globally. The highest Ni contents in olivine in the Luanga Complex occur in distinctively PGE enriched (Pt+Pd > 1 ppm) intervals of the Transition Zone, in both sulfide-poor and sulfide bearing (1-3 vol.%) rocks. The origin of the PGE- and Ni-rich

parental magma of the Luanga Complex is discussed considering the upgrading of magmas through dissolution of previously formed Ni-rich sulfide melts. Our results suggest that high Ni contents in olivine and/or orthopyroxene provide an additional exploration tool for Ni-PGE deposits, particularly useful for target selection in large magmatic provinces.

keywords: layered intrusion, PGE, nickel-rich olivine, mafic-ultramafic magmatism

1.1 - Introduction

The Luanga Complex is part of a cluster of PGE-mineralized mafic-ultramafic intrusions located in the eastern portion of the Carajás Mineral Province, denominated Serra Leste Suite. This suite consists of several small to medium size intrusions that host PGE mineralizations of different styles, including PGE associated with chromitite layers, stratabound magmatic base metal sulfide zones and hydrothermal alteration zones (e.g., Diella et al., 1995; Ferreira Filho et al., 2007; Teixeira et al., 2015). These layered intrusions have Neoarchean ages (e.g., Machado et al., 1991; Teixeira et al., 2015) that overlap with the ca. 2.75 Ga extensive basaltic magmatism of the Carajás Mineral Province (e.g., Trendall et al., 1998), thus representing coeval magmatic events at the scale attributed to large igneous provinces (LIP; Ernst et al., 2005). The spatial association of PGE-mineralized layered intrusions of the Serra Leste suite led to the suggestion that they originated from a PGE-fertile parental magma (Ferreira Filho et al., 2007; Teixeira et al., 2015). How magmas with distinctive geochemical characteristics that enhance the origin of Ni-Cu-PGE deposits are formed and whether such compositions are systematically associated with Ni-Cu-PGE deposits is a debated issue (e.g., Zhang et al., 2008; Fiorentini et al., 2010; Griffin et al., 2013). While some studies have proposed that LIP containing Ni-Cu-PGE deposits have magmas with distinctive geochemical compositions, usually attributed to specific characteristics of the sub-continental lithosphere (e.g., Maier and Groves, 2011; Griffin et al., 2013), others indicate that a systematic association of unusual magmas and magmatic deposits are not supported by current data (e.g., Fiorentini et al., 2010; Barnes et al., 2015). In this study we present anomalously high Ni contents for olivine in rocks of the Luanga Complex. Extensive data on olivine compositions have been used to suggest that high Ni contents

in olivine occur in mantle melts from sources containing high proportions of recycled oceanic crust (i.e., Sobolev et al., 2005 and 2007) due to the predominance of pyroxene over olivine in the source. Ni-rich magmas with elevated PGE contents are also attributed to processes that lead to the dissolution of previously formed sulfides during magma ascent (i.e., Kerr and Leitch, 2005). Our results provide additional data to the ongoing debate about whether Ni-Cu-PGE deposits are favored or not by specific magma compositions.

This paper presents the first extensive geological and geochemical characterization of the Luanga Complex, the layered intrusion that hosts the most significant stratiform/stratabound PGE mineralization in Carajás (Ferreira Filho et al, 2007). Our results provide evidence for an anomalous Ni-rich magmatism associated with the PGE-mineralized Luanga Complex. These results are compared with previous studies of layered intrusions in the Carajás Mineral Province and worldwide in order to evaluate the petrological processes that take place during the evolution of PGE-fertile districts.

1.2 - Regional setting

1.2.1 – The Carajás Mineral Province

The Carajás Mineral Province is one of the most important mineral provinces of the South American continent, hosting several Fe, Cu–Au and Ni world-class deposits. It is located in the southeastern portion of the Amazonian Craton (Fig. 1.1A), bounded by the Neoproterozoic Araguaia Belt in the east and south, and overlain by Paleoproterozoic sequences generically assigned to the Uatumã Supergroup in the west (Araújo and Maia, 1991; Docegeo, 1988). To the north, where Paleoproterozoic gneiss–migmatite–granulite terrains predominate (Vasquez et al., 2008), geological limits are not precisely defined. The Carajás Mineral Province is subdivided into two Archean tectonic domains: the older Mesoarchean Rio Maria Domain to the south and the younger Neoarchean Carajás Domain to the north (Fig. 1.1B; Araújo and Maia, 1991; Araújo et al., 1988; Dall'Agnol et al., 2006; Docegeo, 1988; Feio et al., 2013). A regional E–W shear zone, known as the Transition Subdomain (Feio et al., 2013), separates the Rio Maria and Carajás domains.

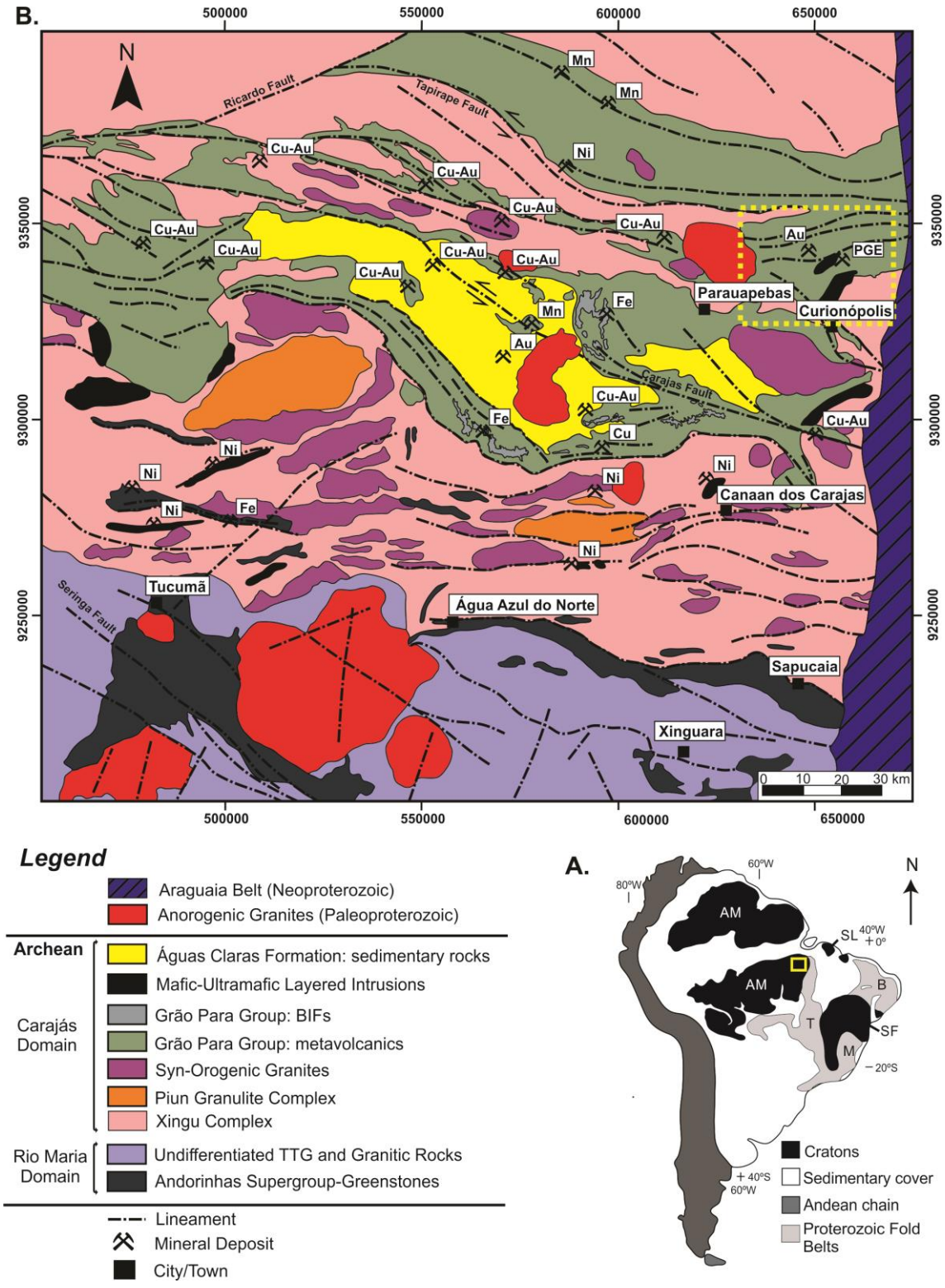

Fig. 1.1: A) Location of the Carajás Mineral Province. AM - Amazonian Craton; B – Borborema Province; M – Mantiqueira Province; SF – São Francisco Craton; T – Tocantins Province. B) Geology and mineral deposits of the Carajás Mineral Province (modified from Vasquez et al., 2008). The dashed rectangle indicates the position of Figure 2.

The Rio Maria Domain is a typical granite–greenstone terrain (Vasquez et al., 2008). The Andorinhas Supergroup (Docegeo, 1988) comprises several individual Mesoarchean greenstone belts (2904 ± 29 Ma;Macambira and Lancelot, 1996) and metasedimentary rocks (Huhn et al., 1986; Souza and Dall'Agnol, 1996; Souza et al., 2001). The recent characterization of spinifex-textured komatiites in a greenstone belt sequence within the Transition Subdomain (Siepierski and Ferreira Filho, 2016) suggests that granite–greenstone terrains extend further north than indicated in previous regional maps.

The basement of the Carajás Domain consists mainly of gneiss– migmatite–granulite terrains of the Xingu Complex (Docegeo, 1988; Machado et al., 1991; Pidgeon et al., 2000). The evolution of the Carajás Domain, where the study area is located, is widely discussed. Different models have been proposed to explain the evolution of the Archean volcano-sedimentary sequences, which includes the large sequence of metabasalts of the Grão Pará Group (ca. 2.75 Ga; Machado et al., 1991; Vasquez et al., 2008). While several studies have proposed an intraplate rift model (Gibbs et al., 1986; Villas and Santos, 2001), others have suggested subduction-related environments (Dardenne et al., 1988; Teixeira and Eggler, 1994). These volcano-sedimentary sequences are covered by low-grade metamorphic sequences of clastic sedimentary rocks of the Águas Claras Formation (i.e., Rio Fresco Group; Araújo et al., 1988; Docegeo, 1988; Nogueira et al., 1994, 2000).

Several mafic–ultramafic complexes intrude into both the Xingu Complex and the Archean volcano-sedimentary sequences (Docegeo, 1988; Ferreira Filho et al., 2007). These intrusions host large Ni laterite deposits (e.g., Onça-Puma, Vermelho, Jacaré) as well as PGE deposits (e.g., Luanga, Lago Grande) and were ascribed as part of the Cateté Suite in regional studies (e.g., Macambira and Ferreira Filho, 2002). Significant differences in the magmatic structure and evolution of the layered intrusions suggest, however, that they belong to different Neoarchean magmatic suites (e.g., Ferreira Filho et al., 2007; Rosa, 2014; Teixeira et al., 2015).

1.2.2 - The Serra Leste Magmatic Suite

The Serra Leste Magmatic Suite (Ferreira Filho et al., 2007) consists of a cluster of small- to medium-size layered mafic-ultramafic intrusions located in the northeastern portion of the Carajás Mineral Province (Fig. 1.2). Mafic-ultramafic complexes are intrusive into gneiss rocks of the Xingu Complex and/or volcanic-sedimentary rocks of

the Grão Pará Group. This suite was originally grouped based on abundant PGE anomalies of the layered intrusions, disregarding any geological, stratigraphic or petrological consideration (Ferreira Filho et al., 2007). Recent studies of the Lago Grande Complex (Teixeira et al., 2015) and Luanga Complex (this study) are the first systematic stratigraphic and petrological investigations of layered intrusions ascribed to the Serra Leste Suite, thus providing data for the composition of their parental magmas and fractionation processes. Geochronological studies of the Serra Leste Suite are restricted to the crystallization age of the Luanga Complex (2,763 ± 6 Ma, U-Pb in zircon, Machado et al. 1991) and Lago Grande Complex (2,722 ± 53 Ma, U-Pb in zircon, Teixeira et al. 2015). Magmatic ages of the layered intrusions overlap with the age of the bimodal volcanism of the Grão Pará Group (2,759 ± 2 Ma, U-Pb in zircon, Machado et al. 1991; 2,760 ± 11 Ma, U-Pb in zircon, Trendall et al. 1998), supporting the interpretation that they are part of a major Neoarchean magmatic event (Machado et al., 1991; Ferreira Filho et al., 2007). The architecture of the intrusion and the crystallization sequence described in the Luanga and Lago Grande complexes (Fig. 1.2) indicate an overturned layered sequence (Ferreira Filho et al., 2007; Teixeira et al., 2015). Even though the tectonic processes leading to the overturned sequence of layered rocks in the Lago Grande and Luanga complexes have so far not been studied in detail, regional structural studies in the Serra Leste region indicate significant tectonic transport that may lead to major overturned blocks (Holdsworth and Pinheiro, 2000; Tavares, 2015).

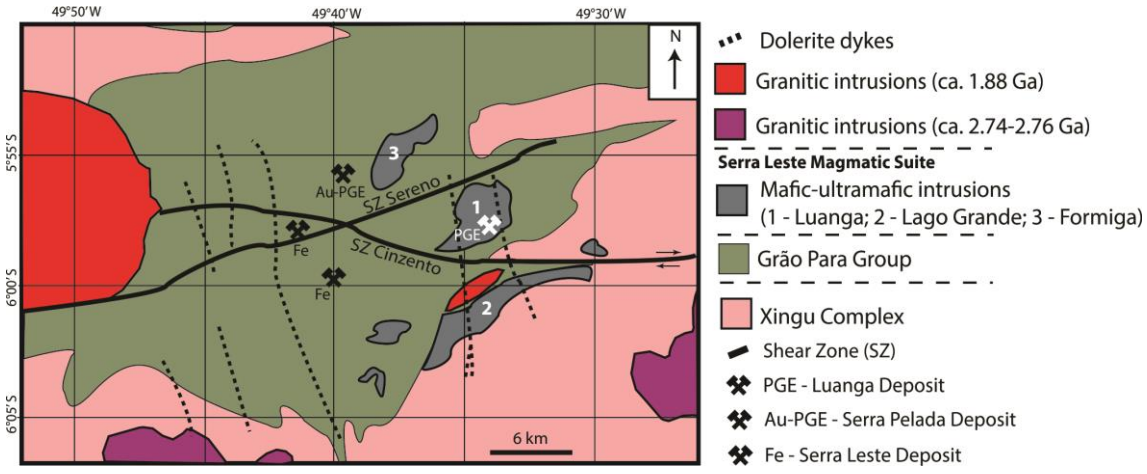

Fig. 1.2: Geology of the Serra Leste region. Partially modified from unpublished report of VALE.

1.3 – Sampling and analytical procedures

For this study, drill core from eleven boreholes and outcrops rocks were systematically sampled in order to select unweathered rocks with primary magmatic minerals and textures. The analytical procedures are described as follows.

1.3.1 - Microprobe analyses

Mineral analyses were performed on polished thin section using a JEOL JXA-8230 SuperProbe with 5 wavelength dispersive (WDS) spectrometers at the Electron Microprobe Laboratory of the University of Brasília (Brazil). Systematic WDS analyses were obtained for olivine, orthopyroxene and plagioclase. Operating conditions for the WDS analyses for orthopyroxene and plagioclase were 15 kV accelerating voltage, with a beam current of 10 nA and probe diameters of 3 μm for orthopyroxene and 5 μm for plagioclase. Count times on peak and on background were 10s and 5s respectively. Operating conditions for Ni were 15 kV accelerating voltage, with a beam current of 100 nA, probe diameters of 3 μm and count times on peak and on background were 60s and 30s, respectively. These different conditions were used because of the importance of Ni values for further discussions. Using these analytical conditions, detection limits for major elements are around 100 ppm while for Ni the detection limit is around 25 ppm. Both synthetic and natural mineral standards were used for the analyses and the same standards and procedure were retained throughout the analytical work. The results are provided in Online Supplementary Table 1.

1.3.2 - Bulk rock analyses

Sample preparation and lithogeochemical analyses were performed at ALS Chemex (Canada). Analytical procedures include the whole-rock package plus LOI (ALS Chemex codes: ME-XRF12st and OA-GRA05x), total S plus total C (ALS Chemex codes: S-IR08 and C-IR07) and the 38 elements fusion ICP-MS package (ALS Chemex code: ME-MS81). A complete description of analytical methods is available in the ALS Chemex Home Page (www.alsglobal.com). Results for representative samples are shown in Table 1.1 (see Online Supplementary Table 2 for all analytical data).

Table 1.1 Whole-rock analyses of representative samples from the Luanga Complex. Serp = erpentinite; Hzb = Harzburgite; Opxt = Orthopyroxenite; Nrt = Norite; Nrt Peg = pegmatoid norite.

Sample		LUFD141	LUFD141	LUFD069	LUFD069	LUFD078	LUFD071	LUFD071	LUFD078	LUFD079	LUFD093	LUFD104	LU-120B
Depth		39	209	106,62	115,64	55	152,55	183,35	157,10	143	103	198,50	*
Rock		Serp	Serp	Hzb	Opxt	Nrt (TZ)	Nrt (TZ)	Hzb	Opxt	Nrt (TZ)	Nrt (TZ)	Nrt (TZ)	Nrt Peg
SiO_2	%	40.30	42.10	38.84	52.37	48.90	49.29	53.21	53.24	49.40	48.20	49.61	54.10
Al_2O_3	%	3.14	5.22	6.37	1.67	19.05	17.00	1.52	4.27	18.80	21.20	14.97	14.25
Fe_2O_3	%	6.33	10.45	12.99	12.06	4.41	4.99	15.55	9.17	3.73	4.20	4.96	8.09
MnO	%	0.07	0.14	0.11	0.18	0.06	0.07	0.25	0.17	0.03	0.07	0.06	0.20
MgO	%	38.10	29.10	29.48	26.79	12.90	13.47	25.52	27.04	13.15	10.20	17.99	6.25
CaO	%	0.14	5.13	2.66	1.45	8.67	8.25	1.64	2.08	7.77	9.74	6.72	14.70
Na_2O	%	0.02	0.21	0.09	0.12	1.20	1.03	0.11	0.32	1.17	0.88	0.84	0.91
K_2O	%	0.03	0.05	<0.01	0.08	0.80	0.96	0.03	0.26	1.13	1.43	0.39	0.05
TiO_2	%	0.12	0.29	0.04	0.11	0.09	0.08	0.13	0.13	0.12	0.06	0.07	0.19
P_2O_5	%	0.01	0.02	<0.01	<0.01	0.01	<0.01	<0.01	<0.01	0.01	0.01	<0.01	0.02
LOI	%	11.57	6.73	8.12	4.89	3.60	3.66	2.26	2.18	4.14	4.61	4.11	1.38
Total		99.83	99.45	98.68	99.71	99.67	98.79	100.21	98.85	99.44	100.58	99.71	100.14
S	%	0.04	0.01	<0.01	<0.01	0.01	<0.01	<0.01	<0.01	0.01	0.01	<0.01	0.02
C	%	0.05	0.04	<0.01	<0.01	0.01	<0.01	<0.01	<0.01	0.01	0.10	<0.01	0.03
Ba	ppm	9.0	17.7	4.0	6.0	180.0	148.0	2.0	137.0	153.5	191.5	66.0	349.0
Sr	ppm	1.8	16.2	3.0	3.0	318.0	392.0	2.0	46.0	261.0	363.0	140.0	197.5
V	ppm	30.0	120.0	47.8	101.2	56.0	53.8	121.7	93.1	52.0	57.0	41.0	135.0
Cr	ppm	2480	2260	2830	2290	1560	803	1840	3340	1600	330	471	120
Co	ppm	99	108	97	137	47	46	96	85	40	38	46	42
Ni	ppm	2410	1740	1440	1510	535	385	613	769	486	281	475	95
Cu	ppm	12	13	<0.1	158	42	60	<0.1	62	17	20	<0.1	314
Ga	ppm	3.30	6.80	6.09	3.85	9.70	10.55	4.28	4.86	9.00	10.20	8.56	18.60
Rb	ppm	4.30	2.90	1.68	2.71	38.40	54.57	<0.1	14.35	52.70	76.90	19.51	1.20
Zr	ppm	9.00	16.00	5.26	12.56	7.00	2.21	3.09	12.14	11.00	6.00	6.45	14.00
Nb	ppm	1.40	1.90	1.70	3.51	1.80	0.59	0.95	0.68	2.40	2.20	0.41	2.80

La	ppm	1.30	3.00	0.68	0.60	5.70	1.67	0.47	2.18	6.80	4.00	1.20	5.80
Ce	ppm	2.80	6.40	1.81	1.39	10.10	2.86	1.17	3.54	12.90	8.30	2.07	10.10
Pr	ppm	0.36	0.70	0.23	0.16	0.83	0.30	0.15	0.34	1.16	0.76	0.22	1.11
Nd	ppm	1.30	3.10	0.99	0.70	2.70	1.18	0.70	1.38	3.80	2.70	0.85	4.50
Sm	ppm	0.24	0.78	0.22	0.18	0.48	0.22	0.22	0.29	0.61	0.58	0.19	0.91
Eu	ppm	0.06	0.27	0.05	0.04	0.27	0.19	0.05	0.12	0.21	0.19	0.12	0.57
Gd	ppm	0.63	1.19	0.23	0.22	0.29	0.19	0.31	0.35	0.42	0.46	0.19	0.86
Tb	ppm	0.11	0.16	0.04	0.05	0.06	0.03	0.07	0.06	0.04	0.05	0.04	0.16
Dy	ppm	0.75	1.19	0.28	0.38	0.28	0.23	0.54	0.43	0.26	0.25	0.24	0.91
Ho	ppm	0.11	0.28	0.06	0.09	0.07	0.05	0.14	0.10	0.08	0.04	0.05	0.21
Er	ppm	0.52	0.50	0.21	0.36	0.19	0.18	0.54	0.36	0.16	0.07	0.16	0.63
Tm	ppm	0.05	0.13	0.03	0.06	0.02	0.03	0.09	0.06	0.03	0.04	0.03	0.07
Yb	ppm	0.47	0.44	0.22	0.42	0.28	0.21	0.66	0.39	0.28	0.25	0.18	0.56
Lu	ppm	0.06	0.09	0.04	0.07	0.02	0.03	0.11	0.06	0.02	0.02	0.03	0.08
Hf	ppm	0.40	0.50	0.16	0.34	0.20	-0.10	0.12	0.32	0.30	0.20	0.18	0.40

1.4 - The Luanga Layered Mafic-Ultramafic Complex

1.4.1 – Geology

The Luanga Complex consists of a 6 km long and up to 3.5 km wide (~18 km²) sequence of mafic-ultramafic layered rocks (Fig. 1.3A). Unweathered rocks are abundant compared to adjacent areas of the Carajás Mineral province and consist mainly of massive blocks and boulders. The most prominent geomorphologic feature consists of an elongated arc-shaped smooth hill sustained mainly by ultramafic rocks, up to 60 meters higher than flat areas where gabbroic rocks prevail. The layering forms an arc-shaped structure (Fig. 1.3A) that matches the morphology. Host rocks of the Luanga Complex consist of highly foliated gneiss and migmatite of the Xingu Complex in the south/southeast and mafic volcanics and iron formations of the Grão Pará Group in the north/west.

The central portion of the complex has the thickest sequence of layered rocks. To the north and northeastern the layered sequence is truncated by granitic intrusions and, to the south, it becomes progressively thinner. The Luanga Complex and host rocks are cross cut by NNW-SSE diabase dykes. These vertical dykes are up to several meters wide and consist of fine- to medium-grained intergranular to ophitic textured rocks with thin aphanitic chilled margins. Diabase dykes consist mainly of clinopyroxene, olivine and plagioclase, with accessory Ti-magnetite. They belong to a Proterozoic swarm of magnetic mafic dykes that occurs in the Serra Leste region (Teixeira, 2013; Teixeira et al., 2015).

Geological sections (e.g., Fig. 1.3B) defined by drilling indicate that igneous layers have steep dip to the SE. These sections indicate that the Ultramafic Zone overlies the Transition Zone, which overlies the Mafic Zone, suggesting thus that the layered sequence is tectonically overturned. An overturned layered sequence was previously described for the Luanga Complex (Ferreira Filho et al., 2007) and for the Lago Grande Complex (Teixeira, et al., 2015). These studies suggest the existence of regional scale structures leading to large overturned blocks in the Serra Leste region.

The subdivision of the Luanga Complex into three zones, Ultramafic, Transition and Mafic, is based on different type and/or proportion of cumulus minerals (Fig. 1.3C). The estimated thickness of the layered sequence indicated in the stratigraphic column (Fig. 1.3C) and schematic block diagram (Fig. 1.4) is constrained by extensive drilling

in the central portion of the complex, likely to represent the axial portion of the original magma chamber.

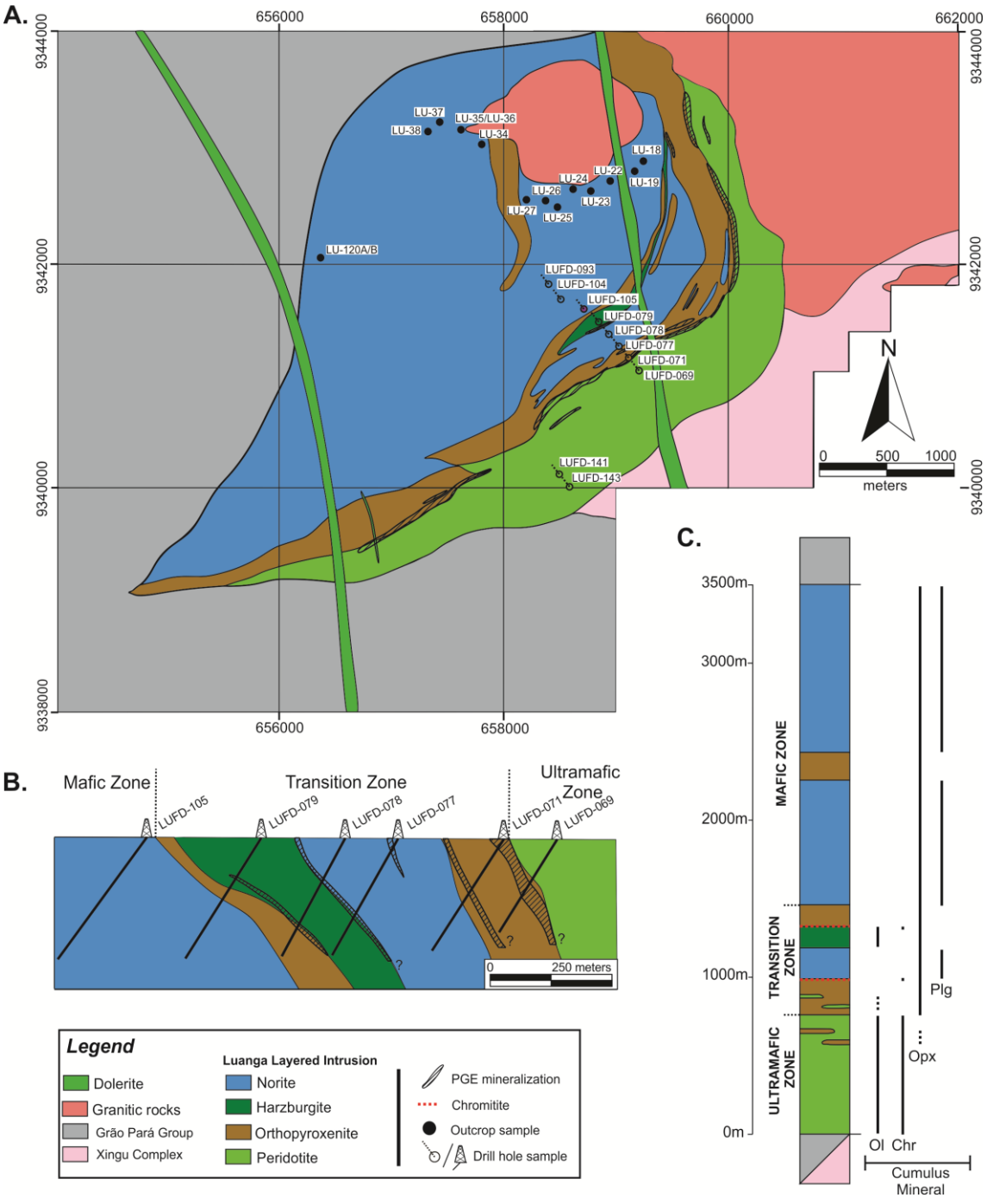

Fig. 1.3: A) Geological map of the Luanga Complex (partially modified from unpublished report of VALE). Note the sampled boreholes and outcrops referred in this study. B) Geological section on the central portion of the complex (partially modified from unpublished report of VALE). C) Representative stratigraphic column for the Luanga Complex. Note the variation of cumulus minerals along the stratigraphy.

1.4.1.1 –Ultramafic Zone

The Ultramafic Zone, about 5 km long and up to 1 km wide, is up to 800 meters thick (Fig. 1.3C) and consists of serpentinites (i.e., metamorphosed peridotite) with a few meters thick orthopyroxenite lenses at the upper portions (facing criteria considering the overturned sequence). The lower contact of the Ultramafic Zone with the Xingu Complex and Grão Pará Group is poorly exposed and was mapped based mainly on soil geochemistry surveys. The contact with the overlying Transition Zone is gradational and characterized by a 5-10 meters thick sequence of interlayered orthopyroxenite and serpentinite. Serpentinite is a massive fine-grained rock (Fig. 1.5A), with discrete cross-cutting domains of foliated magnetite-serpentine schist. These foliated domains are up to several meters thick and probably result of discrete high strain zones. Magmatic textures are usually preserved in massive serpentinites but primary igneous minerals are commonly partially to extensively replaced by metamorphic minerals. Based upon the domains with best preserved textures and minerals, serpentinites are olivine (Ol) cumulates with abundant intercumulus minerals. Chromite (Chr) is a common accessory mineral (~ 2 vol.%) suggesting its occurrence as a liquidus (or cumulus) mineral throughout the Ultramafic Zone. Chromite occurs in relict cores of fine-grained euhedral crystals variably replaced by magnetite (or ferrichromite) in the outer rim or along fractures. Serpentinites have variable modal proportions of serpentine, chlorite, talc, amphibole (tremolite/actinolite) and magnetite, as the result of extensive replacement of olivine and intercumulus minerals. Textural and mineralogical features indicate that the Ultramafic Zone consists mainly of olivine + chromite cumulates with ortho- to mesocumulate textures, the later consisting of abundant intercumulus plagioclase (Pl) and orthopyroxene (Opx).

1.4.1.2 –Transition Zone

The Transition Zone, about 5 km long and up to 1 km wide, comprises an up to 800 meters thick (Fig. 1.3C) pile of interlayered ultramafic and mafic cumulate rocks. Interlayering of different rocks types in different scales (from a few centimeters up to dozens of meters), is a distinctive feature of the Transition Zone. Cumulate rocks have variable textures, from adcumulate to orthocumulate, and variable assemblages of cumulus and intercumulus minerals. The most common rock types are orthopyroxenite,

harzburgite, norite and chromitite, but minor dunite, troctolite, olivine orthopyroxenite and melanorite occur in the Transition Zone.

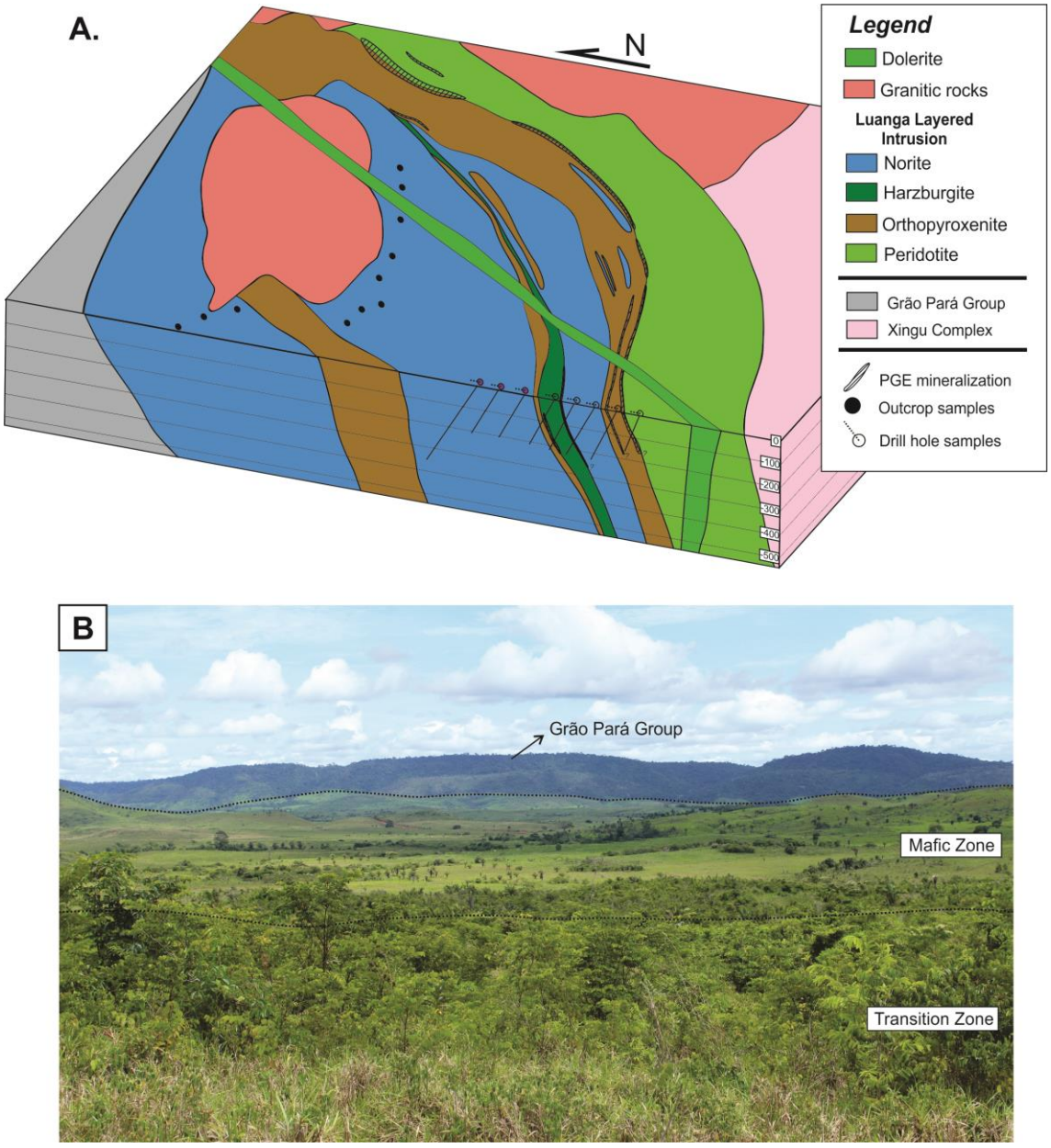

Fig. 1.4: A) Simplified tridimensional model of the Luanga Complex. Note the overturned structure where the Ultramafic Zone overlies the Transition and Mafic Zones. The downward limit of the PGE mineralization is given by drilling. B) Panoramic view of the Luanga Complex. Note the contrasting highest relief of the Transition Zone and the flat terrain of the Mafic Zone. The higher hill in the back consists of iron formation and volcano-sedimentary rocks from the Grão Pará Group.

Orthopyroxenite is a medium- to coarse-grained orthopyroxene cumulate. The texture varies from adcumulate (Fig. 1.5B) to meso- and orthocumulate with plagioclase as the predominant intercumulus mineral. The transition from an adcumulate orthopyroxenite to orthocumulate rocks (i.e., plagioclase orthopyroxenite or melanorite) is commonly gradational and result from continuous upward increase in plagioclase content.

Harzburgite is a medium- to coarse-grained olivine and chromite cumulate with meso- to orthocumululate texture. Most rocks consist of abundant oikocrysts of orthopyroxene (harzburgite) or orthopyroxene and plagioclase (plagioclase harzburgite) enclosing several olivine and chromite crystals (Fig. 1.5C). Olivine crystals included in orthopyroxene oikocrysts show corrosion features (Fig. 1.5D) indicating a peritetic reaction of cumulus olivine and intercumulus liquid (i.e, Ol + liquid = Opx).

Norite is a medium-grained orthopyroxene and plagioclase adcumulate rock (Fig 1.5E). It occurs as discontinuous layers commonly following a gradational upward fractionation from orthopyroxenite, to plagioclase orthopyroxenite and norite.

Chromitite layers with variable thickness and textures occur mainly in the upper portions of the Transition Zone and the lowermost portion of the Mafic Zone (Fig. 1.3C). The thickest chromitite is an up to 60 cm chromite-rich layer located at the contact between the upper harzburgite and orthopyroxenite layers from the Transition Zone. Several thin chromitites (< 10 cm-thick) occur in the Transition Zone and in the lowermost portion of the Mafic Zone. Thin chromitites hosted by noritic rocks are commonly preceded by a thin layer of harzburgite, These chromitites are fine- to medium-grained chromite cumulates with intercumulus plagioclase and orthopyroxene The upward transition from massive chromitite, to chain textured chromitite and disseminated chromite is common and provides a facing criterion for the igneous stratigraphy of the Luanga Complex (Fig. 1.5F).

1.4.1.3 – Mafic Zone

The Mafic Zone, about 5 km long and up to 3 km wide, comprises an up to 2000 meters-thick (Fig. 1.3C) sequence of monotonous noritic rocks (i.e., orthopyroxene and plagioclase cumulates). Minor interlayered ultramafic rocks in the Mafic Zone consist mainly of orthopyroxenite (Fig. 1.3C). These rocks are similar to those described in the Transition Zone. Medium-grained norite consisting of tabular plagioclase and anhedral

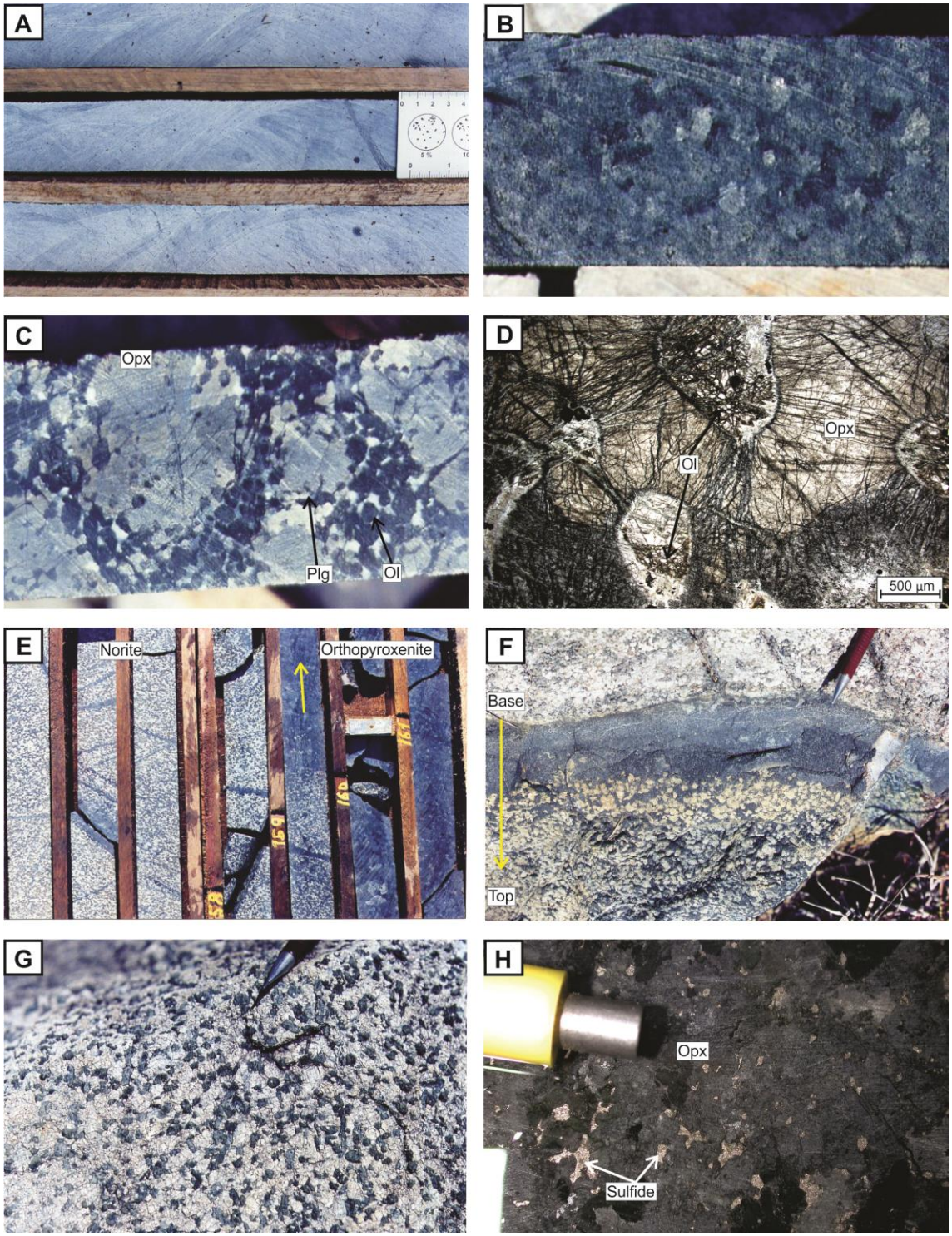

Fig. 1.5: A) Massif serpentinite from the Ultramafic Zone. B) Medium grained orthopyroxenite with adcumulate texture. C) Harzburgite with olivine (dark color) enclosed into orthopyroxene oikocrysts. Note interstitial plagioclase (whitish color). D) Photomicrograph of harzburgite with partially corroded olivine inclusion in orthopyroxene oikocryst. E) Contact of orthopyronenite and norite. The arrow points to the upper portion of the borehole, such that the norite is located stratigraphically below the orthopyroxenite (see geological section in Fig. 3B for orientation). The contact has a thin (~ 10 cm) zone of orthopyroxenite with intertitial plagioclase. F) Chromitite layer associated with norite. The arrow indicates the base-to-top gradational transition from massive chromitite to chain textured chromitite. G) Adcumulate norite consisting of orthopyroxene (greenish color) and plagioclase (white color). H) Interstitial base metal sulfides in PGE mineralized rocks of the Sulfide Zone. The core is 4.7 centimeters wide in all photos. Mineral abbreviations: (Ol) olivine, (Opx) orthopyroxene and (Plg) plagioclase.

orthopyroxene is the characteristic rock type of the Mafic Zone (Fig. 1.5G). These rocks are adcumulates except for rare domains with interstitial quartz and/or clinopyroxene

1.4.1.4 – Sulfide Zone

Several PGE-mineralized intervals occur in the Transtion Zone but the Sulfide Zone hosts the bulk of the PGE resources in the Luanga Complex (Ferreira Filho et al., 2007). A detailed description of the PGE deposit is being developed (Mansur et al., in prep.) and just a brief description of the Sulfide Zone is provided in here. The Sulfide Zone consists of a 10 – 50 meters thick interval with disseminated sulfides located at the contact of the Ultramafic and Transition zones (Figs. 1.3A, 1.3B and 1.4A). This stratabound PGE mineralization consists of disseminated sulfides (~ 1-3-vol. %) hosted mainly by orthopyroxenite. Base metal sulfides (pentlandite > pyrrhotite > >> chalcopyrite) interstitial to cumulus silicates or their pseudomorphs characterize the Sulfide Zone. PGE contents in the Sulfide Zone have strong positive correlation with modal sulfides. Pt+Pd contents are highly variable in the mineralized interval, from a few ppb up to several ppm, have positive correlation with copper and sulfur contents, and show consistent Pt/Pd ratios of about 0.7 (Ferreira Filho et al., 2007; Mansur et al., in prep.). In addition to PGE associated with disseminated sulfides in the Sulfide Zone, distinctively PGE enriched (Pt+Pd > 1 ppm) occur in sulfide-poor intervals in the Transition Zone. These unusual sulfide-poor PGE mineralizations are similar to those described in the Serra da Onça Complex (Ferreira Filho et al., 2007) and in the footwall zone of the Santa Rita deposit in the Mirabela Complex (Ferreira Filho et. al., 2013).

1.4.1.5 – Metamorphism

Metamorphic assemblages commonly replace primary igneous minerals of the Luanga Complex. This metamorphic alteration is heterogeneous and characterized by an extensive hydration that largely preserves primary textures, bulk rock compositions and the compositional domains of igneous minerals. The penetrative fabric is restricted to narrow domains of up to a few meters across, and igneous textures are identified in adjacent nondeformed domains. These assemblages include serpentine + talc + magnetite ± cummingtonite in replaced olivine-bearing ultramafic rocks, talc + serpentine + magnetite ± cummingtonite in replaced orthopyroxenites, and hornblende + chlorite + epidote in replaced mafic rocks. Metamorphic assemblages indicate temperatures up to the amphibolite facies of metamorphism in the Luanga (Ferreira

Filho et al., 2007) and Lago Grande Complexes (Teixeira et al., 2015). The age and type of metamorphism affecting the layered intrusions and their host metavolcanic and metasedimentary rocks in the Serra Leste region is a debated issue (Dardenne et al., 1988; Suita, 1988; Teixeira et al., 2015; Tavares, 2015) and will not be addressed in this study. However, the effect of metamorphism on sulfides is relevant for discussions regarding PGE mineralizations hosted by sulfide-bearing and sulfide-poor cumulate rocks in the Luanga Complex. The metamorphic alteration is heterogeneous as indicated by rocks with magmatic minerals and texture closely associated (i.e., a few to dozen of meters apart in drill core) with rocks where primary textures are preserved but magmatic minerals are extensively replaced. Apart from highly variable hydration, the compositions of variably altered samples are very similar when recalculated on anhydrous basis, thus supporting that metamorphic alteration does not promote a significant change in composition.

1.4.2 – Mineral Chemistry

Systematic studies of mineral chemistry of cumulus minerals from the Luanga Complex (i.e., olivine, orthopyroxene and plagioclase) were performed in samples collected in a representative section along the central and northern parts of the complex (Fig. 1.3A). This composed section comprises drill core samples collected from boreholes intersecting the Ultramafic Zone (LUFD-143, LUFD-141 and LUFD-69), Transition Zone (LUFD-69, LUFD-71, LUFD-77, LUFD-78 and LUFD-79) and Mafic Zone (LUFD-105, LUFD-104 and LUFD-93), together with samples from outcrops of the Mafic Zone (see Fig. 1.3A for the location of boreholes and outcrops). Based on detailed sampling (~ 140 samples) and petrographic studies, 10 samples with olivine, 19 samples with orthopyroxene and 27 samples with plagioclase were chosen for chemical analyses. Olivine was analysed in samples of serpentinite and harzburgite from the Ultramafic and Transition zones, respectively. Orthopyroxene was analysed in samples of orthopyroxenite, harzburgite and norite from the Transition Zone. Plagioclase was analysed in samples of norite from the Transition and Mafic zones. Compositional variation of olivine, orthopyroxene and plagioclase with stratigraphy in the Luanga Complex is shown in figure 1.6.

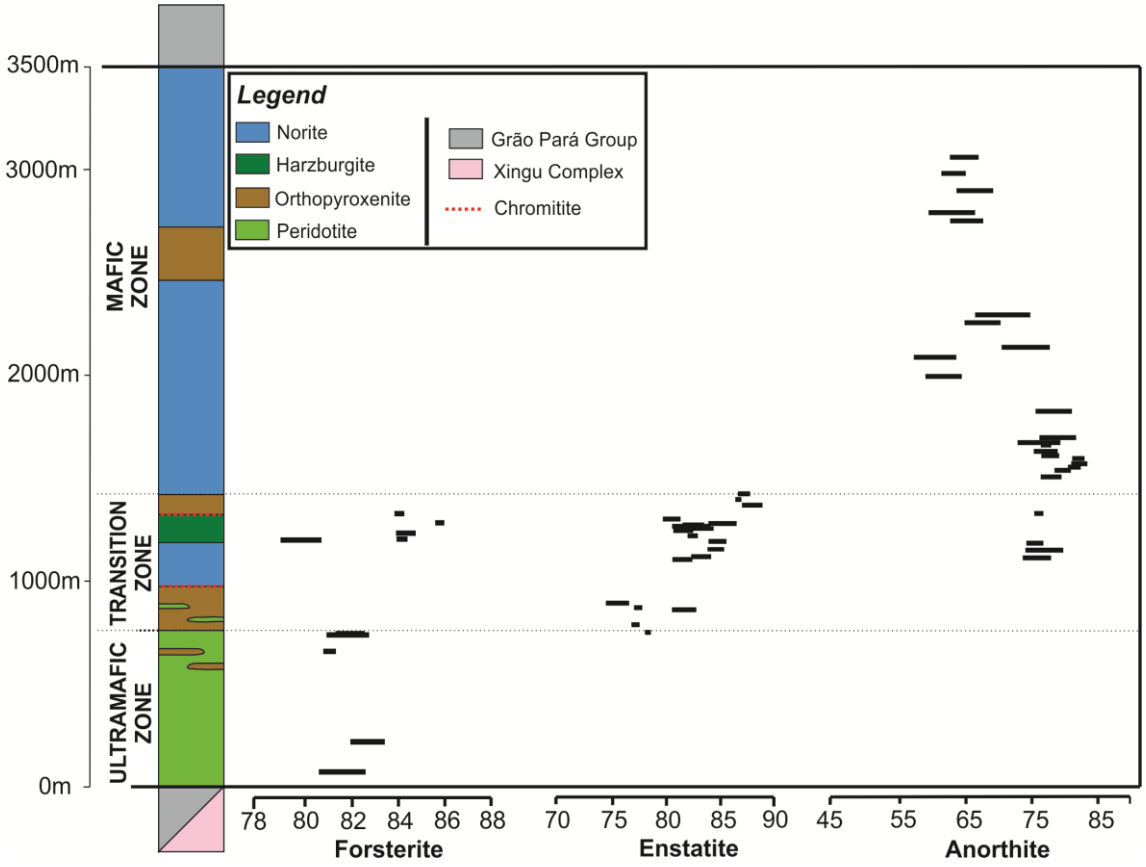

Fig. 1.6: Compositional variations of cumulus minerals throughout the stratigraphy of the Luanga Complex.

Olivine compositions range from $Fo_{78.8}$ to $Fo_{86.7}$ mol% (Fig. 1.6) indicating moderately primitive compositions. A systematic evaluation of cryptic variation of olivine is hampered by the restricted distribution of unaltered crystals throughout the Ultramafic and Transition zones. Nevertheless, our results indicate that higher Fo contents occur in harzburgites of the upper portion of the Transition Zone (Fig. 1.6). Ni contents in olivine from the Ultramafic Zone range from 2800 to 3700 ppm and are positively correlated with Fo contents (Fig. 1.7A). Ni contents in olivine crystals from the Transition Zone range from 4500 to 7400 ppm and are weakly correlated with Fo contents (Fig. 1.7A). Considering the Fo range, the contents of Ni in the Luanga Complex, especially in the Transition Zone, are distinctively high.

Orthopyroxene compositions range from $En_{77.0}$ to $En_{89.9}$ mol% in the Transition Zone. The cryptic variation of orthopyroxene shows many reversals within a consistent upward increase in En contents, suggesting an inverse fractionation in the Transition Zone (Fig. 1.6). This trend is consistent with olivine compositions and indicates

progressively more primitive compositions (i.e., higher Mg/Mg+Fe ratios) toward de upper portions of the Transition Zone. Ni contents in orthopyroxene range from 800 to 1700 ppm with weak positive correlation with En contents (Fig. 1.7B). Ni contents in orthopyroxene of the Transition Zone are distinctively high and consistent with elevated values reported for olivine.

Plagioclase compositions range from $An_{83.2}$ to $An_{57.3}$ mol% in the Mafic Zone and the upper portion of the Transition Zone. The cryptic variation of plagioclase shows several reversals within a consistent upward decrease in An contents, suggesting a normal fractionation in the Mafic Zone (Fig. 1.6). Plagioclase compositions in the Transition Zone, range from $An_{74.28}$ to $An_{78.61}$ indicating An contents lower than those reported in the lower portion of the Mafic Zone.

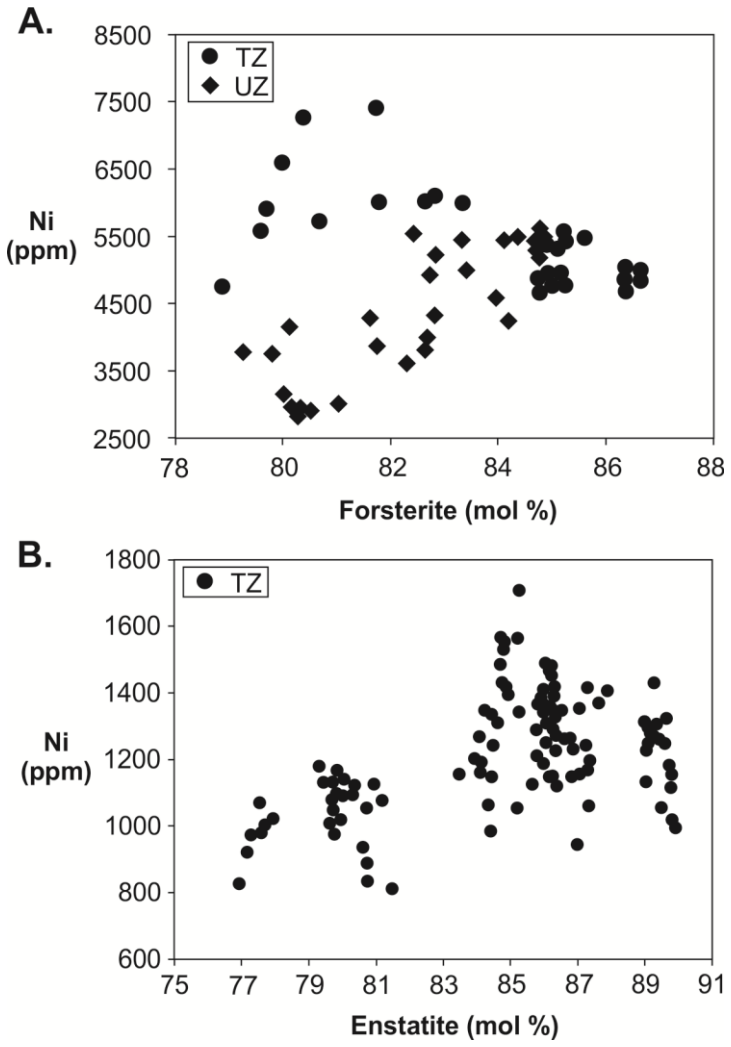

Fig. 1.7: A) Plot of Ni versus forsterite contents for olivine crystals. B) Plot of Ni versus enstatite contents for orthopyroxene crystals.

In summary, cryptic variations shown in figure 1.6 indicate an inverse fractionation trend in the Transition Zone, followed by a normal fractionation trend in the Mafic Zone. These broad compositional trends include several reversals throughout the stratigraphy of the Luanga Complex, thus suggesting a magmatic evolution in a dynamic open system magma chamber, a subject to be considered in the following discussions.

1.4.3 - Bulk rock geochemistry

A group of 21 samples representative of the stratigraphy of the Luanga Complex, comprising 3 samples from the Ultramafic Zone, 11 samples from the Transition Zone and 7 samples from the Mafic Zone, was analysed for major, minor and trace elements (see Table 1.1 and Online Supplementary Table 2). Variable amounts of loss on ignition reflect the degree of alteration and/or different alteration minerals for distinct rock types. Hence, the compositions of major and minor elements are normalized to 100% on an anhydrous basis. The reasoning for normalizing on anhydrous basis is to equilibrate differences originated by various degrees of hydration, especially when olivine cumulates (i.e., 6 to 11 wt.% LOI) are compared with orthopyroxene or orthopyroxene-plagioclase cumulates (i.e., 1 to 5 wt.% LOI).

1.4.3.1 – Major and minor elements

Because the Luanga Complex consists of cumulate rocks, their major and trace element compositions are controlled by the type of cumulus minerals. The plot of MgO vs major element oxides (Fig. 1.8A-F) is consistent with the predominance of olivine, orthopyroxene and plagioclase cumulates, as indicated by petrographic studies. This suggestion is supported by comparing major element compositions with the composition of cumulus minerals obtained in this study (Fig. 1.8A-F).

Rocks with olivine as cumulus mineral (i.e., serpentinite and harzburgite) have MgO content (normalized to 100% on an anhydrous basis) between 26.05 to 43.17 wt.%. These highly variable values are consistent with distinctively different proportions of intercumulus minerals in these rocks, as indicated by samples with adcumulate to orthocumulate textures. The contents of SiO_2, CaO, Al_2O_3, Na_2O and K_2O of these rocks are not controlled just by different proportions of olivine and orthopyroxene (Fig. 1.8A-F). Compositions plotting outside the Ol-Opx tie lines have

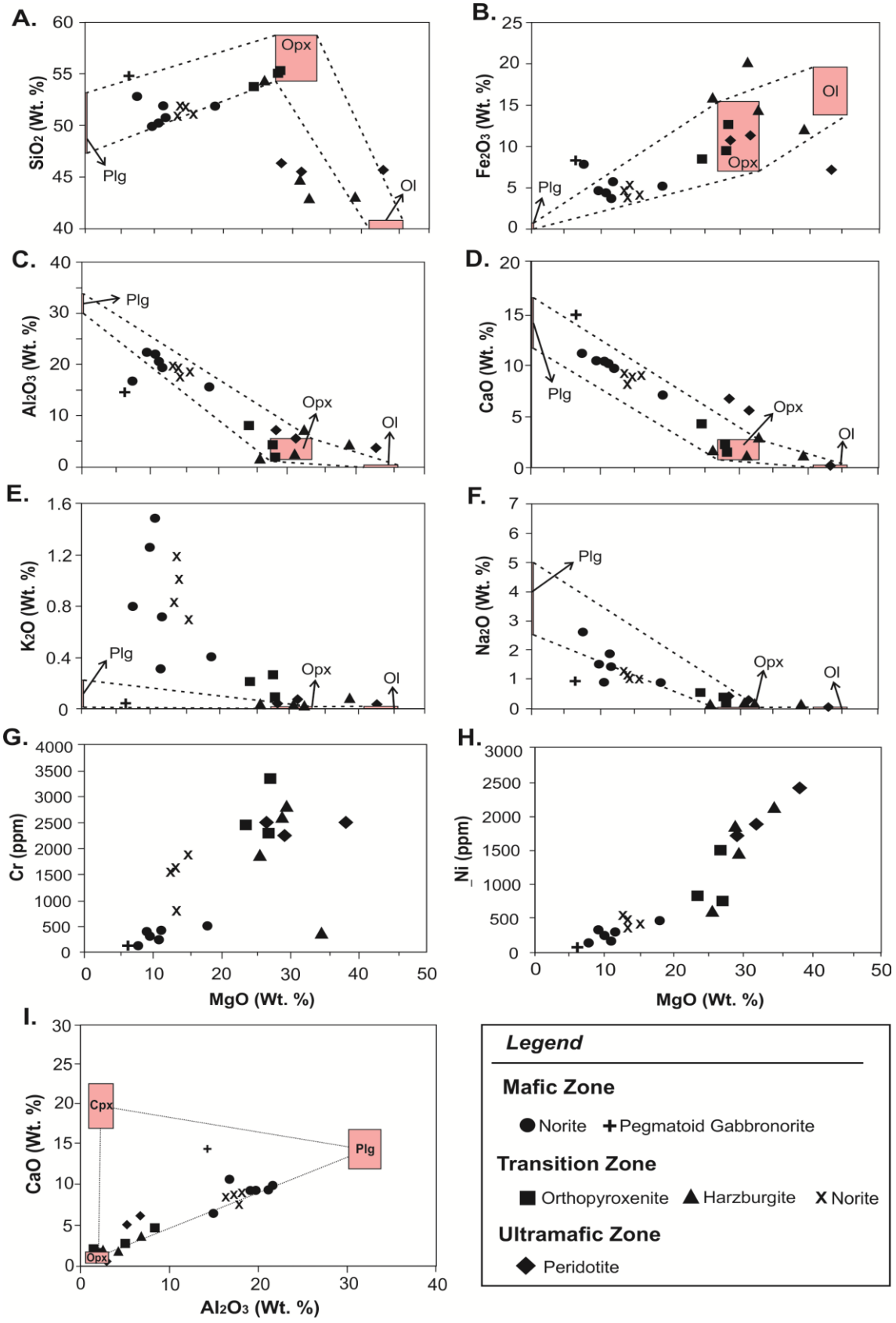

Fig. 1.8: A-H: Plot of MgO versus major element oxides and minor elements for rocks of the Luanga Complex. I: Plot of Al_2O_3 versus CaO for rocks of the Luanga Complex. Data from Table 1 normalized to 100% on an anhydrous basis. Compositions of olivine, orthopyroxene and plagioclase correspond to microprobe analyses reported in this study, whereas the composition of clinopyroxene are from gabbroic rocks of the Serra da Onça Complex (Rosa, 2014).

intercumulus plagioclase, resulting in relatively lower SiO_2 content and higher CaO and Al_2O_3 contents. The contents of Ni and Cr are controlled by olivine and chromite, respectively (Fig. 1.8G-H). Values of Ni and Cr are compatible with Ni content in olivine (~ 3000-6000 ppm of Ni in rocks with approximately 40-50 vol. % olivine) and the presence of chromite as an accessory mineral (~ 1-2 vol.%), respectively. Very low sulfur contents in these rocks (S < 0.04 wt.%) are consistent with the lack of sulfide minerals and Ni contents being controlled mainly by olivine.

Orthopyroxenites have MgO content (normalized to 100% on an anhydrous basis) between 24.52 and 28.25 wt.%, consistent with rocks composed mainly of cumulus orthopyroxene and minor amounts of intercumulus plagioclase. The contents of SiO_2, CaO, Al_2O_3, Na_2O and Fe_2O_3 of these rocks are restricted to compositions plotted along the Opx-Pl tie lines (Fig. 1.8A-F). Cr contents (up to 3500 ppm) are essentially the same of the olivine-bearing samples, attesting that Cr is also controlled by accessory chromite in orthopyroxenites. Ni contents are lower than in olivine-bearing rocks (up to 1500 ppm) due to lower Ni content in orthopyroxene (up to 1600 ppm) compared to olivine.

Norite is the lithotype with the lowest MgO content (from 7.52 to 11.59 wt.%) of the Luanga Complex. The compositions of norites from the Transition and Mafic zones are very similar (Fig. 1.8A-F) with contents of SiO_2, CaO, Al_2O_3, Na_2O and Fe_2O_3 restricted to the plagioclase-orthopyroxene tie line (Fig. 1.8A-F), as expected for plagioclase-orthopyroxene adcumulates. Nevertheless, contents of K_2O above and Na_2O bellow the plagioclase-orthopyroxene tie line may result from minor alteration and/or accessory phlogopite (Fig. 1.8E-F). Cr and Ni contents decrease with decreasing MgO contents as the result of progressive disappearance of chromite and reduction of Ni and Cr contents in orthopyroxene with fractionation (Fig 1.8G-H). Cr contents of up to 1880 ppm are consistent with the common presence of chromite as a liquidus mineral in norites of the Transition Zone.

Primary pyroxenes are not preserved throughout most of the Mafic Zone (Fig. 1.8E-F). While extensive petrographic data indicate that norite is the only mafic rock type in the Transition Zone, direct petrographic evidence is not available for the extensively replaced rocks of the Mafic Zone, This raises the possibility that fractionation in the Luanga Complex led to the crystallization of clinopyroxene as a liquidus mineral in the upper portion of the Mafic Zone, such that the crystallization

sequence evolved from Opx+Pl cumulates to Opx+Cpx+Pl cumulates, as described in several layered intrusions. The plot of CaO vs Al_2O_3, comparing bulk rock and mineral compositions (Fig. 1.8I), indicate that plagioclase and orthopyroxene adcumulates prevail in the Mafic Zone. Sample LUFD-120B, a coarse-grained gabbroic rock collected from an elongated 1-2 meters long pegmatoidal pod has a composition consistent with a gabbronorite (Fig. 1.8I). This sample has the lowest MgO, Ni and Cr contents (Fig. 1.8G-H) and is interpreted as resulting from crystallization of trapped intercumulus liquid.

1.4.3.2 – Trace elements

Mafic-ultramafic rocks of the Luanga Complex have relatively low contents of incompatible trace elements (Table 1.1), as expected for olivine, pyroxene and plagioclase cumulates. Variations in contents of incompatible trace elements in mafic-ultramafic cumulates in layered complexes result from the combined effect of variable assemblages of cumulus minerals, fractionation of the parental magma and variable amounts of trapped intercumulus liquid (e.g., Barnes, 1986; Ferreira Filho et al., 1998). Distinct primitive mantle-normalized rare earth element (REE) profiles characterize different cumulate rocks of the Luanga Complex (Fig. 1.9). REE profiles for serpentinites (i.e., olivine cumulates) have flat to slightly positive slope for LREE and flat slope for HREE (Fig. 1.9A). Sample LUFD-141-39, an extensively replaced serpentinite (11.57 wt.% LOI) with adcumulate texture, has the lowest contents of REE (Fig. 1.9A). This sample has an irregular REE profile with distinct negative Eu anomaly, likely to result from alteration or due to larger analytical errors in samples close to the detection limits of the analytical methods. REE patterns for samples of orthopyroxenite (Fig. 1.9B) have positive slope for LREE and slightly negative slope for HREE. The contents of LREE and primitive mantle normalized La/Sm ratios (La/Sm_{MN}) of orthopyroxenites increase with the amount of intercumulus plagioclase. Samples with intercumulus plagioclase also have positive Eu anomalies, while an adcumulate orthopyroxenite (sample LUFD-69-115.64) has negative Eu anomaly (Fig. 1.9B). REE patterns for harzburgite have slightly positive slope for LREE, flat to slightly negative slope for HREE and weak negative Eu anomalies (Fig. 1.9C). These samples have the lowest LREE contents for the Luanga Complex. Norite from the Transition and Mafic zones has distinctively positive slopes for LREE, flat slopes for

HREE and distinctively positive Eu anomalies (Figs. 1.9D-E), as expected for rocks with abundant plagioclase.

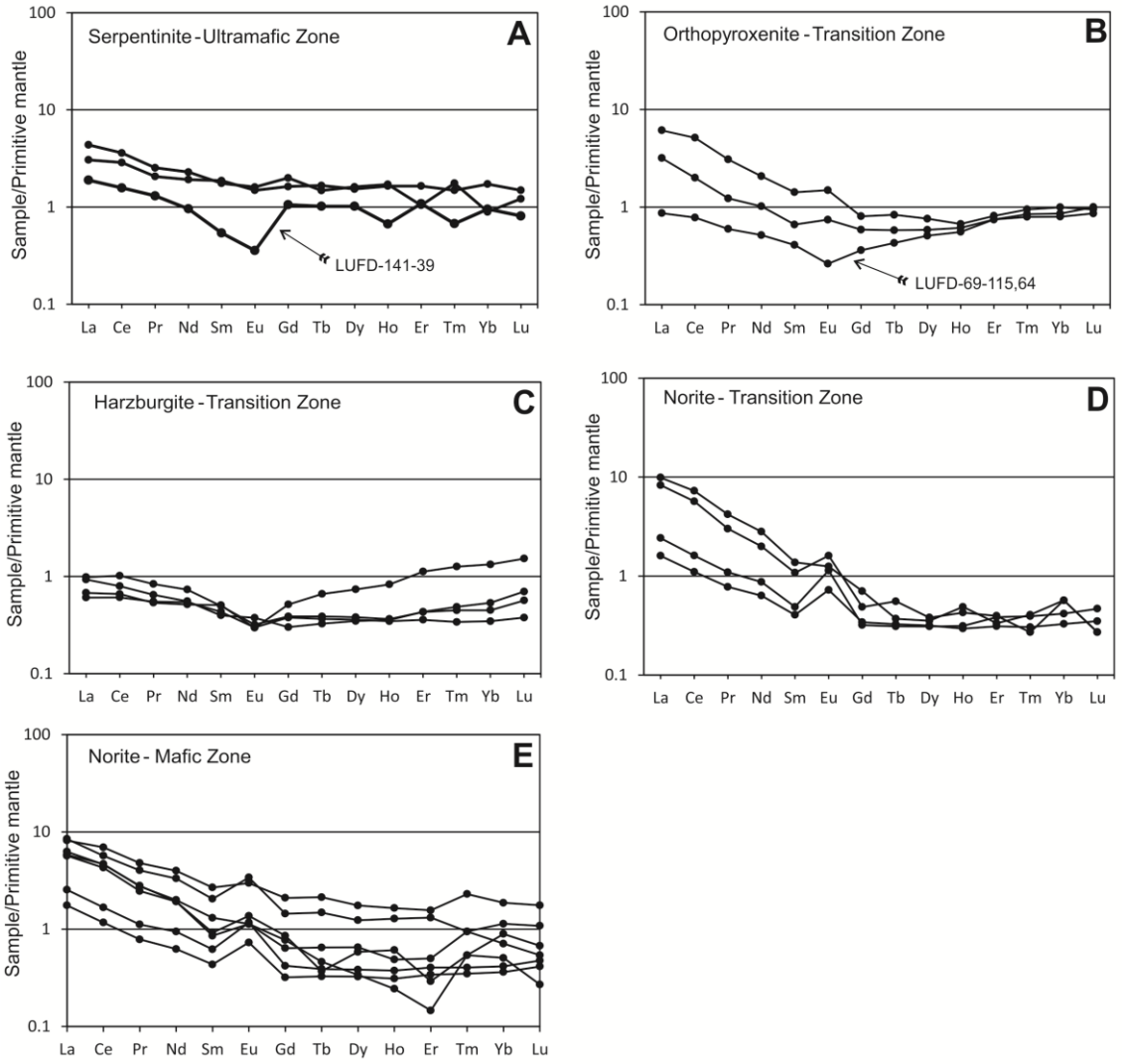

Fig. 1.9: Primitive mantle-normalized REE patterns for samples of the Luanga Complex. A) Serpentinite from the Ultramafic Zone. B) Orthopyroxenite from the Transition Zone. C) Harzburgite from the Transition Zone. D) Norite from the Transition Zone. E) Norite from the Mafic Zone. Data from Table 1 and Supplementary Table 2. Primitive mantle normalization values are from Sun and McDonough (1989).

Contents for several incompatible high field strength elements (e.g., Ta, Nb, Th, Hf) in ultramafic rocks of the Luanga Complex are close to their lower limits of quantification in the analyses of this study (Table 1.1), and should be considered with discretion. In addition, contents for several LILE (large ion lithophile elements) are variable due to the effect of metamorphic alteration. In order to prevent scattering associated with alteration or analytical uncertainties, mantle normalized trace elements

patterns were plot for alteration-resistant trace elements on norite samples, which have the highest trace elements content (Fig. 1.10). The mantle-normalized alteration-resistant trace element patterns for norite samples are fractionated, as indicated by relative enrichment in LREE and Th, with strong negative Nb and Ta anomalies (Fig. 1.10).

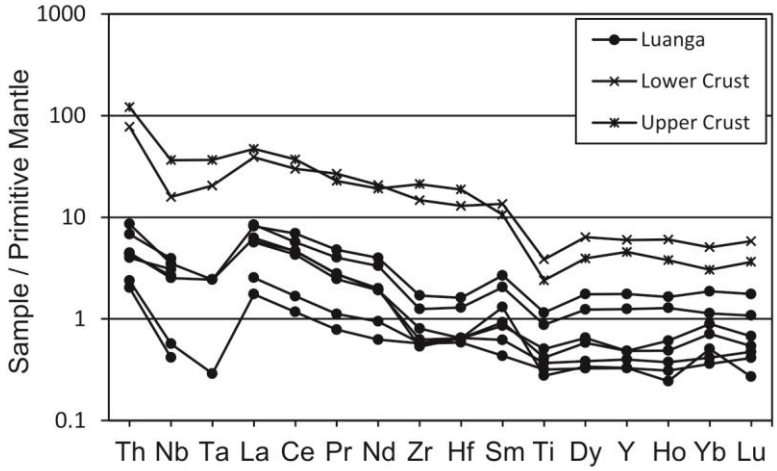

Fig. 1.10: Primitive mantle-normalized alteration-resistant trace elements patterns for samples of norite from the Mafic Zone of the Luanga Complex. Data from Table 1 and Supplentary Table 2. Lower and Upper Crust values are from Wedepohl (1995). Primitive mantle normalization values are from Sun and McDonough (1989).

1.5 – Discussion

1.5.1 – Magmatic structure

Ni-Cu-PGE deposits in mafic-ultramafic intrusion are broadly classified into those associated with magma conduits (or chonoliths) and those associated with layered intrusions (Beresford and Hronsky, 2014). Ore-hosting intrusions come in widely variable architectures and sizes as the result of highly complex mechanisms of mantle magma transport and storage in the crust (Barnes et al., 2016). Although typical tube-like conduits (e.g., Limoeiro, Mota-e-Silva et al., 2013; Nebo-Babel, Seat et al., 2007) have very distinct architecture compared with classical layered intrusions (e.g., Skaergaard, Irvine, 1987; Niquelandia, Ferreira Filho et al., 1992 and 2010), they are just members of a wide range of structures resulting from variable and usually continuous magmatic processes. The main features of the architecture of the Luanga Complex are listed below to provide the framework for the following discussion on the compositional variations through the intrusion.

a) The morphology is broadly an arc-shaped structure with a thicker central portion that becomes thinner toward the edges.

b) Layering in variable scales (from a few centimeters to a few hundred meters thick) is the most characteristic structure.

c) Cyclic units occur in all zones of the Luanga Complex and are abundant in the TZ.

The features mentioned above are characteristic of layered intrusions originated in open-system magma chambers through successive influxes of magma.

1.5.2 – Compositional variations through the Luanga Complex

Geochemical results described in this study provide constraints for the magmatic fractionation of the Luanga Complex. The schematic model in figure 1.11 summarizes these features. The Ultramafic Zone (Fig. 1.11; Stage 1) at the base of the layered sequence results from initial inputs of magma into the chamber. Cryptic variation of olivine in the Ultramafic Zone indicates a narrow compositional range (Fo 79.3 to 84.9) and moderately primitive compositions. The restricted compositional range within the monotonous sequence of olivine and chromite cumulates of the Ultramafic Zone suggests open-system crystallization involving periodic replenishment by new primitive magma pulses (Fig. 1.11; Stage 1). Fractionation following the replenishment of the magma chamber is limited, such that the evolving magma does not usually depart from the field where olivine and chromite are liquidus minerals. The contact of the Ultramafic and Transition zones is marked by the change from a monotonous to a highly variable sequence of rock types, the later interpreted as a sequence of cyclic units. Cryptic variation of orthopyroxene in the Transition Zone (Fig. 1.6) indicates several reversals within a major upward trend of progressively more primitive compositions. From bottom upwards this reversed fractionation consists of several normal fractionating cyclic units of variable thickness, which are indicated by individual cycles consisting of a complete sequence of harzburgite, orthopyroxenite and norite, or an incomplete sequence (usually orthopyroxenite-norite or harzburgite-orthopyroxenite). Chromitite layers or seams commonly occur at the base of cyclic units as reported in several layered intrusions (e.g., Bushveld Complex, Naldrett et al., 2012; Great Dyke, Wilson, 1982), or immediately (~ 10 centimeters) above the most primitive rock type of a new cycle. Cryptic variation of olivine in the Transition Zone indicates a larger compositional range (Fo 78.8 to 86.7) compared to the Ultramafic Zone. Results

indicate that the most primitive olivine in the Luanga Complex occurs at the upper portion of the Transition Zone, which is consistent with cryptic variation of orthopyroxene (Fig. 1. 6). The compositional variation of orthopyroxene and olivine in the Transition Zone suggests and open-system crystallization involving periodic replenishment by new primitive magma pulses followed by significant fractionation (Fig. 1.11; Stage 2). To explain the reversed fractionation of the Transition Zone, the residual magma resident in the magma chamber after fractionation should become progressively more primitive. This upward trend of progressively more primitive compositions may result either from an input of progressively more primitive parental magma, or a progressive increase in the amount of the same parental magma. Despite the fact that the Mafic Zone consists mainly of a monotonous sequence of orthopyroxene and plagioclase adcumulates, cryptic variation of plagioclase along the Mafic Zone indicates multiple reversals within an upward fractionation trend (Fig. 1.6). These reversals indicate several new influxes of fresh magma followed by fractionation, such that the evolving magma does not usually depart from the field where plagioclase and orthopyroxene are liquidus minerals (Fig. 1.11; Stage 3).

Cryptic variation and the crystallization sequence along the stratigraphy of the Luanga Complex (Fig. 1.11) are characteristic of layered intrusions originated in highly dynamic open-system magma chambers, a common feature in PGE-mineralized intrusions.

1.5.3 –Constraints on the composition of the parental melt

The characterization of parental magmas in layered complexes is a key feature to understand the nature of mantle source, the amount of assimilation of crustal rocks during ascent and emplacement and their potential to host economic deposits. The composition of the parental magma of the Luanga Complex cannot be constrained by common approaches used to define their composition in well-exposed intrusions with primary composition and magmatic architecture largely preserved (e.g., chilled margin,

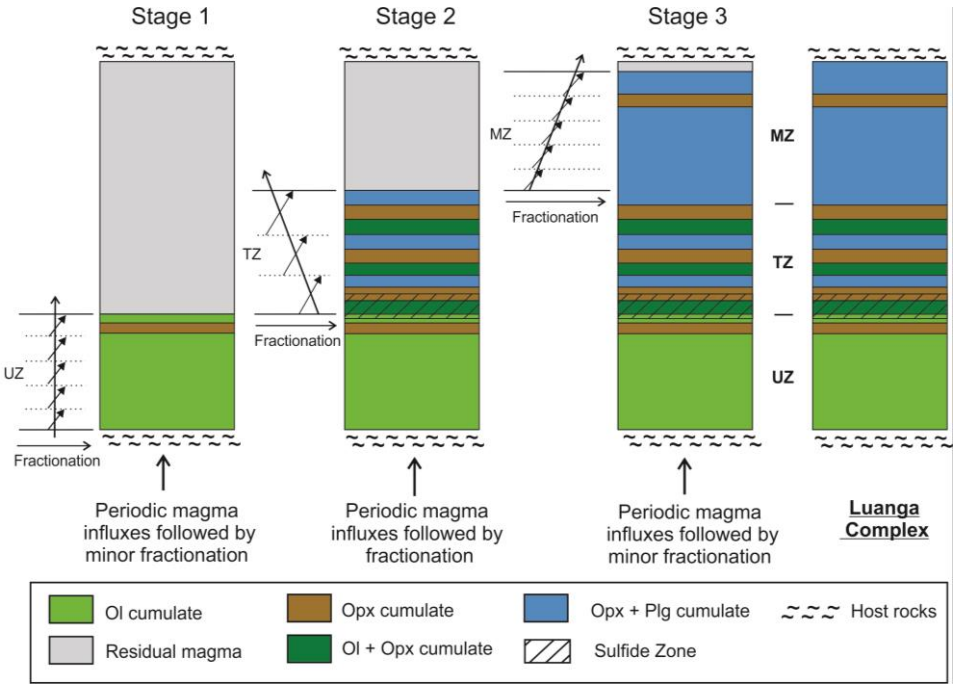

Fig. 1.11: Schematic model illustrating the evolution of the Luanga Complex. See text for explanation. Mineral abbreviations: (Ol) olivine, (Opx) orthopyroxene and (Plg) plagioclase.

bulk composition, extrusive equivalents, related dykes). Once a direct composition of parental magma is not available, its nature can be inferred from the crystallization sequence and cumulate geochemistry. The compositional range of cumulus olivine within the Ultramafic and Transition zones of the Luanga Complex ($Fo_{78.9\text{-}86.4}$) is comparable to those reported for the central zone of the Jinchuan intrusion ($Fo_{83\text{-}86}$; Li et al., 2004) and the Ultramafic Zone of the Lago Grande Complex ($Fo_{80.0\text{-}84.7}$; Teixeira et al., 2015). This range of olivine compositions is typical of layered intrusions originated from moderate primitive parental magmas, as suggested by the MgO and FeO compositions of 11.5 wt.% and 11.2 wt.% respectively, estimated by Chai and Naldrett (1992) for the parental magma of the Jinchuan Complex.

The crystallization sequence of the Luanga Complex is similar to those of the major PGE-bearing intrusions (e.g., Bushveld, Stillwater, Great Dyke) in which orthopyroxene precedes clinopyroxene (Eales and Cawthorn, 1996). In fact, cumulus clinopyroxene does not occur in the Luanga Complex. The early crystallization of orthopyroxene indicates that the primary magma was silica saturated, a feature commonly interpreted as the result of crustal assimilation (Campbell, 1985).

Mantle-normalized trace element profiles for norites of the Luanga Complex show characteristic negative Nb and Ta anomalies with relative enrichment in LREE

and Th (Fig. 1.10). A comparison between alteration-resistant mantle-normalized trace elements of lower and upper crust and norites of the Luanga Complex shows similar profiles (Fig. 1.10), which may be interpreted as the result of crustal assimilation during ascent and/or emplacement of the parental magma. The trace element profiles for gabbroic rocks of the Luanga (Fig. 1.10) and Lago Grande complexes (Teixeira et al., 2015) show the same pattern, characterized by negative Nb and Ta anomalies with relative enrichment in LREE and Th. Additional evidence for crustal contamination of the parental magma of the Lago Grande Complex is provided by Nd model ages between 2.94 and 3.56 Ga, with variably negative $\varepsilon Nd_{(T .= 2.72\ Ga)}$ values (Teixeira et al., 2015). Together with the crystallization sequence, geochemical results obtained for layered intrusions of the Serra Leste region, are consistent with original mantle melts contaminated with older continental crust. This interpretation is consistent with the emplacement of layered intrusions within gneisses and migmatites of the Xingu Complex (ca. 3.0 Ga). Although the distribution of alteration-resistant elements in the Luanga Complex is consistent with contamination of a primitive mantle melt with continental crust, lithogeochemical data from the Luanga Complex may also be interpreted as the result of melting an old lithospheric mantle (Zhang et al., 2008).

1.5.4 - Reasons for high nickel contents in olivine and orthopyroxene

Compared with most layered intrusions, olivine from ultramafic rocks of the Luanga Complex has significantly higher Ni content (Fig. 1.12). In fact, when similar Fo contents are considered, Ni contents in the Luanga Complex stand among the highest values ever reported in layered intrusions. The values reported in this study are much higher than content in olivine with variable Fo contents ($Fo_{70.7}$ to $Fo_{91.5}$) of the Bushveld Complex (Fig. 1.12A), including Ni-rich olivine from the Sandsloot section located below the Platreef (Yudovskaya et al, 2013). The similar high Ni contents in the range of 4,000-14,000 ppm for Fo contents of 77.9-90.6 was reported in olivine from the Ni-PGE sulfide lensoid orebodies of the Kevitsa intrusion (Yang et al., 2013).

Possible reasons for high Ni contents in olivine and orthopyroxene include their crystallization from anomalously Ni-rich magmas or their upgrade through interaction with closely associated sulfide liquids (i.e., diffusion of Ni from sulfide liquid to silicates) or sulfides (i.e., solid state diffusion of Ni from sulfides to silicates). The later may be ruled out as an explanation for the Ni enrichment in olivine and orthopyroxene crystals in rocks of the Luanga Complex, as high contents occur mainly in rocks with no associated sulfides. In fact, the Ni content of olivine crystals within the Sulfide Zone (Ni

contents in the range of 3700 to 5900 ppm) is the same or even lower than Ni content of olivine crystals from outside this zone (Ni contents in the range of 2800 to 7400 ppm). Furthermore, although minor Ni enrichment in zoned olivine crystals closely associated with sulfides was reported in a few Ni-Cu deposits (e.g., Voisey's Bay: Li and Naldrett, 1999; Santa Rita: Barnes et al., 2013), olivine crystals closely associated with sulfides are not Ni-enriched in the majority of deposits.

Possible mechanisms for Ni-enrichment of the parental magma include the generation of magmas from pyroxenitic mantle sources (Sobolev et al., 2005; 2007), or the upgrading of magmas through dissolution of previously formed Ni-rich sulfide melts (Kerr and Leitch, 2005). These two alternative mechanisms to generate unusually Ni-rich magmas will be considered for the Luanga Complex.

The Ni contents in olivine in equilibrium with primary magma from peridotite mantle should not contain more than 3,200 ppm Ni (Herzberg, 2011). On the other hand, magmas derived from pyroxenitic sources are expected to have higher Ni contents (up to a factor of 2) such that olivine in equilibrium with these magmas is expected to have proportionally higher Ni contents (Sobolev et al., 2007; Herzberg, 2011). Sobolev et al. (2007) used a large data set of high-precision analyses of olivine phenocrysts from different tectonic settings to conclude that a pyroxenitic mantle source is a major contributor to tholeiitic (silica-saturated) and transitional (moderately silica-undersaturated) magmas of ocean island basalts and large igneous provinces emplaced on thick oceanic or continental lithosphere. The authors' data set indicates that most olivine crystals from these magma types are significantly enriched in Ni and depleted in Mn. This mechanism was recently considered as an explanation for the high Ni contents of olivine crystals in the mafic-ultramafic intrusion associated with the Santa Rita Ni-Cu-PGE sulfide deposit in Brazil (Fig. 1.12B, Barnes et al., 2013). The highest Ni contents in olivine of the Luanga Complex occur in distinctively PGE enriched (Pt+Pd > 1 ppm) intervals of the Transition Zone, while olivine in the Ultramafic Zone have lower Ni (Fig. 1.7A) and PGE contents (Pt+Pd usually < LDL= 80 ppb).

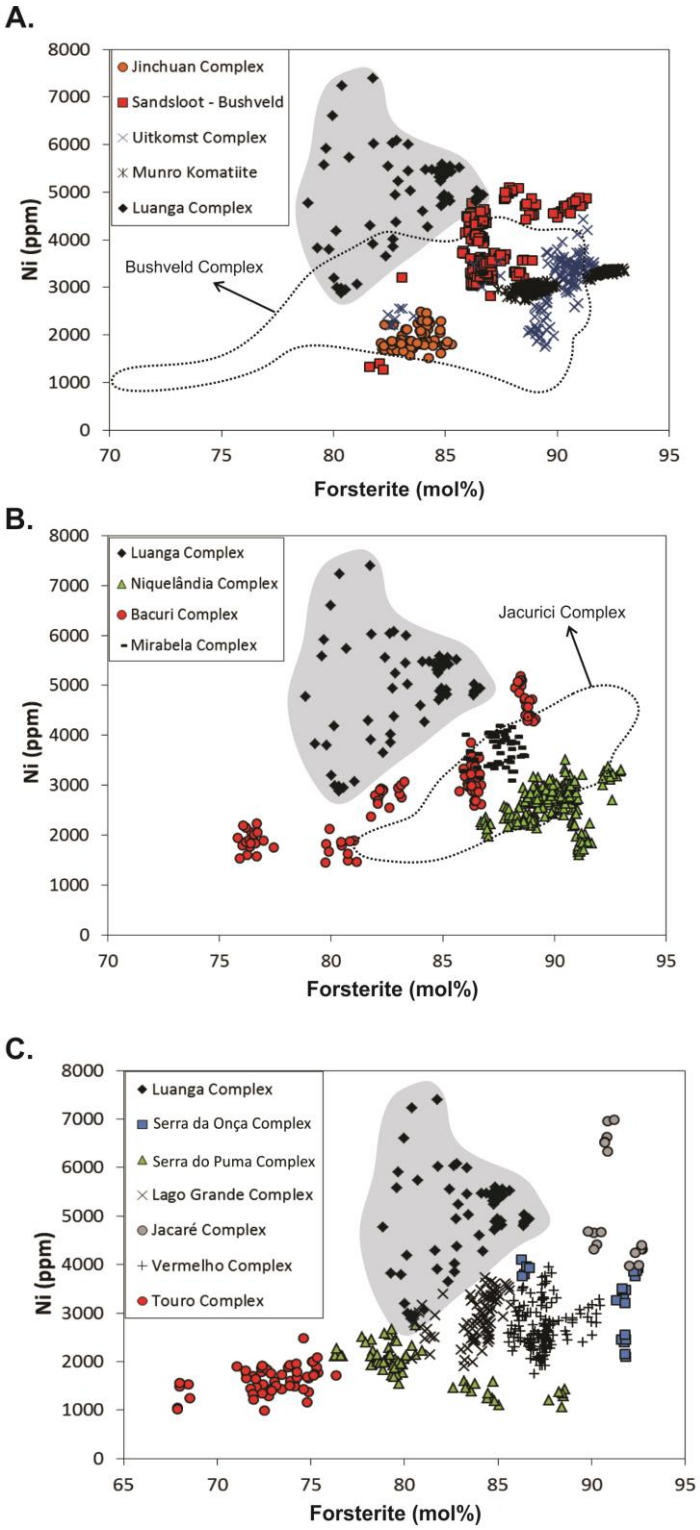

Fig. 1.12: Plot of Ni versus forsterite contents of olivine crystals from mafic-ultramafic complexes and komatiites. A) Data are shown for the Jinchuan Complex (Li et al., 2004), the Bushveld Complex (Yudovskaya et al., 2013 and references therein), the Sandsloot section below the Platreef (Yudovskaya et al., 2013), the Uitkomst Complex (Li et al., 2002; Maier et al., 2004), the Luanga Complex (this study) and the Munro Township komatiites (Sobolev et al., 2007). B) Data are shown for the Niquelândia Complex (Ferreira Filho and Araújo, 2009), the Bacuri Complex (Spier and Ferreira Filho, 2001), the Ipueira-Medrado Sill (Marques and Ferreira Filho, 2003), the Mirabela Complex (Barnes et al., 2013; Ferreira Filho et al., 2013) and the Luanga Complex (this study). C) Data are shown for the Lago Grande Complex (Teixeira et al., 2015), the Serra da Onça and Serra do Puma complexes (Rosa, 2014), the Vermelho and the Touro complexes (Siepierski, 2016), the Jacaré Complex (unpublished internal report) and Luanga Complex (this study).

The association of high Ni contents in olivine with high PGE contents in both sulfide-poor and sulfide-rich intervals is characteristic of the Transition Zone. Because the distribution of PGE during melting of pyroxenitic sources are not well constrained by experimental data, the interpretation for higher Ni contents in olivine crystals due to a pyroxenitic mantle source indicated by Sobolev et al. (2007) does not necessarily provide an explanation for the high PGE contents in the Luanga Complex. Nevertheless, Barnes et al. (2016) noticed that the basaltic crustal component most likely to provide the raw material for deep mantle pyroxenite and eclogite, would be expected to be impoverished in PGE compared with the peridotitic mantle. The authors conclude that melts associated with pyroxenitic sources should be PGE-depleted compared to those derived mainly from peridotitic sources.

The Kerr and Leitch (2005) model of partial dissolution of early formed magmatic sulfides by new fresh inputs of fresh magmas, known as "multistage-dissolution upgrading model", provides a possible explanation to some extremely PGE-rich sulfides. Although the authors' model was mainly applied for the origin of high tenor sulfide liquids, the concept that preexisting sulfide liquid could be partly dissolved by later batches of magma, suggests that this process could also proceed to the sulfide liquid be entirely dissolved and previously extracted metals returned to later batches of silicate magma (Kerr and Leitch, 2005). This process that may lead to the origin of metal enriched magmas was proposed to explain the origin of extremely Ni-rich olivine associated with Ni-PGE orebodies in the Kevitsa intrusion (Yang et al., 2013). The suggested "cannibalization" of proto-sulfide ore model, applied for the Kevitsa PGE-rich magma, may also justify the association of high Ni contents in olivine with high PGE contents in both sulfide-poor and sulfide-rich rocks in the Luanga Complex.

1.5.5 – Tectonic setting of the PGE-mineralized magmatism in the Carajás Mineral Province

The ages of the layered intrusions of the Carajás Mineral Province (2763 ± 6 Ma Luanga Complex: Machado et al., 1991; 2766 ± 6 Ma Serra da Onça Complex: Lafon et al., 2000) overlap with ages of bimodal volcanism in the Grão Pará Group (2759 ± 2 Ma: Machado et al., 1991; 2760 ± 11 Ma: Trendall et al., 1998), supporting the interpretation that mafic volcanics and mafic-ultramafic layered intrusions resulted from coeval major magmatic events in the Carajás region (Machado et al., 1991; Ferreira Filho et al., 2007). The extensive basaltic volcanism is considered to result either from

intra-plate rifting of older continental crust (e.g., Gibbs et al., 1986; Olszewski et al., 1989; Villas and Santos, 2001) or from subduction-related settings (Dardenne et al., 1988; Teixeira and Eggler, 1994; Zucchetti, 2007). The basaltic volcanism in the Carajás Domain shows lithogeochemical and isotopic evidence for significant contamination of mantle-derived melts by continental crust, thus supporting the continental rifting model (Gibbs et al., 1986; Olszewski et al., 1989). The structure and composition of the layered intrusions of the Carajás are also consistent with a Neoarchean intra-plate rifting environment in Carajás. Apart from contentious discussions regarding the tectonic setting of the Carajás Mineral Province, we use results obtained in this study to evaluate the petro-tectonic setting of the PGE-mineralized magmatism in Carajás.

The cluster of PGE-mineralized intrusions in the eastern portion of the Carajás Mineral Province was identified during regional exploration (Ferreira Filho et al., 2007). Mineralized intrusions have similar fractionation sequences, comparable petrological evolution, overlapped U-Pb zircon ages and similar styles of PGE mineralization, supporting the interpretation that they belong to the same magmatic suite (Teixeira et al., 2015). Results obtained for the Lago Grande and Luanga complexes indicate that this magmatic suite originated from siliceous magnesian basaltic magmas, similar to the parental liquids of the world's principal PGE-sulfide deposits (Barnes and Lightfoot, 2005). However, the unusually high contents of Ni obtained in olivine of the Luanga Complex do not occur in the Lago Grande Complex (Fig. 1.12C). Considering the petrological similarities of these complexes, the distinct Ni contents in olivine are a remarkable feature. Distinct Ni contents in olivine suggest that the process leading to Ni enrichment in the parental magma is restricted to the Luanga Complex in the Serra Leste suite. Because the most significant PGE-mineralized intersections with consistently high PGE tenors in the Serra Leste region occur in the Luanga Complex (Ferreira Filho et al., 2007; Mansur et al., in prep.), the same process should promote the enrichment in Ni and PGE in the parental magma. Regardless of the mechanism leading to enrichment of Ni and PGE, the high Ni content in olivine described in the Luanga Complex has implications for mineral exploration. Unusually high Ni contents in olivine and/or orthopyroxene may provide an additional exploration tool for Ni-PGE deposits. We have compared Ni content of olivine for several layered intrusions in the Carajás Mineral Province (Fig. 1.12C). Our data set includes data from complexes located in the Serra Leste region (Luanga and Lago Grande), the Canaã dos Carajás region (Vermelho and Touro), the Tucumã region (Serra do Onça and Serra do Puma)

and a few analyses for the Jacaré Complex located in the westernmost portion of the Carajás Mineral Province. All these intrusions have Ni contents in olivine compatible with values obtained in most layered complexes globally, except Luanga and Jacaré complexes (Fig. 1.12A-B). Olivine in dunite and harzburgite of closely associated samples of the Jacaré Complex has very primitive composition (Fo contents range from 89.8 to 92.7) and very high Ni content (4000 to 7000 ppm). The Jacaré Complex is a very large ultramafic intrusion (~ 100 Km^2) best known for hosting large Ni laterite resources (Carlon et al., 2006). The magmatic structure and petrology of the Jacaré Complex have not been investigated in detail and olivine analyses are limited to a few samples. Nevertheless, preliminary data for olivine compositions are higher than most intrusions and may suggest a favorable potential for Ni-PGE mineralization.

1.6 - Conclusions

Systematic geological and petrological characterization of the Luanga Complex provides additional evidences for a PGE-fertile magmatism at the eastern portion of the Carajás Mineral Province. Our results indicate that Ni contents in olivine in the Luanga Complex (up to 7,500 ppm) stand among the highest values reported in layered intrusions globally. High Ni contents in olivine of the Luanga Complex occur in distinctively PGE enriched (Pt+Pd > 1 ppm) intervals of the Transition Zone, in both sulfide-poor and sulfide-rich rocks. The origin of the PGE- and Ni-rich parental magma of the Luanga Complex is likely to result from the “cannibalization” of previously formed sulfides (Kerr and Leitch, 2005). Regardless of the process that lead to the generation of anomalously Ni- and PGE-rich magmas, our results indicate that an anomalous PGE-fertile magmatism took place at the eastern portion of the Carajás Mineral Province, thus triggering the development of different styles of PGE mineralization.

Acknowledgements

This study was supported by CNPq (Conselho Nacional de Desenvolvimento Científico e Teconológico) and VALE S.A. (Projeto 550398/2010-4). Analytical facilities of the Instituto de Geociências of the University of Brasília (UnB) provided additional support for this research. The authors acknowledge VALE's Exploration Managers for Brazil and Carajás (Mr. Fernando Greco and Mr. Fernando Matos,

respectively) for field support and access of exploration data. Cesar F. Ferreira Filho is a Research Fellow of CNPq since 1996, and acknowledges the continuous support through research grants and scholarships for the "Metalogenênese de Depósitos Associados ao Magmatismo Máfico-Ultramáfico" Research Group. The authors thank the reviewers (Dr. Marina A. Yudovskaya and one anonymous) and editor (Dr. Andrew Kerr) for their constructive and helpful reviews. The authors acknowledge Federico Cuadros, doctoral student at UnB, for the essential contribution over the microanalytical work. Eduardo T. Mansur holds and scholarship from Coordenação de Aperfeiçoamento de Pessoal de Nível Superior (CAPES) and this study is part of his M.Sc. thesis developed at the Instituto de Geociências (Universidade de Brasília). We thank Fernanda A. Ferreira (PhD student at Harvard University) for proof reading the manuscript.

References

Araújo, O.J.B., Maia, R.G.N., João, X.S.J., Costa, J.B.S., 1988. A megaestruturação arqueana da Folha Serra dos Carajás. Congresso Latino Americano de Geologia, Belém-Brazil, Anais, pp. 324-338.

Araújo, O.J.B., Maia, R.G.N., 1991. Projeto especial mapas de recursos minerais, de solos e de vegetação para a área do Programa Grande Carajás; Subprojeto Recursos Minerais; Folha SB.22-Z-A Serra dos Carajás - Estado do Pará: DNPM/CPRM.

Barnes, S.-J., Lightfoot, P.C., 2005. Formation of magmatic nickel sulfide deposits and processes affecting their copper and platinum group element contents. Economic Geology 100th Anniversary Volume, pp. 179–214.

Barnes, S.J., 1986. The effect of trapped liquid crystallization on cumulus mineral compositions in layered intrusions. Contributions to Mineralogy and Petrology 93, 524–531.

Barnes, S.J., Cruden, A.R., Arndt, N., Saumur, B.R., 2016. The mineral system approach applied to magmatic Ni–Cu–PGE sulphide deposits. Ore Geology Reviews 76, 296-316.

Barnes, S.J., Godel, B., Gürer, D., Brenan, J.M., Robertson, J., Paterson, D., 2013. Sulfide-olivine Fe-Ni exchange and the origin of anomalously Ni rich magmatic

sulfides. Economic Geology 108, 1971–1982.

Barnes, S.J., Mungall, J.E., Maier, W.D., 2015. Platinum group elements in mantle melts and mantle samples. Lithos 232, 395–417.

Beresford, S.W., Hronsky, J.M.A., 2014. The chonolith Ni-Cu model: expanding the footprint of Ni-Cu deposits. 12th International Platinum Symposium. Russian Academy of Sciences, Ural Branch, Yekaterinburg, Russia, pp. 102–103.

Campbell, I.H., 1985. The difference between oceanic and continental tholeiites: a fluid dynamic explanation. Contributions to Mineralogy and Petrology 91, 37-43.

Carlon, C.J., Molinari, L., Queiroz, R.., Felix de Melo, J., 2006. The discovery and exploration of the Jacare ("Alligator") nickel laterite-saprolite deposit, Para State, Brazil. Australian Earth Science Convention, AESC2006, Melbourne, Australia, (http://www.publish.csiro.au/paper/ASEG2006ab023.htm).

Chai, G., Naldrett, A.J., 1992. The Jinchuan Ultramafic Intrusion: cumulate of a high-Mg basaltic magma. Journal of Petrology 33, 277–303.

Dall'Agnol, R., Oliveira, M.A., Almeida, J.A.C., Althoff, F.J., Leite, A.A.S., Oliveira, D.C., Barros, C.E.M., 2006. Archean and Paleoproterozoic granitoids of the Carajás metallogenetic province, eastern Amazonian craton. Symposium on Magmatism, Crustal Evolution, and Metallogenesis of the Amazonian Craton, Abstracts Volume and Field Trips Guide, 150 pp.

Dardenne, M.A., Ferreira Filho, C.F., Meirelles, M.R., 1988. The role of shoshonitic and calc-alkaline suites in the tectonic evolution of the Carajás District, Brazil. Journal of South American Earth Sciences 1, 363–372.

Diella, V., Ferrario, A., Girardi, V.A.V., 1995. PGE and PGM in the Luanga mafic-ultramafic intrusion in Serra dos Carajás (Pará State, Brazil). Ore Geology Reviews 9, 445-453.

Docegeo - Rio Doce Geologia e Mineração, 1988. Revisão Litoestratigráfica da Província Mineral de Carajás. 35º Congresso Brasileiro de Geologia, Belém, Brasil, Anais, Sociedade Brasileira de Geologia, pp. 11-59.

Eales, H.V., Cawthorn, R.G., 1996. The Bushveld complex. In: Cawthorn, R.G. (Ed.), Layered Intrusions. Elsevier, Amsterdam, The Netherlands, pp. 181–230.

Ernst, R.E., Buchan, K.L., Campbell, I.H., 2005. Frontiers in large igneous province research. Lithos 79, 271-297.

Feio, G.R.L., Dall'Agnol, R., Dantas, E.L., Macambira, M.J.B., Santos, J.O.S., Althoff, F.J., Soares, J.E.B., 2013. Archean granitoid magmatism in the Canaã dos Carajás area: Implications for crustal evolution of the Carajás province, Amazonian craton, Brazil. Precambrian Research 227, 157-185.

Ferreira Filho, C.F., Araújo, S.M., 2009. Review of Brazilian chromite deposits associated with layered intrusions: geological and petrological constraints for the origin of stratiform chromitites. Applied Earth Science (Trans. Inst. Min. Metall. B) 118, 86-100.

Ferreira Filho, C.F., Cançado, F., Correa, C., Macambira, E.M.B., Siepierski, L., Brod, T.C.J., 2007. Mineralizações estratiformes de EGP-Ni associadas a complexos acamadados em Carajás: os exemplos de Luanga e Serra da Onça. In: Publitec Gráfica & Editora, Contribuições à Geologia da Amazônia, vol. 5, pp. 01-14.

Ferreira Filho, C.F., Cunha, E.M., Lima, A.C., Cunha, J.C., 2013. Depósito de Níquel-Cobre Sulfetado de Santa Rita, Itagibá, Bahia, Brasil. Série arquivos abertos, vol. 39, pp. 59. Salvador – Bahia: Companhia Baiana de Pesquisa Mineral.

Ferreira Filho, C.F., Naldrett, A.J., Gorton, M.P., 1998. REE and pyroxene compositional variation across the Niquelândia layered intrusion, Brazil: petrological and metallogenetic implications. Applied Earth Sciences 107, 1-22.

Ferreira Filho, C.F., Nilson, A.A., Naldrett, A.J., 1992. The Niquelândia Mafic-Ultramafic Complex, Goias, Brazil: A contribution to the ophiolite X stratiform controversy based on new geological and structural data. Precambrian Research 59, 125−143.

Ferreira Filho, C.F., Pimentel, M.M., Araujo, S.M., Laux, J.H., 2010. Layered intrusions and volcanic sequences in Central Brazil: Geological and geochronological constraints for Mesoproterozoic (1.25 Ga) and Neoproterozoic (0.79 Ga) igneous associations. Precambrian Research 183, 617−634.

Fiorentini, M.L., Barnes, S.J., Lesher, C.M., Heggie, G.J., Keays, R.R., Burnham, O.M., 2010. Platinum-group element geochemistry of mineralized and non-mineralized komatiites and basalts. Economic Geology 105, 795–823.

Gibbs, A.K., Wirth, K.R., Hirata, W.K., Olszewski Jr, W.J., 1986. Age and composition of the Grão Pará Group volcanics, Serra dos Carajás. Revista Brasileira de Geociências 16, 201-211.

Griffin, W., O'Reilly, S.Y., Begg, G.C., 2013. Continental-root control on the genesis of magmatic ore deposits. Nature Geoscience 6, 905–910.

Herzberg, C., 2011. Identification of Source Lithology in the Hawaiian and Canary Islands: Implications for Origins. Journal of Petrology 52, 113–146.

Holdsworth, R.E., Pinheiro, R.V.L., 2000. The anatomy of shallow-crustal transpressional structures: insights from the Archean Carajás fault zone, Amazon, Brazil. Journal of Structural Geology 61, 1105-1123.

Huhn, S.R.B., Santos, A.B.S., Amaral, A.F., Ledsham, E.J., Gouveia, J.L., Martins, L.P.B., Montalvão, R.M.G., Costa, V.C., 1986. O terreno granito-greenstone da região de Rio Maria-Sul do Pará. 35º Congresso Brasileiro de Geologia, Belém, Brasil, Anais, Sociedade Brasileira de Geologia, pp. 1438-1452.

Irvine, T. N., 1987. Layering and related structures in the Duke Island and Skaergaard intrusions: similarities, differences and origins. In: Parsons, I. (ed.) Origins of Igneous Layering. NATO ASI Series C 196, 185–245.

Kerr, A., Leitch, A.M., 2005. Self-destructive sulfide segregation systems and the formation of high-grade magmatic ore deposits. Economic Geology 100, 11−332.

Lafon, J.M., Macambira, M.J.B., Pidgeon, R.T., 2000. Zircon U-Pb SHRIMP dating of Neoarchean magmatism in the southwestern part of the Carajás Province (eastern Amazonian Craton, Brazil). 30th International Geological Congress, Abstract Volume, CD-ROM.

Li, C., Naldrett, A.J., 1999. Geology and petrology of the Voisey's Bay intrusion: Reaction of olivine with sulfide and silicate liquids. Lithos 47, 1–31.

Li, C., Ripley, E. M., Maier, W.D., Gomwe, T.E.S., 2002. Olivine and sulfur isotopic compositions of the Uitkomst Ni–Cu sulphide ore bearing complex, South Africa: evidence of sulfur contamination and multiple magma emplacements. Chemical Geology 188, 149–159.

Li, C., Xu Z., de Waal, S.A., Ripley, E.M., Maier, W.A., 2004. Compositional variations of olivine from the Jinchuan Ni-Cu sulfide deposit, western China: Implications for ore genesis. Mineralium Deposita 39, 159–172.

Macambira, E.M.B., and Ferreira Filho, C.F., 2002. Fracionamento Magmático dos Corpos Máfico-Ultramáficos da Suíte Intrusiva Cateté – Sul do Pará. In: Contribuições à Geologia da Amazônia v. 3. SBG-Núcleo Norte, pp. 105-114.

Macambira, M.J.B., Lancelot, J.R., 1996. Time constraints for the formation of the Archean Rio Maria crust, Southeastern Amazonian Craton, Brazil. International Geology Review 38, 1134-1142.

Machado, N., Lindenmayer, Z.G., Krogh, T.E., Lindenmayer, D., 1991. U-Pb geochronology of Archean magmatism and basement reactivation in the Carajás area, Amazon shield, Brazil. Precambrian Research 49, 329-354.

Maier, W. D., Gomwe, T., Barnes, S.-J., Li, C., Theart, H., 2004. Platinum group elements in the Uitkomst Complex, South Africa. Economic Geology 99, 499–516.

Maier, W.D., Groves, D.I., 2011. Temporal and spatial controls on the formation of magmatic PGE and Ni-Cu deposits. Mineralium Deposita 46, 841-857.

Mansur, E.T., Ferreira Filho, C.F., *in prep*. Chromitites from the Luanga Complex, Carajás, Brazil: clues to processes leading to chromite concentration and post-magmatic alteration. To be submitted to Ore Geology Reviews.

Mansur, E.T., Ferreira Filho, C.F., Oliveira, D.P.L., *in prep*. The platinum group element deposit of the Luanga Complex, Carajás Mineral Province, Brazil. To be submitted to Economic Geology.

Marques, J.C., Ferreira Filho, C.F., 2003. The chromite deposits of the Ipueira-Medrado Sill, Bahia, Brazil. Economic Geology 98, 87–108.

Mota-e-Silva, J., Ferreira Filho, C.F., Della Giustina, M.E.S., 2013. The Limoeiro deposit: Ni– Cu–PGE sulfide mineralization hosted within an ultramafic tubular magma conduit in the Borborema Province, Northeast Brazil. Economic Geology 108, 1753–1771.

Naldrett, A.J., Wilson, A., Kinnaird, J., Yudovskaya, M., Chunnett, G., 2012. The origin of chromitites and related PGE mineralization in the Bushveld Complex: new

mineralogical and petrological constraints. Mineralium Deposita 47, 209–232.

Nogueira, A.C.R., Truckenbrod, W., Costa, J.B.S., Pinheiro, R.V.L., 1994. Análise faciológica e estrutural da Formação Águas Claras, Pré-Cambriano da Serra dos Carajás. Simpósio de Geologia da Amazônia, Belém, Brasil, Resumos Expandidos, pp. 363–364.

Nogueira, A.C.R., Truckenbrod, W., Pinheiro, R.V.L., 2000. Storm and tide-dominated siliciclastic deposits of the Archean Águas Claras Formation, Serra dos Carajás, Brazil. 31st International Geological Congress, Rio de Janeiro, Brazil, Extended Abstracts, CD-ROM.

O'Driscoll, B., Emeleus, C.H., Donaldson, C.H., Daly, J.S., 2010. Cr-spinel seam petrogenesis in the Rhum layered suite, NW Scotland: cumulate assimilation and in situ crystallization in a deforming crystal mush. Journal of Petrology 51, 1171–1201.

Olszewski, W.J., Wirth, K.R., Gibbs, A.K., Gaudette, H.E., 1989. The age, origin, and tectonics of the Grão Pará Group and associated rocks, Serra dos Carajás, Brazil: Archean continental volcanism and rifting. Precambrian Research 42, 229–254.

Pidgeon, R.T., Macambira, M.J.B., Lafon, J.M., 2000. Th-U-Pb isotopic systems and internal structures of complex zircons from enderbite from the Pium Complex, Carajás Province, Brazil: evidence for the ages of granulite facies metamorphism and the protolith of the enderbite. Chemical Geology 166, 159-171.

Rosa, W.D., 2014. Complexos acamadados da Serra da Onça e Serra do Puma: Geologia e petrologia de duas intrusões Máfico-Ultramáficas com sequência de cristalização distinta na Província Arqueana de Carajás, Brasil. Unpublish M.Sc. Thesis, Universidade de Brasília, p. 65 pp.

Seat, Z., Beresford, S.W., Grguric, B.A., Waugh, R.S., Hronsky, J.M.A., Gee, M.A.M., Groves, D.I., Mathison, C.I., 2007. Architecture and emplacement of the Nebo-Babel gabbronorite-hosted magmatic Ni-Cu-PGE sulphide deposit, West Musgrave, Western Australia. Mineralium Deposita 42, 551–581.

Siepierski, L., Ferreira Filho, C.F., 2016. Spinifex-textured komatiites in the south border of the Carajas ridge, Selva Greenstone belt, Carajás Province, Brazil. Journal of South American Earth Sciences 66, 41-55.

Siepierski, L., 2016. Geologia, petrologia e potencial para mineralizações magmáticas dos corpos máfico-ultramáficos da região de Canaã dos Carajás, Província Mineral de Carajás, Brasil. Unpublish Ph.D. Thesis, Universidade de Brasília, p. 156 pp.

Sobolev, A.V., Hofmann, A.W., Sobolev, S.V., Nikogosian, I.K., 2005. An olivine-free mantle source of Hawaiian shield basalts. Nature 434, 590.

Sobolev, A.V., Hoffman, A., Kuzmin, D., Yaxley, G., Arndt, N., Chung, S.-L., Danyushevsky, L., Elliott, T., Frey, F., Garcia, M., Gurenko, A., Kamenetsky, V., Kerr, A., Krivolutskaya, N., Matvienkov, V., Nikogosian, I., Rocholl, A., Sigurdson, I., Sushchevskaya, N., Teklay, M., 2007. The amount of recycled crust in sources of mantle-derived melts. Science 316, 412−417.

Souza, Z.S., Dall'Agnol, R., 1996. Caracterização geoquímica e tectônica de rochas meta vulcânicas de "greenstone belts" arqueanos da região de Rio Maria, SE do Pará. Boletim. IG-USP, special publication, online, vol.18, pp. 97-101. ISSN 0102-6275.

Souza, Z.S., Potrel, A., Lafon, J.M., Althoff, F.J., Pimentel, M.M., Dall'Agnol, R., Oliveira, C.G., 2001. Nd, Pb and Sr isotopes in the Identidade Belt, an Archean greenstone belt of Rio Maria region (Carajás Province, Brazil): implications for the geodynamic evolution of the Amazonian Craton. Precambrian Research 109, 293-315.

Spier, C.B., Ferreira Filho, C.F., 2001. The chromite deposits of the Bacuri mafic-ultramafic layered complex, Guyana shield, Amapá State, Brazil. Economic Geology 96, 817–835.

Suita, M.T.F., 1988. Geologia da área Luanga com ênfase na petrologia do Complexo Básico-Ultrabásico Luanga e depósitos de cromita associados. Unpublish, M.Sc. Thesis, Universidade de Brasília, p. 322 pp.

Sun, S.-S., McDonough, W.F., 1989. Chemical and isotopic systematics of oceanic basalts: implications for mantle composition and processes. In: Saunders, A.D., Norry, M.J. (Eds.), Magmatism in the Ocean Basins, vol. 42. Geological Society Special Publication, pp. 313–345.

Tavares, F.M., 2015. Evolução geotectônica do nordeste da Província Carajás. Unpublish, Ph.D. Thesis, Universidade Federal do Rio de Janeiro, p. 115 pp.

Teixeira, A.S., 2013. Geologia, Petrologia e Geocronologia do Complexo Acamadado Lago Grande: Evidencia para uma Suite Magmática Mineralizada a PGE na Província Carajás – Brasil. Unpublish, M.Sc. Thesis, Universidade de Brasília, Brazil, p. 108 pp.

Teixeira, J.B.G., Eggler, D.H., 1994. Petrology, Geochemistry, and Tectonic Setting of Archaean Basaltic and Dioritic Rocks from the N4 Iron Deposit, Serra dos Carajás, Pará, Brazil. Acta Geologica Leopoldensia 17, 71-114.

Teixeira, A.S., Ferreira Filho, C.F., Giustina, M.E.S.D., Araujo, S.M., Silva, H.H.A.B., 2015. Geology, petrology and geochronology of the Lago Grande layered complex: Evidence for a PGE-mineralized magmatic suíte in the Carajás mineral province, Brazil. Journal of South American Earth Sciences 64, 116-138.

Trendall, A.F., Basei, M.A.S., De Laeter, J.R., Nelson, D.R., 1998. SHRIMP zircon U-Pb constraints on the age of the Carajás Formation, Grão Pará Group, Amazon Craton. Journal of South American Earth Sciences 11, 265–277.

Vasquez, M.L., Carvalho, J.M.A., Sousa, C.S., Ricci, P.S.F.; Macambira, E.M.B.; Costa, L.T.R., 2008. Mapa Geológico do Pará em SIG. Brazilian Geological Survey - CPRM.

Villas, R.N., Santos, M.D., 2001. Gold deposits of the Carajás Mineral Province: deposit types and metallogenesis. Mineralium Deposita 36, 300–331.

Wedepohl, K.H., 1995. The composition of the continental crust. Geochimica et Cosmochimica Acta 59, 1217-1232.

Wilson, A.H., 1982. The geology of the Great 'Dyke', Zimbabwe: the Ultramafic Rocks. Journal of Petrology 23, 240-92.

Yang, S-H., Maier, W.D., Hanski, E., Lappalainen, M., Santaquida, F., Määttä, S., 2013. Origin of ultra-nickeliferous olivine in the Kevitsa Ni-Cu-PGE mineralized intrusion, northern Finland. Contributions to Mineralogy and Petrology 166, 81–95.

Yudovskaya, M.A., Kinnaird, J.A., Sobolev, A.V., Kuzmin, D.V., McDonald, I., Wilson, A.H., 2013. Petrogenesis of the Lower Zone olivine-rich cumulates beneath the Platreef and their correlation with recognized occurrences in the Bushveld Complex. Economic Geology 108, 1923–1952.

Zhang, M., O'Reilly, S., Wang, K.-L., Hronsky, J., Griffin, W., 2008. Flood basalts and metallogeny: the lithosphere mantle connection. Earth-Science Reviews 86, 145–174.

Zuchetti, M., 2007. Rochas máficas do Supergrupo Grão Pará e sua relação com a mineralização de ferro dos depósitos N4 e N5, Carajás, PA. Unpublish. Ph.D. Thesis, Universidade Federal de Minas Gerais, Brazil, 165pp.

CAPÍTULO 2

Chromitites from the Luanga Complex, Carajás, Brazil: stratigraphic distribution and clues to processes leading to post-magmatic alteration

Chromitites from the Luanga Complex, Carajás, Brazil: stratigraphic distribution and clues to processes leading to post-magmatic alteration

Eduardo Teixeira Mansur[1] and Cesar Fonseca Ferreira Filho[1]

[1] Instituto de Geociências, Universidade de Brasília, Brasília-DF, 70910-900, Brazil.

Abstract

The Neoarchean (ca. 2.75 Ga) Luanga Complex, located in the Carajás Mineral Province in Brazil, is a medium-size layered intrusion consisting, from base to top, of ultramafic cumulates (Ultramafic Zone), interlayered ultramafic and mafic cumulates (Transition Zone) and mafic cumulates (Mafic Zone). Chromitite layers in the Luanga Complex occur in the upper portion of interlayered harzburgite and orthopyroxenite of the Transition Zone and associated with the lowermost norites of the Mafic Zone. The stratigraphic interval that hosts chromitites (~ 150 meters thick) consists of several cyclic units interpreted as the result of successive influxes of primitive parental magma. The compositions of chromite in chromitites from the Transition Zone (Lower Group Chromitites) have distinctively higher Cr# (100Cr/(Cr+Al+Fe3+)) compared with chromite in chromitites from the Mafic Zone (Upper Group Chromitites). Chromitites hosted by noritic rocks are preceded by a thin layer of harzburgite located 15-20 cm below each chromitite layer. Lower Cr# in chromitites hosted by noritic rocks are interpreted as the result of increased Al2O3 activity caused by new magma influxes. Electron microprobe analyses on line transverses through 35 chromite crystals indicate that they are rimmed and/or extensively zoned. The composition of chromite in chromitites changes abruptly in the outer rim, becoming enriched in Fe3+ and Fe2+ at the expense of Mg, Cr, Al, thus moving toward the magnetite apex on the spinel prism. This outer rim, characterized by higher reflectance, is probably related to the metamorphic replacement of the primary mineralogy of the Luanga Complex. Zoned chromite crystals indicate an extensive exchange between divalent (Mg, Fe2+) cations

and minor to none exchange between trivalent cations (Cr3+, Al3+ and Fe3+). This Mg-Fe zoning is interpreted as the result of subsolidus exchange of Fe2+ and Mg between chromite and coexisting silicates during slow cooling of the intrusion. A remarkable feature of chromitites from Luanga Complex is the occurrence of abundant silicate inclusions within chromite crystals. These inclusions show an adjacent inner rim with higher Cr# and lower Mg# (100Mg/(Mg+Fe2+)) and Al# (100Al/(Cr+Al+Fe3+)). This compositional shift is possibly due to crystallization from a progressively more fractionated liquid trapped in the chromite crystal. Significant modification of primary cumulus composition of chromite, as indicated in our study for the Luanga Complex, is likely to be common in non-massive chromitites and the rule for disseminated chromites in mafic intrusions.

keywords: chromitite; chromite; corona; silicate inclusion; layered intrusion; Carajás

2.1 - Introduction

Cr-bearing spinels have been used as important petrogenetic indicators in many studies (e.g., Irvine, 1965; Stowe, 1994; Barnes and Roeder, 2001). The composition of chromite, a mineral relatively resistant to alteration that crystallizes over a wide range of mafic and ultramafic magmas, is particularly useful as an indicator of magmatic processes in rocks submitted to metamorphism or hydrothermal alteration. However, chromite is susceptible to significant post-magmatic modification, as indicated by several studies of chromite in komatiites (e.g., Barnes, 2000) and ophiolitic complexes (e.g., Evans and Frost, 1975; Gole and Hill, 1990). Primary chromite compositions inherited from the magma may also be modified due to reaction with intercumulus liquid or subsolidus reaction with silicates (e.g., Barnes and Roeder, 2001; Barnes, 1998). Mass balance arguments are commonly used to indicate that massive chromitites with > 70 % vol. chromite are likely to preserve its original igneous compositions because there are few other phases available for element exchange (e.g., Eales and Reynolds, 1986). This reasoning was successfully used in several studies of chromitites (e.g., Bacuri Complex, Spier and Ferreira Filho, 2001; Ipueira-Medrado Sill, Marques and Ferreira Filho, 2003; Nuasahi and Sukinda Massifs, Mondal et al., 2006). However, apart from massive chromitites, post-magmatic modifications should be carefully

evaluated before using chromite compositions to indicate magma types, tectonic environments and magmatic fractionation.

This study, the first systematic description of chromitites throughout the stratigraphy of the Luanga Complex, provides an additional example of chromitites hosted by mafic cumulates. The stratigraphic distribution of chromitites and mineral composition data of chromite support previous results from host cumulate rocks suggesting that the Luanga layered intrusion originated in a dynamic open-system magma chamber (Mansur and Ferreira Filho, 2016). Our results also indicate extensive modification of primary cumulus composition of chromite in chromitites of the Luanga Complex. We discuss this composition modification considering both late-magmatic and metamorphic processes. Our results indicate that the common use of chromite composition as a petrogenetic indicator for mafic intrusions should be considered with caution.

2.2 - Regional setting

2.2.1- The Carajás Mineral Province

The Carajás Mineral Province, located in the southeastern portion of the Amazonian Craton (Fig. 2.1A), is one of the most important mineral provinces of the South American continent, hosting several world-class Cu-Au and Ni deposits along with the largest iron resources of the world. The Carajás Mineral Province is subdivided in two Archean tectonic domains: the Rio Maria Domain to the south and the Carajás Domain to the north (Fig. 2.1B; Vasquez et al., 2008). A poorly defined zone characterized by regional EW faults, designated as the Transition Subdomain (Feio et al., 2013), separates these two domains.

The Rio Maria Domain is a typical granite–greenstone terrain (Vasquez et al., 2008). The Andorinhas Supergroup (Docegeo, 1988) comprises several individual Mesoarchean (ca. 2.94 Ga) greenstone belts (Macambira and Lancelot, 1996; Souza et al., 2001). The recent characterization of spinifex-textured komatiites in a greenstone belt sequence within the Transition Subdomain (Siepierski and Ferreira Filho, 2016), suggests that the Andorinhas Supergroup extends further north than indicated in previous regional maps.

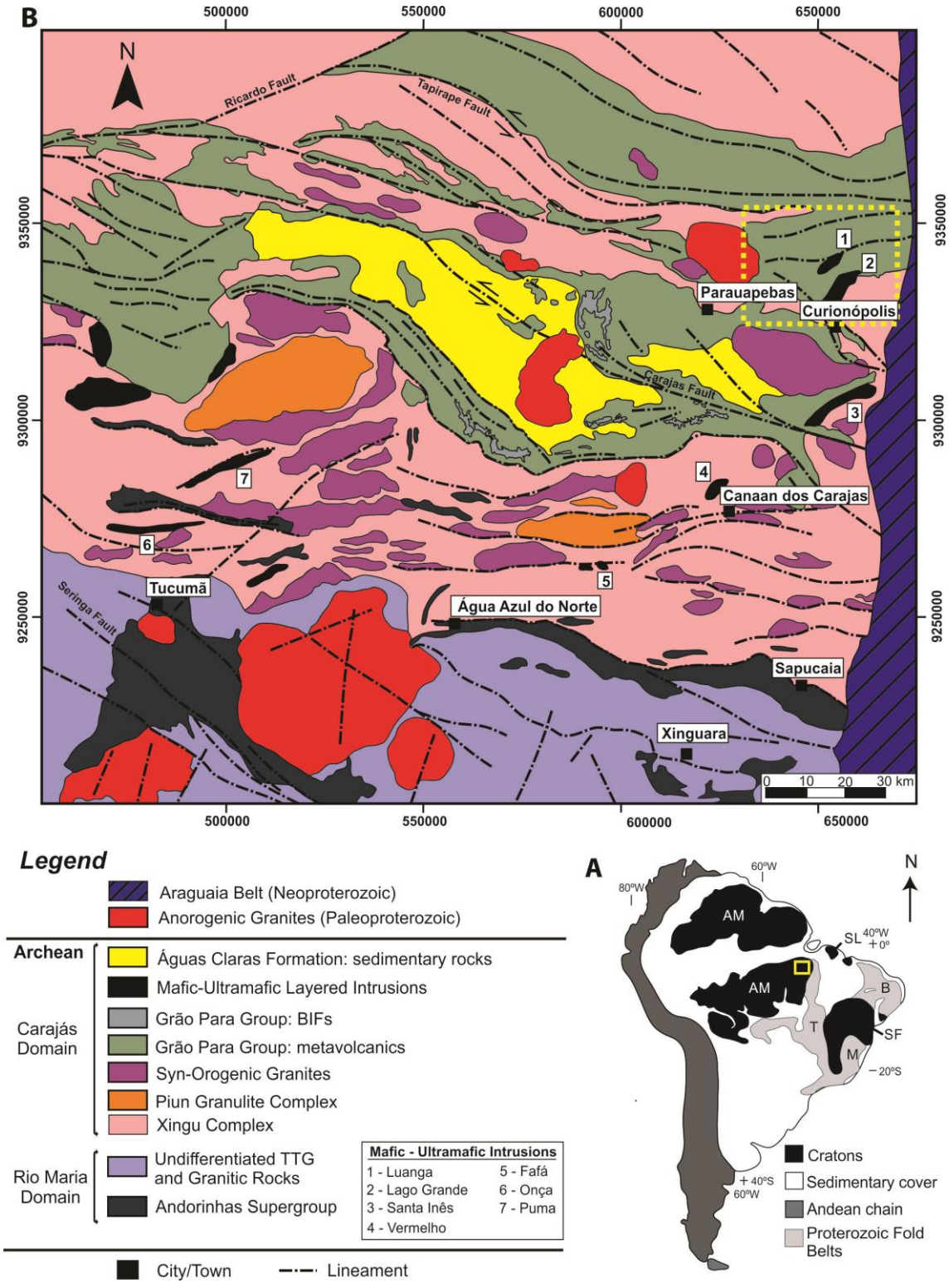

Fig. 2.1: A) Location of the Carajás Mineral Province. AM- Amazonic Craton; B – Borborema Province; M – Mantiqueira Province; SF – São Francisco Craton; T – Tocantins Province. B) Geological map of the Carajás Mineral Province (modified from Vasquez et al., 2008). The dashed rectangle indicates the location of the Serra Leste magmatic suite.

The Archean basement of the Carajás Domain consists mainly of gneiss-migmatite-granulite terrains, generally related to the Xingu Complex (Docegeo, 1988; Machado et al., 1991; Pidgeon et al., 2000). Different models have been proposed to explain the evolution of the Neoarchean volcano-sedimentary sequences, which include the large sequence of metabasalts of the Grão Pará Group (ca. 2.75 Ga; Machado et al., 1991; Vasquez et al., 2008) and associated banded iron formations. An intra-plate rift model is presented in several studies (e.g., Gibbs et al., 1986; Villas and Santos, 2001) but subduction-related environments have also been proposed (e.g., Dardenne et al., 1988; Teixeira and Eggler, 1994). These volcano-sedimentary sequences are covered by low-grade metamorphic sequences of clastic sedimentary rocks from the Águas Claras Formation (Araújo et al., 1988).

Several mafic-ultramafic complexes intrude rocks of the Xingu Complex and the volcanic-sedimentary sequences in the Carajás Domain (Docegeo, 1988; Ferreira Filho et al., 2007). These intrusions host large Ni laterite deposits (e.g., Onça-Puma, Vermelho, Jacaré) as well as PGE deposits (e.g., Luanga, Lago Grande). Distinct magmatic structures and petrological evolution of the layered intrusions suggest that they include different Neoarchean magmatic suites (e.g., Rosa, 2014; Siepierski, 2016; Teixeira et al., 2015).

2.2.2 - The Serra Leste Magmatic Suite

The Serra Leste Magmatic Suite (Ferreira Filho et al., 2007) consists of a cluster of small- to medium-size layered mafic-ultramafic intrusions located in the northeastern portion of the Carajás Mineral Province (Fig. 2.1). Mafic-ultramafic complexes are intrusive into gneiss and migmatites of the Xingu Complex and/or into volcano-sedimentary rocks of the Grão Pará Group. This suite was originally grouped based on abundant PGE anomalies of the layered intrusions, disregarding geological, stratigraphic or petrological consideration (Ferreira Filho et al., 2007). Systematic geological and petrological studies of the Lago Grande (Teixeira et al., 2015) and Luanga (Mansur and Ferreira Filho, 2016) Complexes provided the geological-petrological framework of the Serra Leste Magmatic Suite described in here.

2.2.2.1 - Lago Grande Complex

The Lago Grande Complex is a NE-trending medium-size (12 km long and average 1.7 km wide) layered intrusion consisting mainly of mafic cumulate rocks (Mafic Zone) and minor ultramafic cumulates (Ultramafic Zone). Recent studies (Teixeira et al., 2015) indicate that igneous layers are overturned, such that the Ultramafic Zone overly the Mafic Zone. The Ultramafic Zone comprises an up to 250 m thick sequence of interlayered harzburgite and orthopyroxenite at the base and orthopyroxenite at the top. The Mafic Zone consists of an up to 1000 m thick monotonous sequence of gabbroic rocks. Primary igneous minerals are partially replaced by metamorphic assemblages that indicate temperatures up to the amphibolite facies of metamorphism. This metamorphic replacement is heterogeneous and characterized by an extensive hydration of primary minerals that largely preserves magmatic textures and bulk chemical composition. PGE mineralizations occur in chromitites (up to 10 ppm) and associated with base metal sulfides in the Ultramafic Zone (Teixeira et al., 2015).

2.2.2 Luanga Complex

The Luanga Complex is a 6 km long and up to 3.5 km wide layered intrusion (Fig. 2.2) consisting, from base to top, of ultramafic cumulates (Ultramafic Zone), an intercalation of ultramafic and mafic cumulates (Transition Zone), and mafic cumulates (Mafic Zone). Similar to the configuration of the Lago Grande Complex, the Ultramafic Zone overlies the Transition Zone, which overlies the Mafic Zone, suggesting thus that the layered sequence in the Luanga Complex is also tectonically overturned (Fig. 2.2B; Mansur and Ferreira Filho, 2016). The Ultramafic Zone comprises an up to 800 m thick sequence of serpentinite (i.e., metamorphosed peridotite) with thin (< 10 m thick) interlayered orthopyroxenite lenses. The Transition Zone consists of an up to 800 m thick pile of interlayered ultramafic and mafic cumulate rocks. Interlayering of variably textured orthopyroxenite, harzburgite and norite (Fig. 2.2C) in different scales (from few centimeters up to hundreds of meters thick) is a remarkable feature of the Transition Zone. Interlayering and reversals in cryptic variation of orthopyroxene and olivine in the Transition Zone (Mansur and Ferreira Filho, 2016) support an open and dynamic magmatic system. The Mafic Zone consists of an up to 2000 m thick sequence of

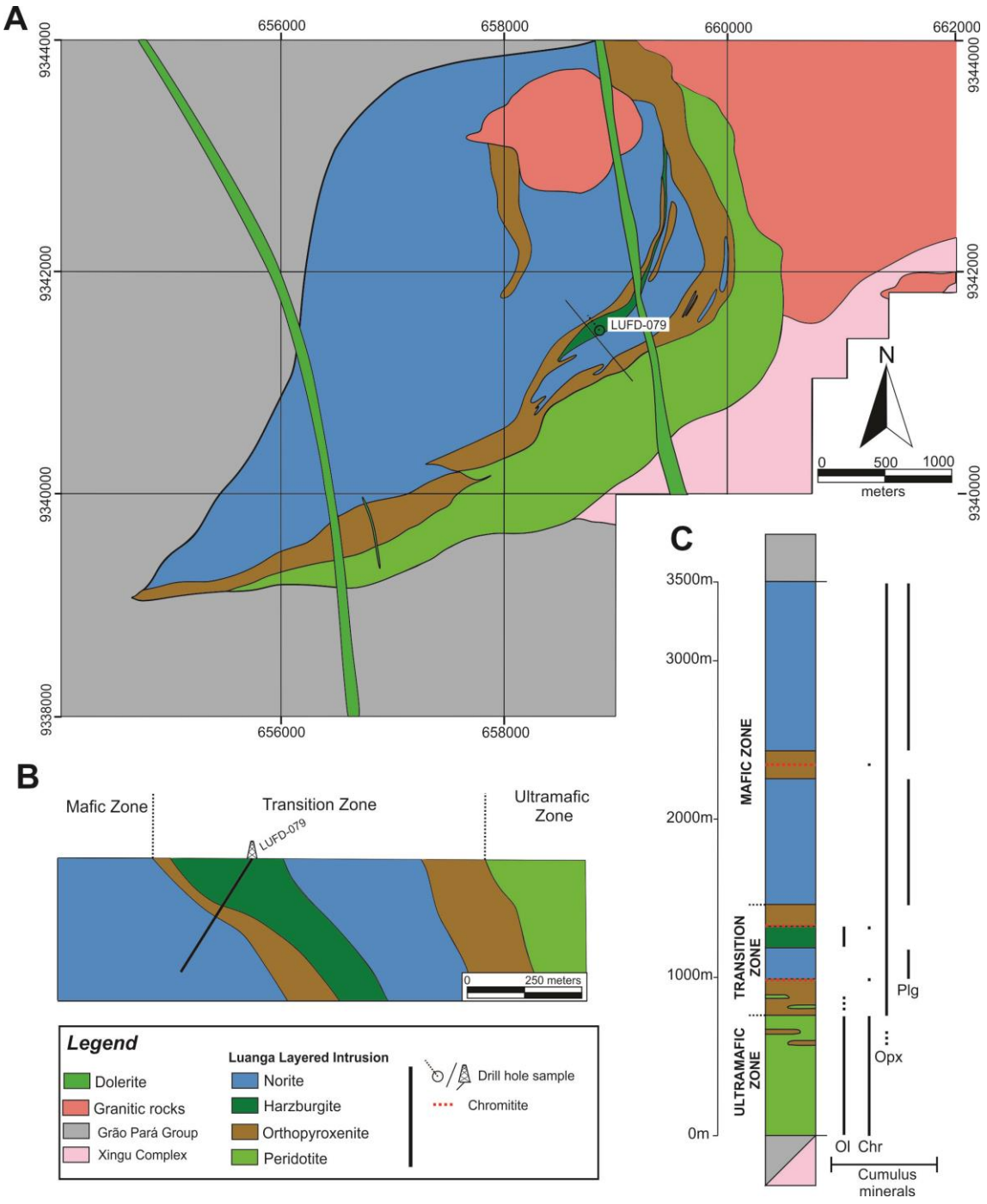

Fig. 2.2: A) Geological map of the Luanga Complex (partially modified from unpublished report of VALE). Note the location of drill hole LUFD-079 referred to in this study. B) Geological section on the central portion of the complex (partially modified from Mansur and Ferreira Filho, 2016). C) Representative stratigraphic column for the Luanga Complex (partially modified from Mansur and Ferreira Filho, 2016). Note the variation of cumulus minerals through the stratigraphy

monotonous norite and minor interlayered orthopyroxenite (Fig. 2.2C). Chromitite layers with variable thickness (from few centimeters up to 0.6 m thick) and textures (Fig. 2.3) occur mainly in the upper portions of the Transition Zone and the lowermost

portion of the Mafic Zone. Chromitites are better preserved in the central portion of the complex, where primary igneous textures and/or minerals prevail, becoming tectonically disturbed on its southern and northern limits (Mansur and Ferreira Filho, 2016). PGE mineralizations occur associated with base metal sulfides in the contact zone of the Ultramafic and Transition Zones and associated with chromitite layers in the Transition Zone (Diella et al., 1995; Ferreira Filho et al., 2007).

2.3 - Sampling and analytical procedures

For this study, a drill hole representative of the Transition Zone in the central portion of the Luanga Complex was systematically sampled for unweathered rocks with primary magmatic textures and minerals (drill hole LUFD-079; Fig. 2.2A and 2.2B). A total of 24 samples were collected for petrographic and mineral analyses, including one sample of each thin chromitite layers (06 samples), six samples from the thickest (~ 60 cm) chromitite layer, and 12 samples from host cumulate rocks (Fig. 2.3).

Scanning Electron Microscope (SEM) photos were taken with a JEOL JCM-5000 Neoscope, at the Micropaleontology Laboratory of the University of Brasília (Brazil), using carbon coating to enhance the contrast and definition.

Mineral analyses were performed on polished thin section using a 5 wavelength dispersive (WDS) spectrometer JEOL JXA-8230 SuperProbe at the Electron Microprobe Laboratory of the University of Brasília (Brazil). Systematic WDS analyses were obtained for chromite, orthopyroxene and plagioclase. Operating conditions for the WDS analyses were 15 kV accelerating voltage, with a beam current of 10 nA and probe diameters of 3 μm for chromite and orthopyroxene and 5 μm for plagioclase. Count times on peak and on background were 10 sec and 5 sec, respectively. Using these analytical conditions, detection limits are around 80 ppm. Both synthetic and natural mineral standards were used for the analyses and the same standards and procedure were retained throughout the analytical work. For chromite analysis, the cation compositions were calculated following the method described by Haggerty (1976) and Robin et al. (1992), Fe^{3+} was calculated assuming perfect stoichiometry. Chromite data are presented in terms of Cr# ($100Cr/(Cr+Al+Fe^{3+})$), Fe^{3+}# ($100Fe^{3+}/(Fe^{3+}+Cr+Al)$), Al# ($100Al/(Al+Cr+Fe^{3+})$), Mg# ($100Mg/(Mg+Fe^{2+})$) and Fe^{2+}# ($100Fe^{2+}/(Fe^{2+}+Mg)$) throughout the paper. The complete dataset for chromite analyses is given on the Online Supplementary Table A1.

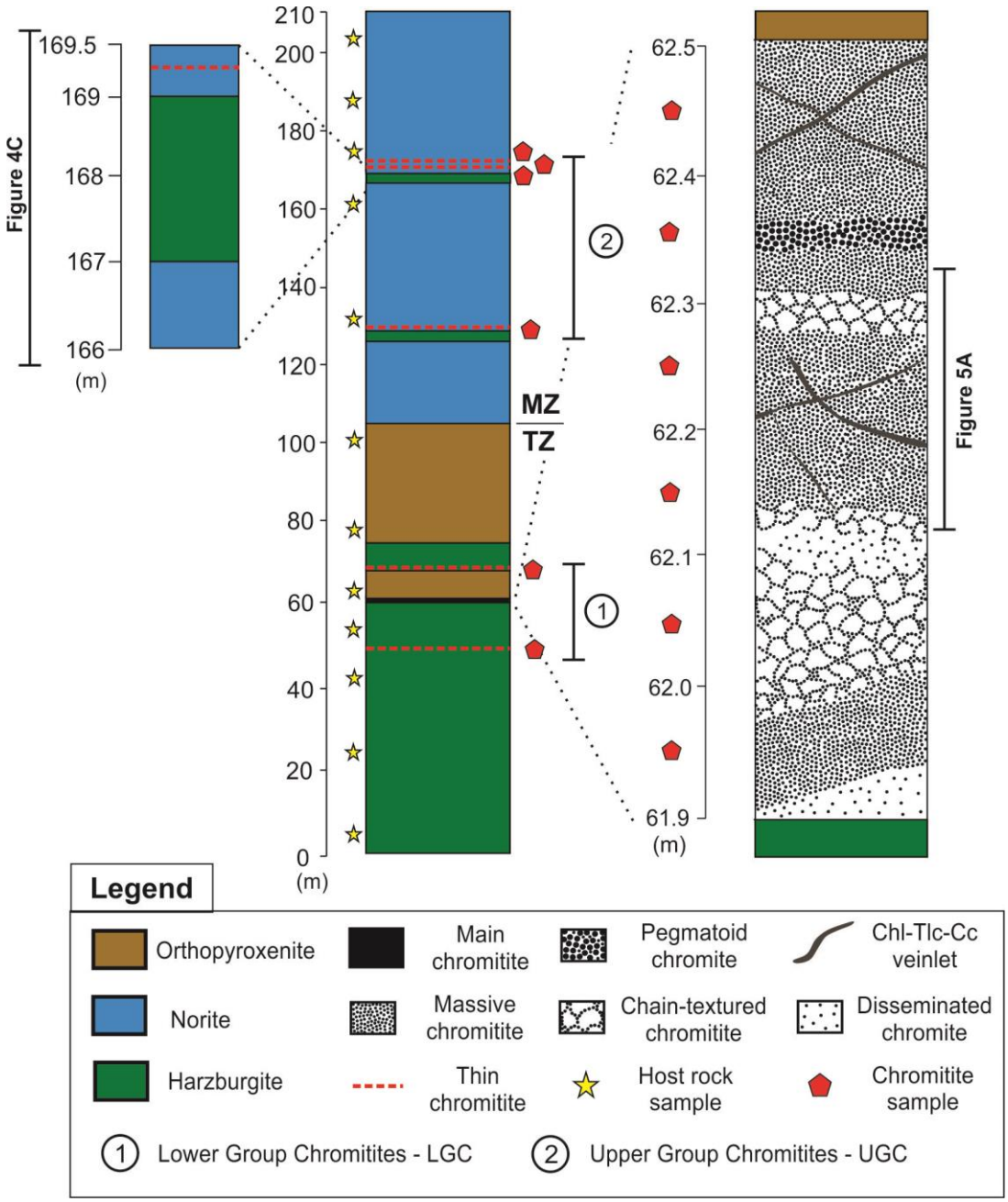

Fig. 2.3: Stratigraphic section of the drill core LUFD-079 (i.e., 210 meters deep; left) and a detailed section of the main chromitite (right). Note that the Luanga Complex comprises an overturned intrusion, but the stratigraphy of the drill core is shown in the original position. The location of the samples is indicated. MZ = Mafic Zone; TZ = Transition Zone.

2.4 - Geology and stratigraphy through the drill hole LUFD-079

The drill hole LUFD-079, located at the central portion of the Transition Zone (Fig. 2.2A and 2.2B), intersects several chromitite layers hosted by different rock types (Fig. 2.3). From the stratigraphic base to top the drill core comprises interlayered harzburgite and orthopyroxenite from the upper portion of the Transition Zone, and a

monotonous sequence of norite with minor thin layers of harzburgite from the base of the Mafic Zone (Fig. 2.3). The chromite-rich layers (Fig. 2.3) are divided into those located in the Transition Zone (Lower Group Chromitites - LGC), and those located in the lowermost portion of the Mafic Zone (Upper Group Chromitites - UGC).

Harzburgite is a medium- to coarse-grained olivine + chromite cumulate with intercumulus orthopyroxene. Coarse-grained harzburgite usually consists of large orthopyroxene oikocrysts enclosing several olivine crystals (Fig. 2.4A). The modal composition is variable due to different amount of interstitial minerals, including plagioclase as an additional common intercumulus mineral. Orthopyroxenite is a medium- to coarse-grained rock with tabular orthopyroxene as cumulus mineral. The texture varies from meso to orthocumulate with plagioclase as the predominant intercumulus mineral (Fig. 2.4B). The thickest chromitite layer (designated main chromitite) is ~ 60 cm thick and occurs at the contact between harzburgite and orthopyroxenite (Fig. 2.3). Norite is a medium-grained orthopyroxene and plagioclase adcumulate rock. A thin (i.e., 2-3 m thick) harzburgite layer always occur 15-20 cm below thin chromitite layers hosted by norite (Figs 2.3, 2.4C, 2.4D and 2.4E).

Primary igneous minerals of these cumulate rocks are commonly partially replaced by metamorphic assemblages. This replacement is heterogeneous and characterized by an extensive hydration that preserves primary textures and the compositional domains of igneous minerals. These assemblages include serpentine + talc + magnetite ± cummingtonite in replaced harzburgite, talc + serpentine + magnetite ± cummingtonite in replaced orthopyroxenite (Fig. 2.4B), and hornblende + chlorite + epidote in replaced norite. Metamorphic assemblages indicate temperatures up to the amphibolite facies of metamorphism, thus consistent with those described in previous studies of the Luanga (Ferreira Filho et al., 2007) and Lago Grande Complexes (Teixeira et al., 2015).

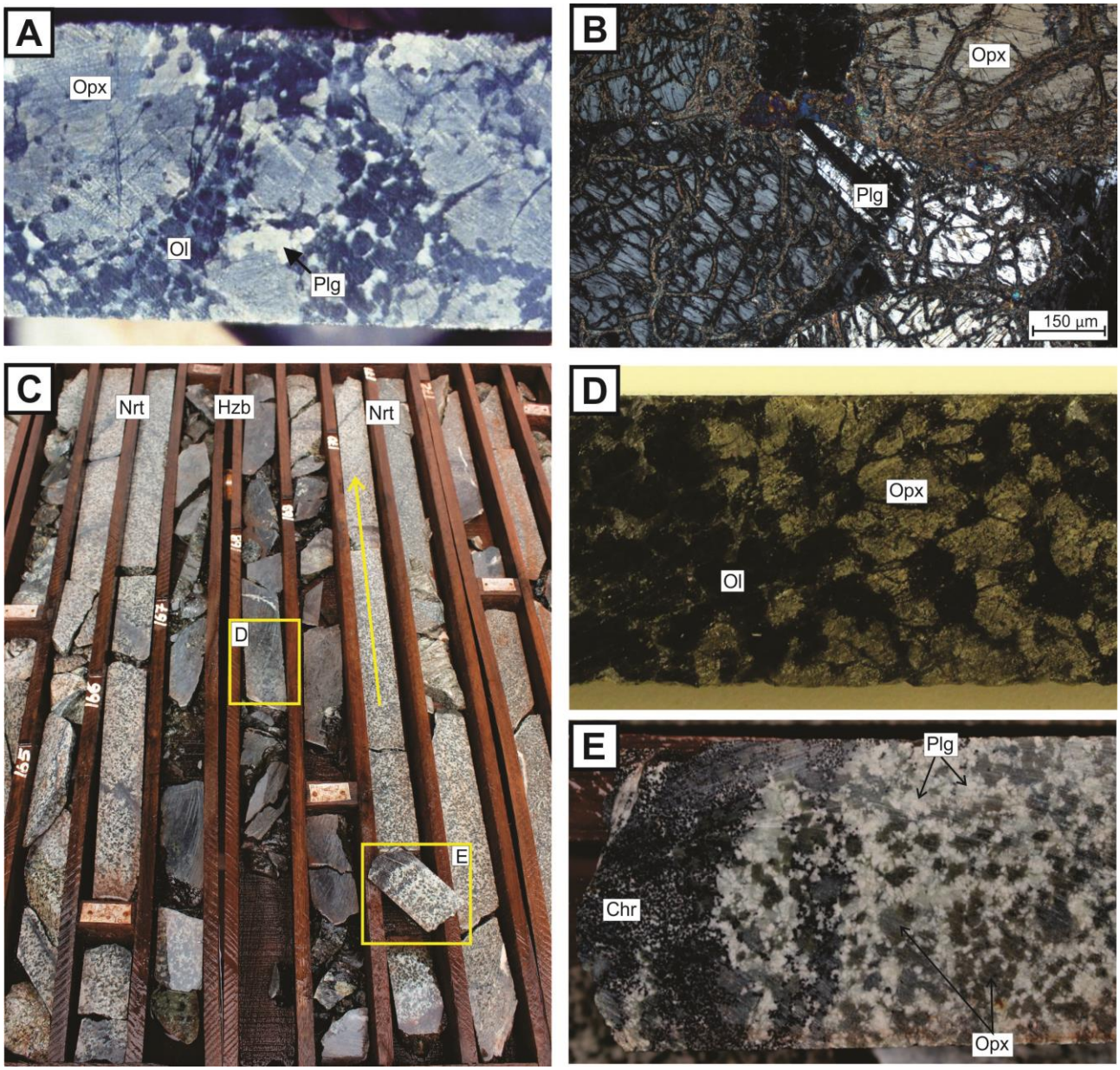

Fig. 2.4: Textures in chromitites and host rocks from drill core LUFD-079 A) Coarse-grained harzburgite (Hzb) consisting of large orthopyroxene (Opx) oikocrysts enclosing several olivine (Ol - black color) crystals and minor interstitial plagioclase (Plg - white color). B) Photomicrograph (crossed polarizers) of orthopyroxenite consisting of cumulus orthopyroxene and minor intercumulus plagioclase. C) Harzburgite layer preceding the appearance of thin chromitite layer hosted by noritic rocks (Nrt) of the Mafic Zone. The arrow points to the bottom of the drill core, indicating that the harzburgite is located stratigraphically below the chromitite (see stratigraphic section in Fig. 3 for the location of the core). The yellow rectangles indicate the areas of photos D and E. D) Detail of harzburgite consisting of cumulus olivine and orthopyroxene. E) Thin chromitite (Chr) layers hosted by noritic rocks of the Mafic Zone. Note cumulus chromite grains and intercumulus plagioclase (white) and orthopyroxene (light brown). For all the photos the core is 4.7 centimeters wide.

2.5 - The chromitite layers

2.5.1 – Petrography

Chromitite layers intersected by drill core LUFD-079 include the main chromitite and 6 thin layers (< 10 cm thick) (Fig. 2.3). The main chromitite is an up to 60 cm chromite-rich layer located at the contact between harzburgite and orthopyroxenite layers from the upper portion of the Transition Zone (LGC; Figs. 2.2C and 2.3). It has sharp contacts with both the underlying harzburgite and the overlying orthopyroxenite, suggesting abrupt changes in the sequence of cumulate minerals in both contacts. The main chromitite extends for 1-2 hundred meters along strike, as indicated by drill core information, but the continuity beyond that is not constrained due to poor outcropping. Massive chromitite prevails (~ 65 vol. %) and is associated with irregular domains of chain-textured and disseminated chromitite (Figs. 2.3 and 2.5A). Massive chromitite is a fine- to medium-grained chromite cumulate with chromite grains representing more than 50 vol. % (Fig. 2.5A). Orthopyroxene and plagioclase, commonly replaced by fine-grained aggregates of serpentine, amphibole, chlorite and talc, are typically the main interstitial minerals. Chromite occurs as euhedral to subhedral annealed crystals with discrete alteration along crystal borders and fractures (Fig. 2.5B). Rounded silicate inclusions inside chromite grains are common and have variable sizes (Fig. 2.5). These inclusions consist of the same fine-grained replacement minerals described for the matrix. Chain-textured chromitite, consisting of 15-20 vol. % chromite, is characterized by orthopyroxene pseudomorphs surrounded by dozens of medium- to fine-grained chromite crystals (Figs. 2.5C). Fine-grained chromite grains are also enclosed by orthopyroxene pseudomorphs in chain-textures chromitites (Fig. 2.5C). The transition from massive to chain-textured chromitite is gradational and marked by the progressive decrease on the chromite modal composition. The same type of silicate inclusions observed in massive chromitites occurs in chain-textured chromitites, but they are less abundant in the latter. The disseminated chromitite contains 5-10 vol. % of cumulus chromite and 95-90 vol. % of variably replaced orthopyroxene and plagioclase. Chromite grains in disseminated chromitite are extensively altered and rarely have silicate inclusions. Coarse-grained chromitite is restricted to a 2 cm thick layer (see pegmatoid chromitite in Fig. 2.3) characterized by coarse chromite grains containing a large volume of silicate inclusions (Fig. 2.5D). Both coarse chromite crystals and silicate inclusions show irregular shapes in the pegmatoidal chromitite (Fig. 2.5D), different from

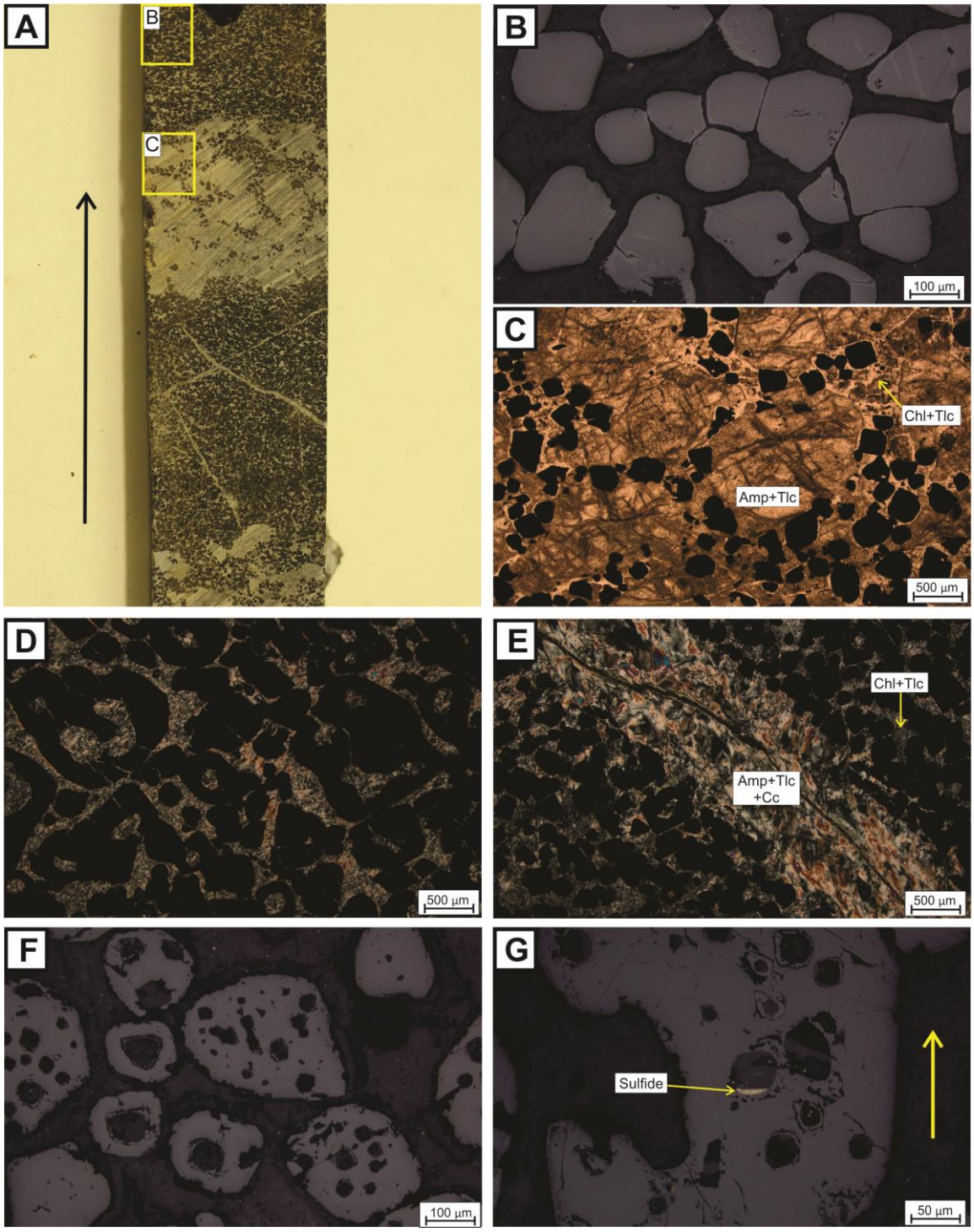

Fig. 2.5: Textures in chromitites. A) Textures varying from massive, chain-textured and disseminated in the main chromitite (see Fig. 3 for location of the drill core). Primary silicates (light gray color) are replaced by a fine-grained aggregate of serpentine and talc. Carbonate-rich veinlets cross cut the chromitite. The arrow points upward the stratigraphy. B) Photomicrograph (reflected light) of massive chromitite with polygonal contact between chromite grains. Note that chromite grains are partially altered along borders and fractures (light gray color). C) Photomicrograph of chain-textured chromitite. Chromite crystals are interstitial to orthopyroxene pseudomorphs replaced by amphibole (Amp) and talc (Tlc). Note interstitial fine-grained aggregates of chlorite (Chl) and talc, probably resulting from alteration of intercumulus plagioclase in contact with Opx.

Fig. 2.5 (cont.) : D) Photomicrograph (crossed polarizers) of pegmatoid chromitite. Note silicate inclusions with irregular shape in chromite grains. The intercumulus and inclusion-hosted minerals are replaced by a fine-grained aggregate of chlorite and talc. E) Photomicrograph (crossed polarizers) of carbonate (Cc)-amphibole-talc veinlet cross cutting massive chromitite. Note that chromite grains are surrounded by a fine-grained aggregated of chlorite and talc, probably resulting from alteration of intercumulus silicates. F) Photomicrograph (reflected light) of inclusion-bearing chromite crystals from a thin chromitite of the Mafic Zone. Note the characteristic sector zoning of inner rims adjacent to silicate inclusions. G) Photomicrograph (reflected light) of inclusion-bearing chromite crystal highlighting the presence of a sulfide droplet at the bottom of the inclusion. The thin section is oriented and the sulfide droplet faces the base of the chromite-rich layer (the arrow points upward the stratigraphy).

the euhedral crystals with rounded inclusions characteristic of the main chromitite. All three types of chromitites are cross-cut by fine grained amphibole-chlorite-carbonate veinlets (Fig. 2.5E). These veinlets do not appear to extensively affect the composition of chromite grains (i.e., no significant zonation or reaction border is observed).

Thin chromitites (< 10 cm thick) are mainly hosted by noritic rocks of the Mafic Zone (UGC; Fig. 2.3). These chromitites are fine- to medium-grained chromite cumulates with intercumulus plagioclase and orthopyroxene (Fig. 2.4E). Chromite grains are euhedral and show many rounded silicate inclusions with well-developed inner rims (Fig. 2.5F). These inclusions consist of the same aggregate of fine-grained silicates that replace the original intercumulus minerals in the main chromitite of the LGC. Locally, sulfide minerals occur at the bottom of the inclusions, facing the base of the chromitite layer (i.e., based on oriented thin sections; Fig. 2.5G).

2.5.2 - Spatial analysis of silicate inclusions and their variation through the stratigraphy

Silicate inclusions and “atoll-like” structures are common features in chromite grains of the studied chromitites (Fig. 2.5). The three-dimensional shape of these inclusions and hosting crystals were described utilizing a SEM (Fig. 2.6). Chromite grains are euhedral with well-defined faces without any indication of reaction or reabsorption features (Fig. 2.6A). Inclusion-bearing crystals have the same morphology of inclusion-free crystals, except for the presence of predominantly rounded inclusions in the first (Fig. 2.6B). Inclusion-bearing chromite grains usually have the inclusions locked within the crystals, with no physical connection of the included silicates and outside matrix minerals. However, few silicate inclusions are connected with the outside

matrix (Fig. 2.6C). The inclusions are composed of the same silicate minerals that occur in the matrix of chromite grains, consisting of extensively replaced plagioclase and/or orthopyroxene (Fig. 2.6D).

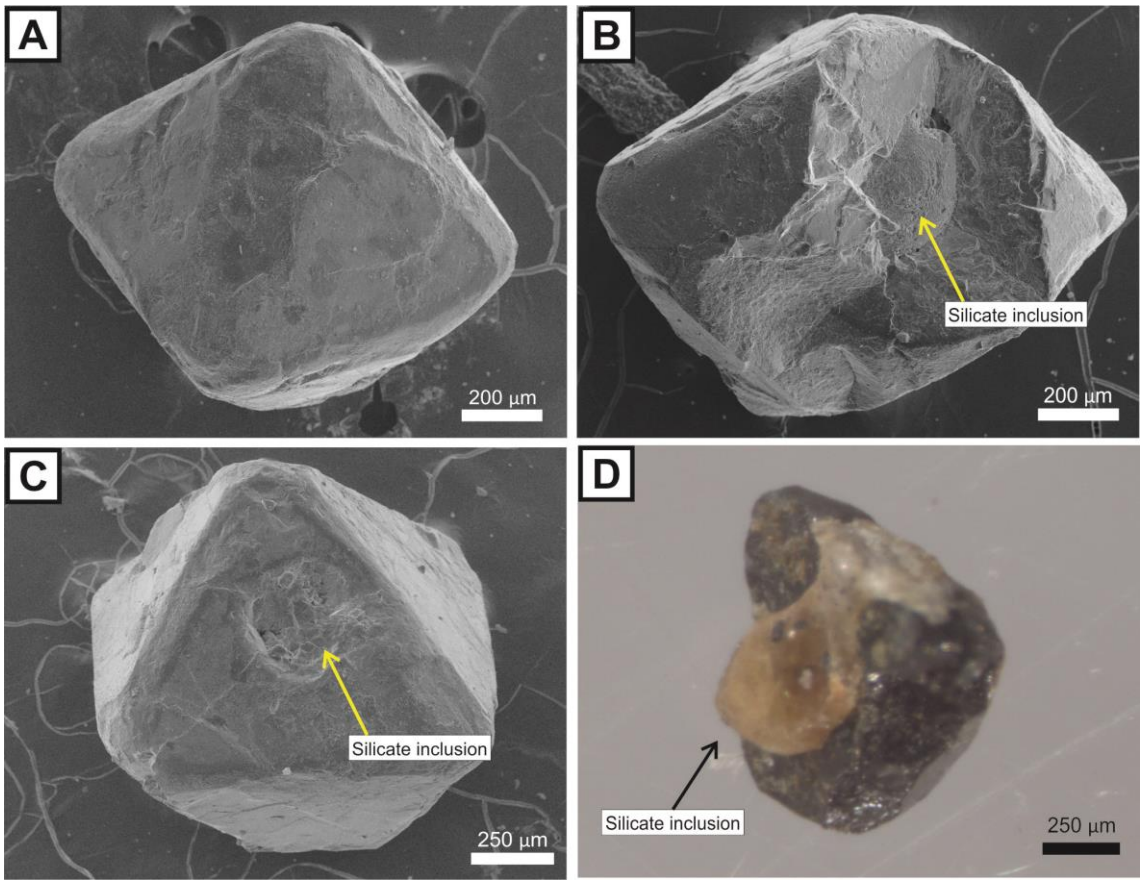

Fig. 2.6: Scanning Electron Microscope (SEM) back scattered photos of chromite crystals. A) SEM photo of an euhedral chromite crystal. B) SEM photo of an euhedral chromite crystal showing one rounded silicate inclusion. C) SEM photo of chromite crystal with a partially-enclosed silicate inclusion. The silicate inclusion appears as a sub-circular shape in one face of the octahedral chromite crystal. D) Photo (using a magnifying glass) of chromite grain enclosing a coalescent silicate inclusion. The inclusion shape indicates that the inclusion and interstitial minerals surrounding the chromite grain are connected.

The silicate inclusions show significant variations in the shape, number and volume proportions in chromite crystals from chromitites of the LGC and UGC (Fig. 2.7). Chromite grains from the LGC commonly have just one large silicate inclusion (Fig. 2.7A). The thin pegmatoid chromitite (Fig. 2.3) has chromite crystals with the larger silicate inclusions (up to 0.65 mm of diameter enclosed within chromite crystals around 1 mm diameter) of all the studied samples (Fig. 2.7B). Upward in the

stratigraphy, UGC are characterized by chromite grains with several small silicate inclusions (Fig. 2.7C).

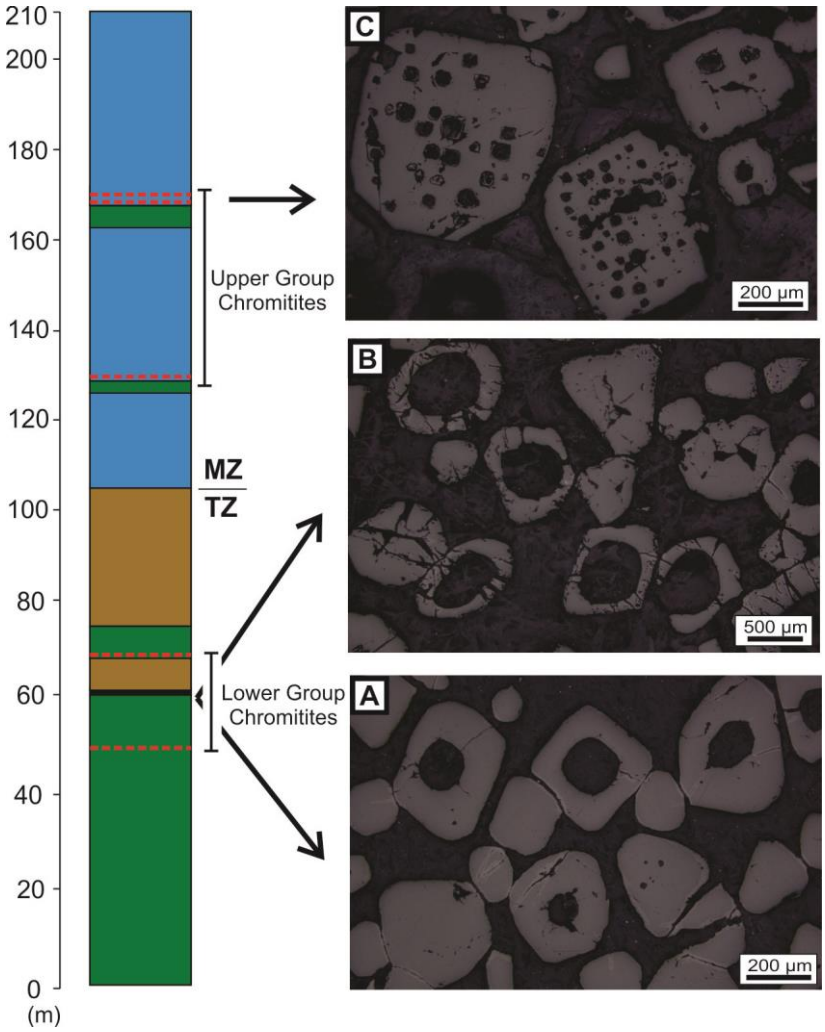

Fig. 2.7: Morphology of chromite grains in the stratigraphic section of drill hole LUFD-079. A) Representative inclusion-bearing chromite grains from chromitite of the Transition Zone. Chromite grains have one single rounded inclusion. B) Representative inclusion-bearing grains from the pegmatoid-textured chromitite. Chromite grains have one large inclusion or atoll-like texture. C) Representative inclusion-bearing chromite grains from thin chromitites of the Mafic Zone. Chromite grains have several inclusions. Note the characteristic sector zoning of inner rims adjacent to silicate inclusions. MZ = Mafic Zone; TZ = Transition Zone.

2.6 - Mineral Chemistry

2.6.1- Orthopyroxene and plagioclase

Systematic studies of mineral chemistry of cumulus minerals from drill core LUFD-079 (i.e., orthopyroxene and plagioclase) were limited by metamorphic replacement of igneous minerals in several samples. Orthopyroxene was analysed in samples of orthopyroxenite and harzburgite from the Transition Zone and norite from the Mafic Zone, while plagioclase was just analysed in samples of norite from the Mafic Zone. Representative analyses of orthopyroxene and plagioclase are reported in Tables 2.1 and 2.2, respectively.

Orthopyroxene compositions range from En83.49 to En89.9 mol % through the top of the Transition Zone and the base of the Mafic Zone (Fig. 2.8). The cryptic variation of orthopyroxene shows a few reversals and relatively more fractionated compositions (En83.49 to En86.45 mol %) in the Transition Zone, whereas the compositions of orthopyroxene in norite of the Mafic Zone are more primitive (En89.0 to En89.84 mol %) (Fig. 2.8). Plagioclase compositions range from An76.61 to An83.20 mol % in the lower portion of the Mafic Zone. The cryptic variation of plagioclase shows a consistent upward increase in An contents, indicating a reversed fractionation in the lower portion of the Mafic Zone (Fig. 2.8). Cryptic variations of orthopyroxene and plagioclase in drill core LUFD-079 are consistent with the common reversals within a general inversed fractionation trend of the Transition Zone and lower portion of the Mafic Zone, as described in previous studies of the Luanga Complex (Ferreira Filho et al., 2007; Mansur and Ferreira Filho, 2016).

2.6.2 – Chromite

Chromite grains show alteration rims (Figs. 2.5 and 2.7) that are probably associated with different compositions. In order to evaluate the compositional variation in chromite grains, EMP analyses were performed on line transverses through 35 chromite crystals with different morphologies (Fig. 2.9 shows 4 representative line traverses), totaling ~ 700 analyses. Investigated chromite crystals were separated into inclusion-free and inclusion-bearing crystals (see Table 2.3 and Table 2.4 for representative analyses from line traverses of inclusion-free and inclusion-bearing crystals, respectively). An outer alteration rim characterized by higher reflectance (see Fig. 2.9B) is common in both inclusion-free and inclusion-bearing crystals. These alteration rims have variable thickness and are commonly continuous along fractures in

extensively altered chromite crystals. Composition of chromite changes abruptly in this outer rim, becoming enriched in Fe^{3+} and Fe^{2+} (i.e., Fe^{3+}# up to 91) at the expense of Mg, Cr, Al. This alteration is easily recognized in petrographic studies and have highly different compositions compared with the core of the crystals. These rims were avoided in the systematic probe investigation and analyses are limited to few line traverses.

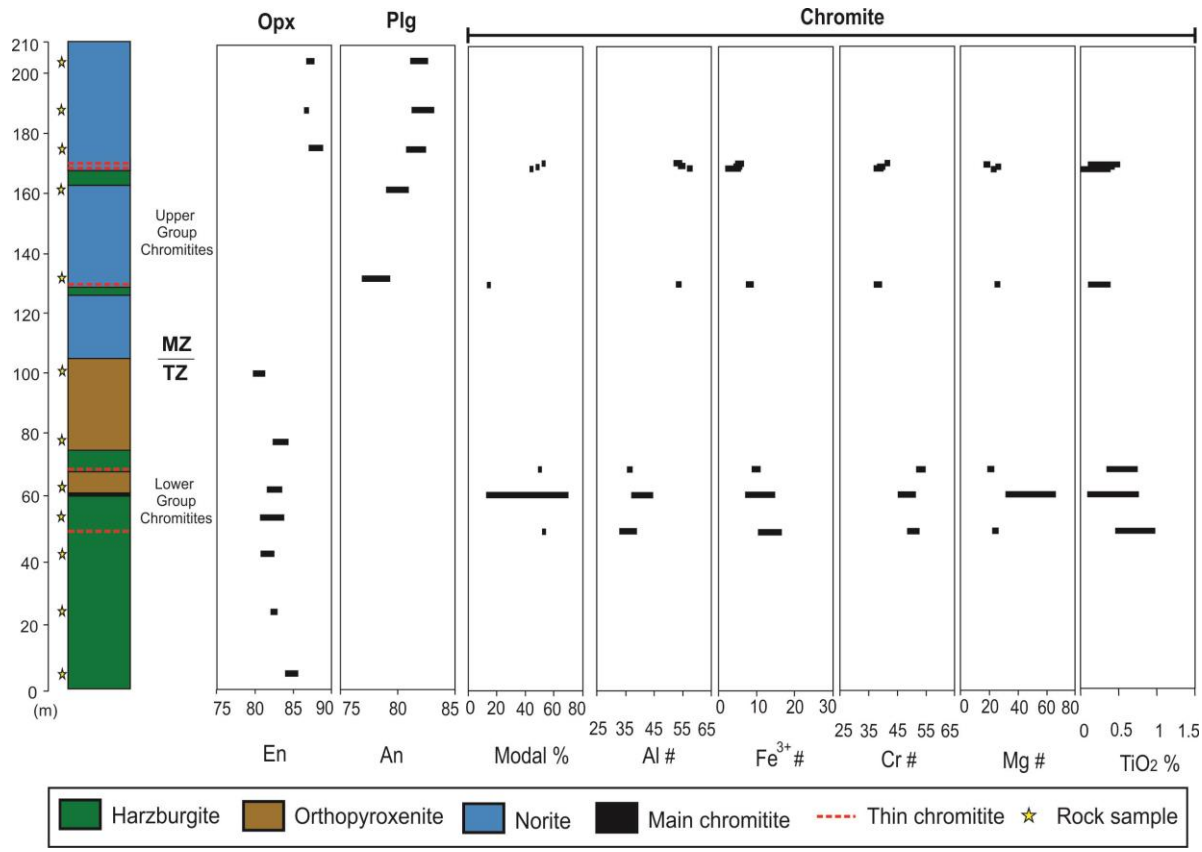

Fig. 2.8: Compositional variations of orthopyroxene (Opx), plagioclase (Plg) and chromite throughout drill core LUFD-079. Orthopyroxene and plagioclase compositions are indicated as enstatite (En) and anorthite (An) contents (mol. %), respectively. Chromite compositions are indicated as Al# = 100Al/(Al + Cr + Fe^{3+}), Cr# = 100Cr/(Cr + Al + Fe^{3+}), Fe^{3+}# = 100Fe^{3+}/(Fe^{3+} + Cr + Al), Mg# = 100Mg/(Mg + Fe^{2+}) and TiO_2 (wt. %)Modal % indicates the chromite percentage of each chromitite. The black bar indicates the variation in composition for each sample. MZ = Mafic Zone; TZ = Transition Zone.

Table 2.1 – Representative analyses of orthopyroxene.

Drill Hole		LUFD-079	LUFD-079	LUFD-079	LUFD-079	LUFD-079	LUFD-079	LUFD-079	LUFD-079	LUFD-079	LUFD-079
Depth (m)		63.75	78.92	101.5	176.4	176.4	176.4	188.8	205.57	205.57	205.57
Rock		Orthopyroxenite	Orthopyroxenite	Orthopyroxenite	Norite	Norite	Norite	Norite	Norite	Norite	Norite
SiO_2	(wt. %)	54.96	55.43	54.87	54.95	54.96	55.03	55.17	55.23	55.41	55.43
TiO_2		0.06	0.13	0.03	0.09	0.24	0.17	0.00	0.06	0.00	0.08
Al_2O_3		2.01	1.72	1.64	2.40	2.77	2.41	1.89	1.82	1.53	1.74
Cr_2O_3		0.46	0.69	0.47	0.79	0.51	0.60	0.40	0.36	0.29	0.40
FeO		10.18	9.10	10.33	7.04	7.25	6.91	7.43	6.90	7.05	7.02
MgO		31.85	32.03	29.31	33.15	33.76	33.60	33.73	34.44	34.66	34.61
MnO		0.22	0.14	0.12	0.05	0.03	0.15	0.17	0.19	0.18	0.12
NiO		0.20	0.18	0.15	0.16	0.18	0.17	0.17	0.13	0.15	0.15
CaO		0.67	1.10	2.65	1.42	0.77	0.76	1.01	1.07	1.03	0.71
Total		100.60	100.52	99.56	100.04	100.47	99.80	99.97	100.20	100.30	100.26
Normalization based on 24 oxygens											
Si	(atoms %)	7.660	7.718	7.798	7.614	7.568	7.629	7.638	7.602	7.617	7.625
Al		0.330	0.282	0.202	0.386	0.432	0.371	0.308	0.295	0.248	0.281
Mg		6.619	6.650	6.210	6.848	6.931	6.944	6.961	7.069	7.103	7.098
Ca		0.100	0.164	0.403	0.211	0.113	0.112	0.150	0.158	0.152	0.105
Ti		0.006	0.013	0.003	0.009	0.024	0.018	0.000	0.006	0.000	0.008
Cr		0.050	0.076	0.053	0.086	0.055	0.066	0.044	0.039	0.032	0.044
Fe^{2+}		1.186	1.059	1.228	0.815	0.835	0.801	0.860	0.795	0.811	0.808
Ni		0.018	0.016	0.014	0.014	0.016	0.015	0.015	0.013	0.014	0.014
Mn		0.026	0.017	0.014	0.006	0.003	0.018	0.020	0.022	0.020	0.014
Total		15.996	15.995	15.924	15.990	15.978	15.973	15.996	15.999	15.997	15.998
En (%)		84.80	86.26	83.49	89.36	89.25	89.66	89.00	89.89	89.75	89.78

Table 2.2 - Representative analyses of plagioclase.

Drill Hole	LUFD-079	LUFD-079	LUFD-079	LUFD-079	LUFD-079	LUFD-079
Depth (m)	132.2	132.2	161	161	188.8	188.8
Rock	Norite	Norite	Norite	Norite	Norite	Norite
SiO2 (wt. %)	49.06	48.77	48.12	47.85	47.60	47.31
Al2O3	32.78	32.82	33.07	33.45	33.65	33.48
FeO	0.25	0.23	0.24	0.19	0.22	0.25
CaO	15.44	15.90	16.18	16.55	16.65	16.87
Na2O	2.59	2.41	2.45	2.18	2.08	2.02
K2O	0.03	0.05	0.04	0.05	0.07	0.03
Total	100.15	100.17	100.10	100.27	100.25	99.96
Normalization based on 8 oxygens						
Si (atoms %)	2.24	2.23	2.20	2.19	2.18	2.17
Al	1.76	1.77	1.79	1.80	1.82	1.81
Fe^{2+}	0.01	0.01	0.01	0.01	0.01	0.01
Ca	0.75	0.78	0.79	0.81	0.82	0.83
Na	0.23	0.21	0.22	0.19	0.18	0.18
K	0.00	0.00	0.00	0.00	0.00	0.00
Total	5.00	5.00	5.01	5.01	5.01	5.01
An	76.61	78.22	78.32	80.53	81.28	82.07

Table 2.3 - Representative analyses of chromite from a line transverse across the inclusion-free chromite grain shown in figure 2.9A.

Drill Hole		LUFD - 79	LUFD - 79	LUFD - 79	LUFD - 79	LUFD - 79	LUFD - 79	LUFD - 79	LUFD - 79	LUFD - 79	LUFD - 79
Depth (m)		62.40	62.40	62.40	62.40	62.40	62.40	62.40	62.40	62.40	62.40
SiO_2	(wt. %)	<0.01	<0.01	<0.01	<0.01	<0.01	<0.01	<0.01	0.02	<0.01	<0.01
TiO_2		0.57	0.55	0.16	0.41	0.47	0.38	0.64	0.38	0.38	0.29
Al_2O_3		18.92	19.54	20.23	20.82	20.85	21.03	20.61	20.29	19.51	18.87
Cr_2O_3		35.68	35.80	35.46	35.69	36.88	36.38	36.49	35.71	35.82	35.43
Fe_2O_3		10.25	11.35	12.66	12.96	12.55	12.82	12.31	12.07	10.97	11.31
FeO		23.90	21.71	16.54	14.04	13.15	13.33	15.55	18.38	23.11	24.10
MnO		0.29	0.19	0.27	0.29	0.14	0.17	0.27	0.30	0.32	0.42
MgO		6.26	8.26	11.24	13.28	14.07	13.90	12.54	10.27	7.00	5.92
CaO		<0.01	<0.01	<0.01	<0.01	<0.01	<0.01	<0.01	<0.01	<0.01	<0.01
NiO		0.20	0.25	0.21	0.25	0.27	0.24	0.25	0.29	0.19	0.18
ZnO		0.49	0.00	0.06	0.06	0.05	0.04	0.13	0.16	0.27	0.51
V_2O_3		0.17	0.16	0.17	0.21	0.15	0.19	0.21	0.17	0.18	0.14
Total		95.74	96.67	95.75	96.74	97.33	97.19	97.78	96.83	96.68	96.06
Number of cations per 32 oxygen ions											
Si	(atoms %)	<0.01	<0.01	<0.01	<0.01	<0.01	<0.01	<0.01	0.01	<0.01	<0.01
Ti		0.12	0.11	0.03	0.08	0.09	0.07	0.12	0.07	0.08	0.06
Al		6.02	6.06	6.17	6.20	6.14	6.20	6.12	6.17	6.10	6.00
Cr		7.61	7.44	7.26	7.13	7.29	7.20	7.27	7.29	7.52	7.55
Fe^{3+}		2.08	2.25	2.46	2.46	2.36	2.42	2.33	2.35	2.19	2.29
Fe^{2+}		5.39	4.78	3.58	2.96	2.75	2.79	3.28	3.97	5.13	5.44
Mn		0.07	0.04	0.06	0.06	0.03	0.04	0.06	0.07	0.07	0.10
Mg		2.52	3.24	4.34	5.00	5.24	5.19	4.71	3.95	2.77	2.38
Ca		<0.01	<0.01	<0.01	<0.01	<0.01	<0.01	<0.01	<0.01	<0.01	<0.01
Ni		0.04	0.05	0.04	0.05	0.05	0.05	0.05	0.06	0.04	0.04

Zn	0.10	0.00	0.01	0.01	0.01	0.01	0.02	0.03	0.05	0.10
V	0.04	0.03	0.03	0.04	0.03	0.04	0.04	0.03	0.04	0.03
Total	24.00	24.00	23.99	24.00	24.00	24.00	24.00	24.00	24.00	24.00
Al#	38.30	38.47	38.85	39.26	38.90	39.22	38.92	39.05	38.60	37.85
Cr#	48.44	47.27	45.69	45.14	46.15	45.51	46.23	46.11	47.55	47.67
Fe^{3+}#	13.25	14.26	15.46	15.60	14.95	15.27	14.84	14.84	13.86	14.48
Fe^{2+}#	68.16	59.59	45.21	37.22	34.40	34.99	41.02	50.11	64.94	69.56
Mg#	31.84	40.41	54.79	62.78	65.60	65.01	58.98	49.89	35.06	30.44

Table 2.4 - Representative analyses of chromite from a line transverse across the inclusion-bearing chromite grain shown in figure 2.9D.

Drill Hole	LUFD - 79	LUFD - 79	LUFD - 79	LUFD - 79	LUFD - 79	LUFD - 79	LUFD - 79	LUFD - 79	LUFD - 79	LUFD - 79
Depth (m)	62.40	62.40	62.40	62.40	62.40	62.40	62.40	62.40	62.40	62.40
SiO_2 (wt. %)	<0.01	<0.01	<0.01	<0.01	<0.01	<0.01	<0.01	0.02	<0.01	<0.01
TiO_2	0.57	0.55	0.16	0.41	0.47	0.38	0.64	0.38	0.38	0.29
Al_2O_3	18.92	19.54	20.23	20.82	20.85	21.03	20.61	20.29	19.51	18.87
Cr_2O_3	35.68	35.80	35.46	35.69	36.88	36.38	36.49	35.71	35.82	35.43
Fe_2O_3	10.25	11.35	12.66	12.96	12.55	12.82	12.31	12.07	10.97	11.31
FeO	23.90	21.71	16.54	14.04	13.15	13.33	15.55	18.38	23.11	24.10
MnO	0.29	0.19	0.27	0.29	0.14	0.17	0.27	0.30	0.32	0.42
MgO	6.26	8.26	11.24	13.28	14.07	13.90	12.54	10.27	7.00	5.92
CaO	<0.01	<0.01	<0.01	<0.01	<0.01	<0.01	<0.01	<0.01	<0.01	<0.01
NiO	0.20	0.25	0.21	0.25	0.27	0.24	0.25	0.29	0.19	0.18
ZnO	0.49	0.00	0.06	0.06	0.05	0.04	0.13	0.16	0.27	0.51
V_2O_3	0.17	0.16	0.17	0.21	0.15	0.19	0.21	0.17	0.18	0.14
Total	95.74	96.67	95.75	96.74	97.33	97.19	97.78	96.83	96.68	96.06

Number of cations per 32 oxygen ions											
Si	(atoms %)	<0.01	<0.01	<0.01	<0.01	<0.01	<0.01	<0.01	0.01	<0.01	<0.01
Ti		0.12	0.11	0.03	0.08	0.09	0.07	0.12	0.07	0.08	0.06
Al		6.02	6.06	6.17	6.20	6.14	6.20	6.12	6.17	6.10	6.00
Cr		7.61	7.44	7.26	7.13	7.29	7.20	7.27	7.29	7.52	7.55
Fe^{3+}		2.08	2.25	2.46	2.46	2.36	2.42	2.33	2.35	2.19	2.29
Fe^{2+}		5.39	4.78	3.58	2.96	2.75	2.79	3.28	3.97	5.13	5.44
Mn		0.07	0.04	0.06	0.06	0.03	0.04	0.06	0.07	0.07	0.10
Mg		2.52	3.24	4.34	5.00	5.24	5.19	4.71	3.95	2.77	2.38
Ca		<0.01	<0.01	<0.01	<0.01	<0.01	<0.01	<0.01	<0.01	<0.01	<0.01
Ni		0.04	0.05	0.04	0.05	0.05	0.05	0.05	0.06	0.04	0.04
Zn		0.10	0.00	0.01	0.01	0.01	0.01	0.02	0.03	0.05	0.10
V		0.04	0.03	0.03	0.04	0.03	0.04	0.04	0.03	0.04	0.03
Total		24.00	24.00	23.99	24.00	24.00	24.00	24.00	24.00	24.00	24.00
Al#		38.30	38.47	38.85	39.26	38.90	39.22	38.92	39.05	38.60	37.85
Cr#		48.44	47.27	45.69	45.14	46.15	45.51	46.23	46.11	47.55	47.67
Fe^{3+}#		13.25	14.26	15.46	15.60	14.95	15.27	14.84	14.84	13.86	14.48
Fe^{2+}#		68.16	59.59	45.21	37.22	34.40	34.99	41.02	50.11	64.94	69.56
Mg#		31.84	40.41	54.79	62.78	65.60	65.01	58.98	49.89	35.06	30.44

2.6.2.1 - Line traverses through inclusion-free crystals

Inclusion-free crystals have a core-to-rim variation in composition (or concentric rim) that varies in thickness according to the modal percentage of chromite. Chromite crystals from massive chromitites (i.e., > 50 vol % of chromite) have thinner concentric rims compared with chain-textured and disseminated chromitites (i.e., < 50 vol % of chromite). Line traverses through inclusion-free crystals (Figs. 2.9A and 2.9B) show significant progressive core to rim changes in Mg# (i.e., a Mg-Fe core-rim zoning). The core of the crystals has higher Mg and lower Fe^{2+} contents than the rims, resulting in an up to 40% difference in Mg# across a chromite crystal. Difference in Mg# from core to rim progressively decreases for chromitites with higher amount of intercumulus minerals, as illustrated by line traverses through chromite crystals from massive (Fig. 2.9A), chain-textured (Fig. 2.9B) and disseminated (Fig. 2.9C) chromitites. This feature (i.e., the progressively lower difference in Mg# for chromitites with higher amounts of intercumulus minerals) is matched with progressively lower Mg# in the core of chromite grains. Significant differences in Mg# of chromite crystals suggest extensive Mg and Fe^{2+} exchange, a subject to be addressed in the discussion of this study. The Cr#, Al# and Fe^{3+}# are constant in line traverses through different types of chromite crystals (Figs. 2.9A, 2.9B and 2.9C), except for few analyses located in the outer bright colored rim in some crystals (not analysed for line traverses represented in Figs. 2.9A, 2.9B and 2.9C). This feature indicates that the suggested extensive exchange between divalent cations in chromite crystals (i.e., Mg and Fe^{2+}) does not affect trivalent cations (i.e., Cr, Al and Fe^{3+}).

2.6.2.2 - Line traverses through inclusion-bearing crystals

Inclusion-bearing crystals (Figs. 2.5G, 2.5H and 2.7) have an outer alteration rim, similar to the one described for inclusion-free crystals, and a variably developed rim adjacent to the silicate inclusions (Fig. 2.9D). The latter, designated inner rim, has a distinctive morphology consisting of rounded contacts with the silicate inclusion and a characteristic sector zoning following the octahedral form of the hosting chromite crystals (Fig. 2.9D). The existence and/or extent of the inner rim do not have any systematic relation with the size of host chromite crystal and silicate inclusion, the number of inclusions, or the chromite modal percentage and texture of the chromitite. Line traverses through inclusion-bearing crystals (Fig. 2.9D) indicate significant compositional changes close to silicate inclusions.

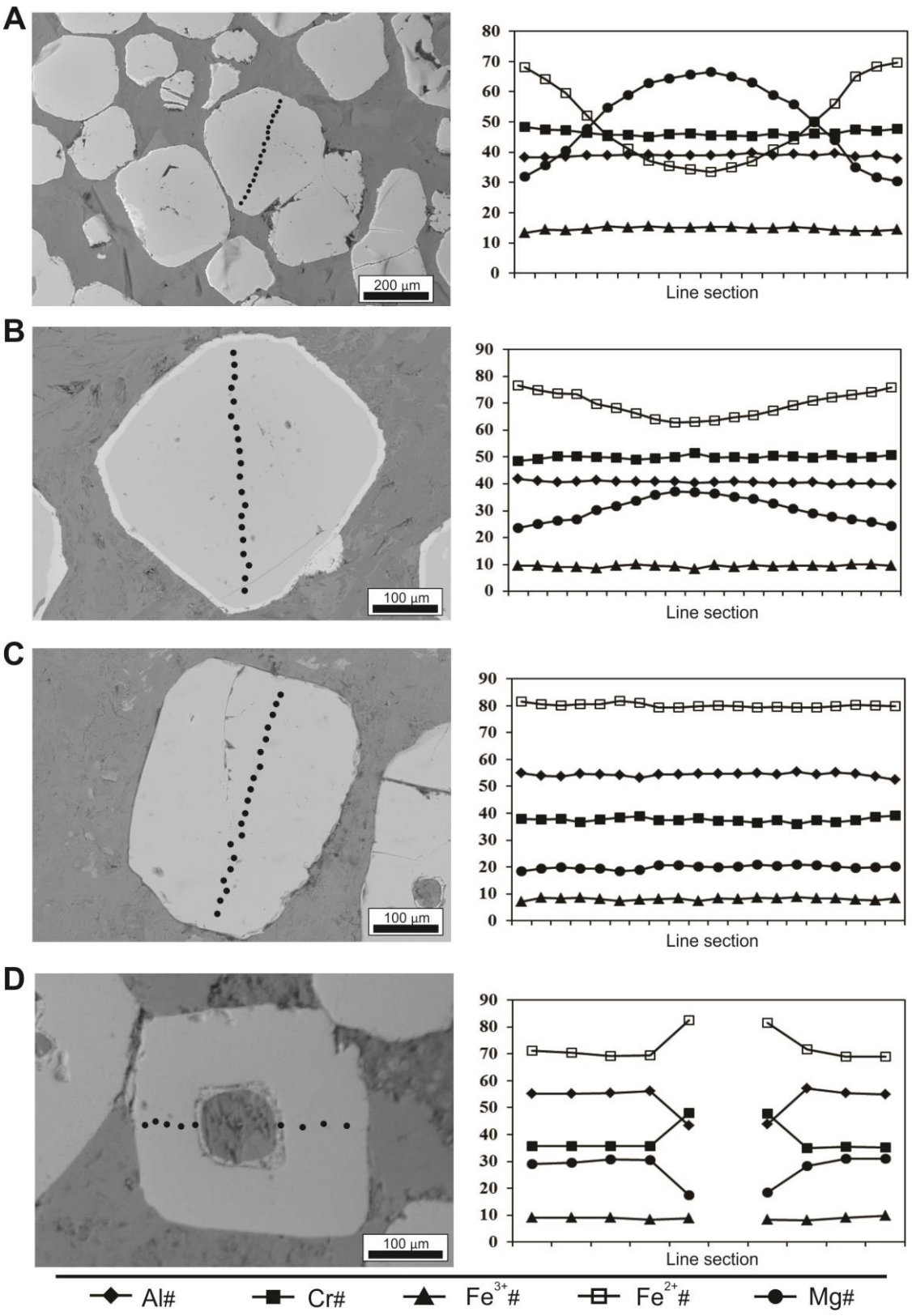

Fig. 2.9: EMP Back-scattered images of chromite grains analysed in line transverses and plots of the results. A) Massive chromitite from the main chromitite of the Transition Zone. B) Chain-textured chromitite from the main chromitite of the Transition Zone. C) Disseminated chromitite from the main chromitite of the Transition Zone. D) Inclusion-bearing chromite grain from a thin chromitite of the Mafic Zone.

Compared to the host chromite, compositions within the rims adjacent to silicate inclusions have higher Cr#, lower Al# and Mg# and similar Fe^{3+}# (Fig. 2.9D). These relative compositional changes are described for all studied rims regardless the size and/or composition of the host chromite.

2.6.2.3 - Cryptic variation of chromite

Line traverses across chromite crystals of several chromitites from drill core LUFD-079 indicate that chromite compositions are highly variable for each sample. Compositional variation occurs within a single grain (i.e., zoning) as well as when different grains from the same sample are compared. These compositional variations pose limits for the use of chromite composition as a parameter for the composition and fractionation of the parental magma. The cryptic variation study of chromite through drill core LUFD-079 (Fig. 2.8) includes just compositions obtained in homogenous core of inclusion-free chromite crystals from chain-textured or massive chromitites. These compositions are interpreted to be close to primary crystallization compositions and largely reduce the variability resulting from zoned crystals.

Chromite compositions in crystals from chromitites through drill core LUFD-079 indicate an increase in Al# along with a decrease in Cr# (Fig. 2.8). Cr# and Al# of LGC (including samples from the main chromitite), respectively 45-54 and 32-44, are distinctively different from those obtained in UGC, respectively 36-42 and 52-58. The Fe^{3+}# follows the Cr# and decrease from LGC (6-19) to UGC (1-9). The Mg# in chromite is largely controlled by textural features of chromite and the modal composition of the chromitite, as indicated in the description of line traverses. Mg# are low and close to ~ 20 for all chromitites, except for higher and highly variable values (30-66) for samples of the main chromitite. The low values of Mg# obtained for most chromitites are likely to result from later alteration processes and, therefore, not useful as an indication of magmatic evolution.

Chromite compositions in crystals from samples through the main chromitite do not provide any significant base-to-top compositional trend (Fig. 2.10). Cr# and Al# in chromite crystals show negative correlation and a limited compositional range, respectively 47-51 and 36-42., except for the unusually Fe^{3+} rich (8-15) and Cr-poor (45-50) uppermost sample. Highly variable Mg# (22-62) are likely to result from heterogeneous effects of alteration processes, as previously described for other chromitites from drill core LUFD-079.

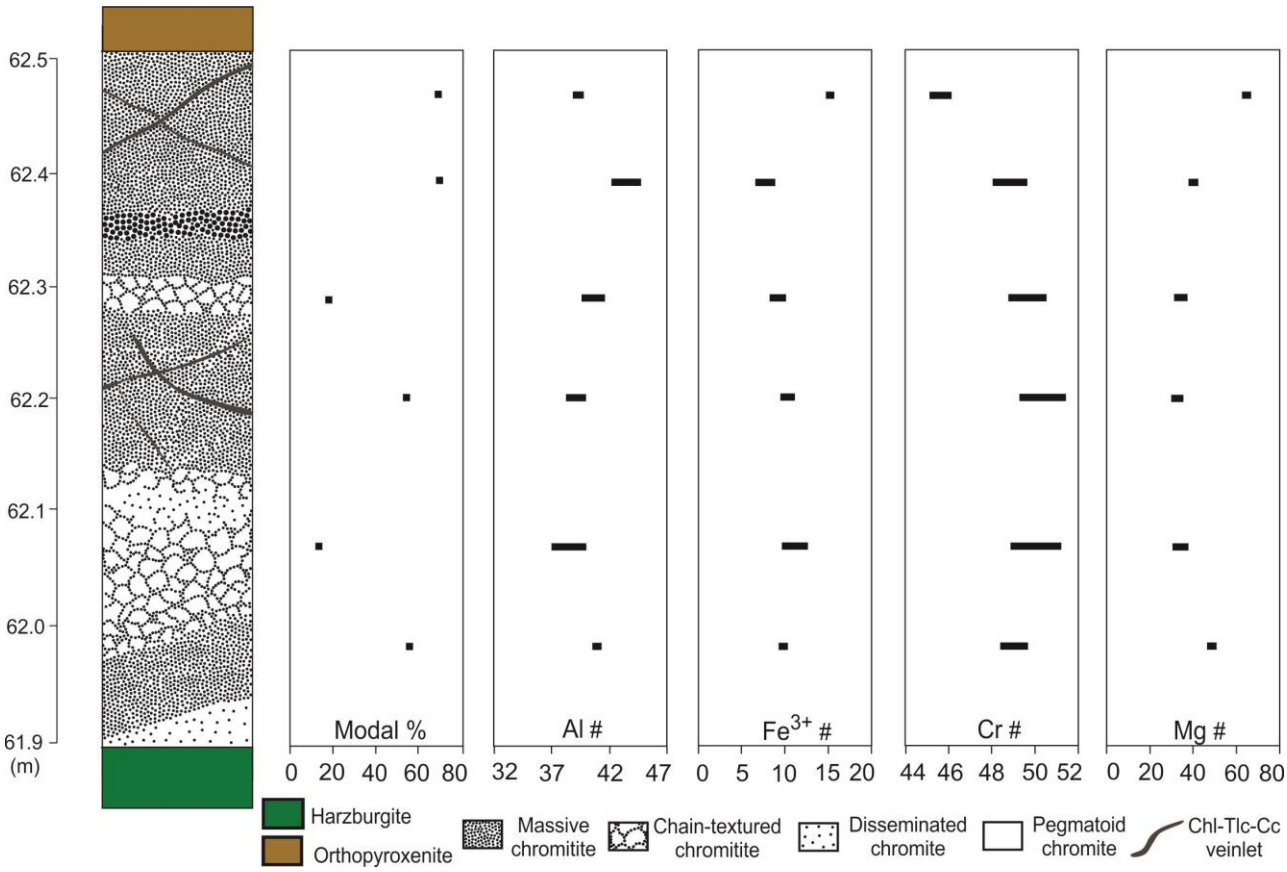

Fig. 2.10: Compositional variations of chromite throughout the main chromitite of the Transition Zone (see stratigraphic section in Fig. 3 for orientation). Chromite compositions are expressed in terms of Al# = 100Al/(Al + Cr + Fe^{3+}), Cr# = 100Cr/(Cr + Al + Fe^{3+}), Fe^{3+}# = 100Fe^{3+}/(Fe^{3+} + Cr + Al) and Mg# = 100Mg/(Mg + Fe^{2+}). Modal % indicates the chromite percentage of each sample. The black bar indicates the variation for each sample.

2.7 - Discussion

2.7.1 - Magmatic compositions of chromite

The extensive database of chromite analyses (~ 700 analyses) for chromitites of the Luanga Complex obtained in this study indicates a large range of compositions. Two common projections of the spinel compositional prism, the triangular Cr-Al-Fe^{3+} plot (Fig. 2.11) and the plot of Fe^{2+}/(Mg+Fe^{2+}) vs Cr/(Cr+Al) (Fig. 2.12), are used to illustrate the compositional variation of chromite in chromitites. Results indicate that LGC have distinctively higher Cr# compared with UGC. The upward decrease of Cr# in chromitites of the Luanga Complex matches the fractionation of the magma from ultramafic cumulates (olivine and/or orthopyroxene cumulates) in the Transition Zone to plagioclase-bearing cumulates in the Mafic Zone (Fig. 2.8). Our results also indicate

that compositions of chromite from the UGC are distinctively different from those hosted in chromitites from continental layered intrusions (Fig. 2.12). While most chromitites in continental layered intrusions are located within ultramafic cumulates, our results for the UGC add another case for the few examples of chromitites hosted within mafic cumulate (e.g., Rum layered intrusion, Henderson, 1975; Upper Group chromitites of the Bushveld Complex, Eales and Reynolds, 1986). Due to extensive Fe^{+2} and Mg compositional variation in chromite, our data is highly scattered in a Fe# vs Cr# plot (Fig. 2.12). Therefore, typical trends indicating either a positive correlation between Fe# (or otherwise a negative correlation if Mg# is plotted) and Cr# (known as the Cr-Al trend by Barnes and Roeder, 2001), or a negative correlation (known as the Rum trend by Barnes and Roeder, 2001) are not obvious for chromitites from the Luanga Complex (Fig. 2.12). Nevertheless, the very low Cr# of the UGC and the abrupt upward decrease in Cr# from the LGC to the UGC are remarkable compositional features. Lower Cr# in the UGC results from the increase in Al at the expense of Cr and some Fe^{3+} (Fig. 2.8 and 2.12). The upward decrease in the Cr# through a layered intrusion has been ascribed to the depletion of Cr in the melt during fractionation (Irvine, 1977; Hulbert and Von Gruenewaldt, 1985). However, the content of TiO_2 in chromite from chromitites of the Luanga Complex (Fig. 2.8) does not show an upward increase as expected for progressively more fractionated magmas. It should also be noted that chromite in the Upper Group of the Bushveld Complex chromitites have higher Cr# compared with chromite in the underlying Middle Group chromitites, a feature interpreted as the result of reduced Al_2O_3 activity by the appearance of cumulus plagioclase in cumulates hosting the Upper Group chromitites (Eales and Marsh, 1983; Naldrett et al., 2009). The previous discussion suggests that the unusual composition of the UGC chromitites are not satisfactory explained by models and processes indicated for chromitites from other locations. We suggest that compositions of the UGC chromite may be linked to petrological processes associated with peridotites underlying each chromitite, an issue addressed in the following discussion.

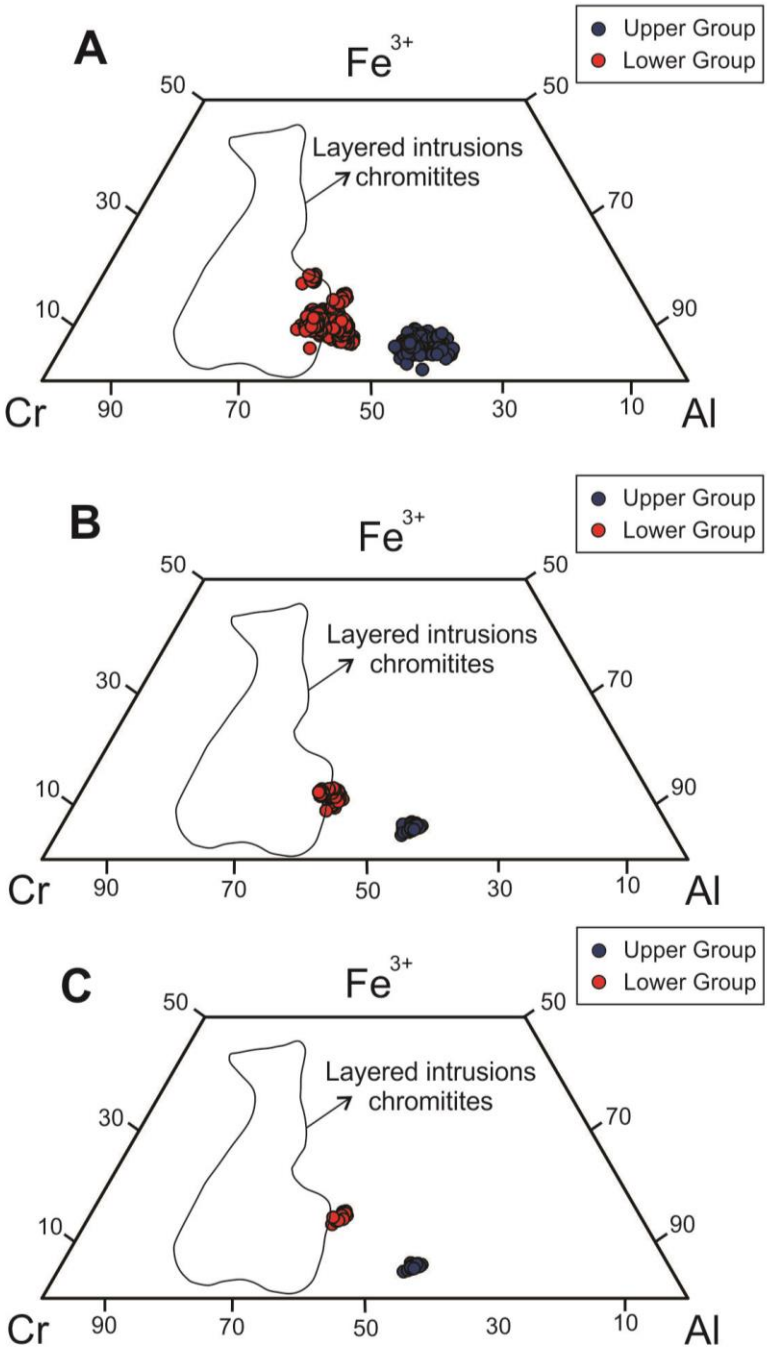

Fig. 2.11: Ternary plot (Fe^{3+}#-Cr#-Al# of chromites from chromitites of the Luanga Complex. A) Chromite analyses from all chromitites investigated. B) Analyses of chromite from one chromitite of the Transition Zone (Lower Group) and one of the Mafic Zone (Upper Group). C) Analyses of chromite from a line traverse of one representative chromite crystal from the chromitites indicated in B). The field of chromite compositions in layered intrusions is from Barnes and Roeder (2001).

2.7.2 - Petrological implications of the stratigraphic distribution of chromitites

As commonly described in layered intrusions, chromitites in the Luanga Complex occur in specific stratigraphic intervals with distinct petrological characteristics. Chromitites occur mainly in the upper portions of the Transition Zone and through the immediate contact with the Mafic Zone (Fig. 2.2C), a stratigraphic interval consisting of several cyclic units interpreted as the result of successive influxes of parental magma (Mansur and Ferreira Filho, 2016). Different models were proposed to explain the common association of chromitites and cyclic units. They include, among others, the mixing of an injection of primitive magma with a more fractionated magma residing in the magma chamber, thus causing chromite to be the sole liquidus mineral (e.g., Irvine, 1977) and the result of slumping of semi-consolidated cumulates in a chromite-rich slurry (e.g., Mondal and Mathez, 2007; Maier and Barnes 2008; Voordouw et al., 2009). It is not the aim of this paper to discuss the processes that lead to the accumulation of chromite-rich layers, a highly controversial subject (see Mondal and Mathez, 2007 and Naldrett et al., 2012 for reviews and references). We rather want to focus on possible petrological implications provided by the stratigraphic sequence associated with chromitites in the Mafic Zone (Fig. 2.3). Thin chromitites hosted by noritic rocks are always preceded by a thin layer of harzburgite located 15-20 cm below each chromitite layer (Figs 2.4C to E). Because this unusual stratigraphic association of harzburgite and chromitite is consistently repeated, a petrological link of harzburgite layers and chromitites located above them is suggested. Thin chromitites closely associated with peridotite-troctolite are also reported in the Rum Complex (O'Driscoll et al., 2010). Although chromitites in the Rum Complex occur mainly at the base of several peridotite-troctolite cyclic units, thin chromitites also occur a few centimeters away from the basal peridotite. O'Drisoll et al. (2010) suggested that chromitites were formed by *in situ* crystallization following assimilation of troctolitic cumulate by a new influx of primitive magma at the crystal mush-magma interface. The authors' also suggested that chromitites located above the unit boundaries resulted from coeval syn-magmatic deformation of the crystal mush. This interpretation may be also applied for chromitites hosted in noritic rocks of the Luanga Complex. When the new influx of primitive magma assimilated norite the concentration (and thus activity) of Al_2O_3 should have increased. The relatively lower Cr# and Fe^{+3} of chromite in the UGC may result from an increase in Al_2O_3 activity right in the crystal mush-primitive magma interface, just preceding the first appearance of liquidus plagioclase. This suggesting

follows O'Driscoll et al. (2010) idea that unusually aluminous composition of chromite in the Rum Complex resulted from high Al_2O_3 content of hybrid liquids originated from assimilation of plagioclase-rich cumulate from a picritic magma.

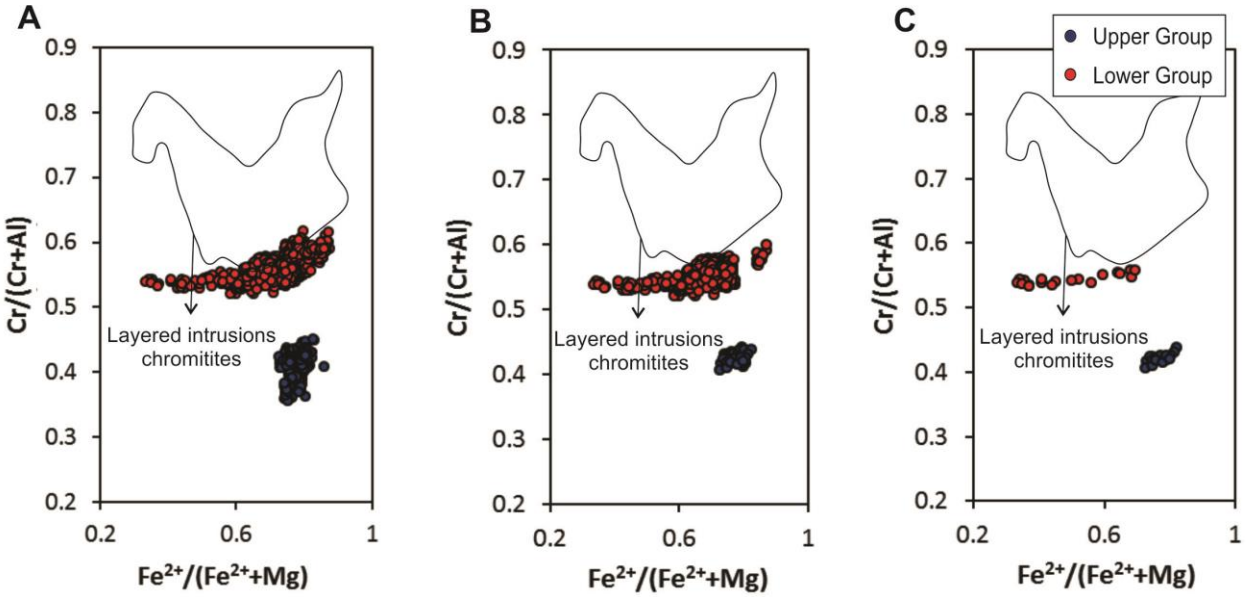

Fig. 2.12: $Fe^{2+}/(Mg + Fe^{2+})$ versus Cr/(Cr + Al) of chromites from chromitites of the Luanga Complex. A) Chromite analyses from all chromitites investigated. B) Analyses of chromite from one chromitite of the Transition Zone (Lower Group) and one of the Mafic Zone (Upper Group). C) Analyses of chromite from a traverse section of one representative chromite crystal from the chromitites indicated in B). The field of chromite compositions in layered intrusions is from Barnes and Roeder (2001).

2.7.3 - Compositional zonation in chromite grains and its implications for the interpretation of chromite compositions

Our results indicate that extensive compositional variation occurs in different scales, as indicated by large variation obtained in analyses of one chromitite (Fig. 2.11B and 2.12B) or even within a chromite crystal (Fig. 2.11C and 2.12C). Compositional traverses in chromite crystals from several chromitites of the Luanga Complex indicate three distinct types of rim or compositional zoning: i. an outer alteration rim, ii. a Mg-Fe core-rim zoning, iii. an inner rim adjacent to silicate inclusions. Distinct textures and compositions of these three types of rim or zoning suggest that they originated from different processes.

An outer alteration rim characterized by higher reflectance (see Fig. 2.9B and photomicrographs in Sack and Ghiorso, 1991) is common in chromite crystals from chromitites overprinted by metamorphism, especially under lower to intermediate grades of the regional metamorphism (i.e., up to amphibolite facies) (e.g., Evans and Frost, 1975; Sack and Ghiorso, 1991; Liipo et al., 1995). This alteration is also common in chromite crystals in serpentinized and/or hydrothermally altered mafic-ultramafic rocks (e.g., Barnes and Roeder, 2001; Mukherjee et al., 2010). The composition of chromite in samples of the Luanga Complex changes abruptly in the outer rim, becoming enriched in Fe^{3+} and Fe^{2+} at the expense of Mg, Cr, Al, thus moving toward the magnetite apex on the spinel prism. The formation of the outer rim is probably related to the metamorphic replacement of the primary mineralogy of the Luanga Complex. This interpretation is supported by progressively larger outer rims in chromite associated with extensively replaced rocks. While chromite grains are commonly completely altered to magnetite-ferrichromite in extensively replaced rocks, chromite enclosed in relicts of olivine or orthopyroxene have just minor alteration along fractures. Once this alteration is easily recognized in petrographic studies and have highly different compositions compared with the core, analyses of the outer rim were disregarded as far as the magmatic and sub-solidus interpretation of chromite compositions of the Luanga Complex is concerned.

The Mg-Fe zoning in chromite crystals has a strong correlation with the modal percentage of chromite in a given layer (Fig. 2.9A to 2.9C). This is indicated by thinner concentric rims in chromite crystals from massive chromitites (i.e., > 50 vol % of chromite) compared with chain-textured and disseminated chromitites (i.e., < 50 vol % of chromite), and has been described in several studies of chromitites (e.g., Danyushevsky et al., 2000; Marques and Ferreira Filho, 2003; Spandler et al., 2005). The Mg-Fe zoning in chromite crystals results of significant core-to-rim difference in Fe^{2+} and Mg contents with none to minor difference in Fe^{3+}, Al and Cr contents. The progressive core-to-rim decrease in Mg# of chromite crystals may result either from an evolving melt composition during crystallization, or by subsolidus exchange of Fe^{2+} and Mg between chromite and coexisting silicates during slow cooling of the intrusion. The first option is favored by the progressive fractionation of the trapped intercumulus liquid coexisting with cumulus chromite (e.g., Henderson and Wood, 1981; Roeder and Campbell, 1985). However, the fractionated trapped melt should become enriched in TiO_2 and Fe^{3+} and therefore, a negative correlation of Mg# and Fe^{3+}# along with TiO_2

contents would be expected for Mg-Fe zoned chromite crystals. Because these correlations do not occur in the Mg-Fe zoned crystals of the Luanga Complex (Fig. 2.9), the first option is not an appropriate interpretation. The second option demands an extensive exchange between divalent cations hosted in tetrahedral sites in chromite crystals (i.e., Mg and Fe^{2+}) and coexisting silicates. This extensive exchange would not be accompanied with exchange between trivalent cations hosted in octahedral sites (i.e., Cr, Al and Fe^{3+}) in chromite and coexisting silicates due to their lower diffusion rates (Sack and Ghiorso, 1991). The second option has been proposed as an explanation for Fe^{2+} and Mg variation across chromite grains in chromitites (e.g., Danyushevsky et al., 2000; Spier and Ferreira Filho, 2001; Spandler et al., 2005), and provides an appropriate interpretation for Mg-Fe zoned chromite crystals of the Luanga Complex.

Inclusion-bearing chromite crystals have the same Mg-Fe zoning but also show additional inner rims adjacent to the silicate inclusions (Fig. 2.9D). The chromite composition adjacent to the silicate inclusion (i.e., in the inner rim) have higher Cr#, lower Mg# and Al#, and similar Fe^{3+}# (Fig. 2.9D), possibly due to crystallization from a progressively more fractionationed liquid trapped in the chromite crystal (i.e., following the process suggested for progressive fractionation of the trapped intercumulus liquid by Henderson and Wood, 1981). Borisova et al. (2012) describe chromites with similar compositional variation in coronas adjacent to silicate inclusions from the Oman ophiolite. Based on the hydrous Na-Cl-rich composition of the melt inclusions, the authors proposed a subsolidus process for the origin of the coronas in chromite from the Oman ophiolite, suggesting that hydrothermal or metamorphic processes induced higher Cr# in chromite close to the hydrous silicate inclusions. Because silicate inclusions in the Luanga Complex are eventually connected to intercumulus minerals, and no evidence for hydrous Na-Cl melt inclusions exists, such a hydrothermal-metamorphic process is not favored for the inner rim coronas described in our study. In particular, reaction of Cr-spinel with intercumulus liquid, as suggested for the inner rim coronas of the Luanga Complex, results in both divalent (Fe^{2+} and Mg) and trivalent (Cr, Al, Fe,) cation exchange. On the other hand, subsolidus reaction of Cr-spinel and intercumulus silicates, as suggested for the Fe-Mg zoning, results mainly in exchange of divalent cations.

Our results indicate that chromite compositions from chromitites of the Luanga Complex (Figs. 2.11 and 2.12) have their primary cumulus composition extensively

modified by postcumulus magmatic processes. Although distinct primary magmatic compositions are indicated by different Cr# for chromites from the Transition Zone and Mafic Zone, the extensive variation of Mg# for a single chromite crystal indicates that the compositional field of the Luanga Complex chromitites are not entirely primary magmatic. Due to the indicated modification of primary magmatic compositions, it is critical to determine what range of compositions of the Luanga Complex chromites represents the closest composition of original cumulus chromite. These are the compositions useful for defining magmatic trends and/or comparison with other layered intrusions. Mass balance arguments are commonly used to indicate that massive chromitites with > 70 % vol. chromite are likely to preserve its original igneous compositions because there are few other phases available for element exchange (e.g., Eales and Reynolds, 1986). This reasoning was used in several studies of chromitites (e.g., Bacuri Complex, Spier and Ferreira Filho, 2001; Ipueira-Medrado Sill, Marques and Ferreira Filho, 2003), but is not appropriate for chromitites of the Luanga Complex, where modal compositions rarely exceed 70 vol. %. Our results suggest, in fact, that just the compositions from analyses in the very core of chromite from massive portions of the main chromitite (e.g., Fig. 2.9A) represent compositions close to original cumulus compositions of the Luanga Complex. None of the other analyses represent cumulus compositions. These altered compositions represent > 90 % of the analyses of this study, including all analyses of chromite from chromitites of the Mafic Zone. The range of chromite compositions likely to represent primary cumulus composition for chromitites of the Transition Zone, as well as the range of Fe^{+2}-Mg exchange, is indicated in figure 2.13. The range of cumulus compositions of chromite of the Transition Zone is restricted to analyses with high Mg# in the core of chromite from massive portions of the main chromitite (as indicated in Fig. 2.9A).

The extensive modification of primary cumulus composition of chromite, indicated in our study for the Luanga Complex, is likely to be common in non-massive chromitites (i.e., < 70 vol. % chromite), and the rule for disseminated chromites in mafic intrusions. Therefore, the common use of spinel compositions as a petrogenetic indicator for mafic intrusions (e.g., Sack and Ghiorso, 1991; Power et al., 2000; Barnes and Roeder, 2001) should be considered with caution and always supported by extensive petrographic/analytical investigation of post-magmatic alteration.

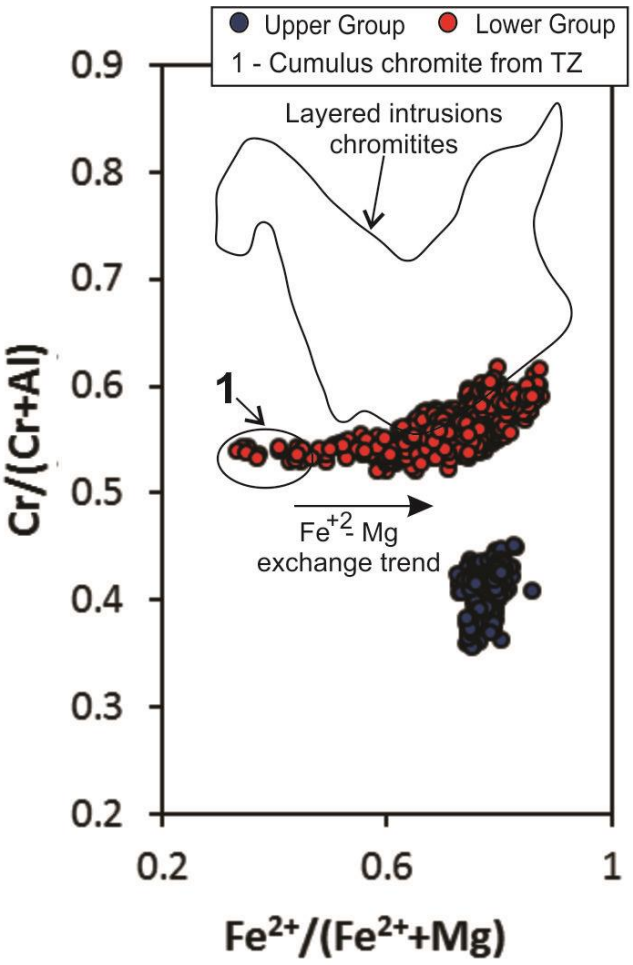

Fig. 2.13: $Fe^{2+}/(Mg + Fe^{2+})$ versus Cr/(Cr + Al) of chromites from chromitites of the Luanga Complex. The field of primary cumulus composition for chromitites of the Transition Zone (1) is indicated. The field of chromite compositions in layered intrusions is from Barnes and Roeder (2001).

2.7.4 - Why different types of inclusion-bearing chromite crystals are formed?

Silicate inclusions of distinct types are common in chromitites through the stratigraphy of the Luanga Complex (Figs. 2.5, 2.6 and 2.7). Different models have been proposed to explain the formation of silicate inclusions in chromite (e.g., Augé, 1987; Ballhaus and Stumpfl, 1986; Hulbert and Von Gruenewaldt, 1985; Li et al., 2005; Lorand and Cottin, 1987; Lorand and Ceulenner, 1989; Roeder et al., 2001; Spandler et al., 2005). It is beyond the scope of this article to enter into a thorough discussion of the mechanisms of formation of these inclusions, and just a parallel of our observation and available models is considered in here.

Based on the size and number of inclusions, the inclusion-bearing chromite grains of the Luanga Complex split into two groups. LGC commonly have chromite crystals with just one large inclusion (Fig. 2.7A), while UGC consist mainly of chromite

grains with several small inclusions (Fig. 2.7C). Both groups show inclusion coalescence (Figs. 2.5E and 2.6D), minor accumulation of sulfides at the bottom of inclusions (Fig. 2.5G) and rounded shapes (Figs. 2.5 to 2.7). These features support the concept that inclusions were formed due to the entrapment of melt during chromite growth, a process that requires fast growth rate as described for chromite grains in komatiites (e.g., Arndt et al., 1977; Barnes 1985; Godel et al., 2013) and modern picritic basalts (Roeder et al., 2001). High growth rate allows the crystallization of chromite with skeletal shapes and the entrapment of melt between dendritic branches (Fig. 2.14). Different types of inclusion-bearing crystals, as described for chromitites from different stratigraphic portions of the Luanga Complex, would thus require different growth rates during the evolution of the complex. Chromite crystals hosting just one large inclusion demand lower growth rates than those hosting several inclusions, thus allowing the coalescence between the entrapped liquid and the development of just one inclusion (Fig. 2.14A). On the other hand, chromite crystals hosting several inclusions are formed under higher growth rates, allowing the entrapment of many physically isolated melt droplets in each crystal (Fig. 2.14B). High growth rate in chromite is generally related to high diffusion and cooling rates (Arndt et al., 1977; Barnes and Hill, 1995; Godel et al., 2013). This reasoning suggests that the entrapment of many silicate melt droplets within UGC is a response to higher cooling rates, caused by new primitive magma injections within mafic cumulates. In contrast, chromite crystals from LGC would have a slower growth rate due to no major difference in temperature between primitive magmas and hosting ultramafic cumulates.

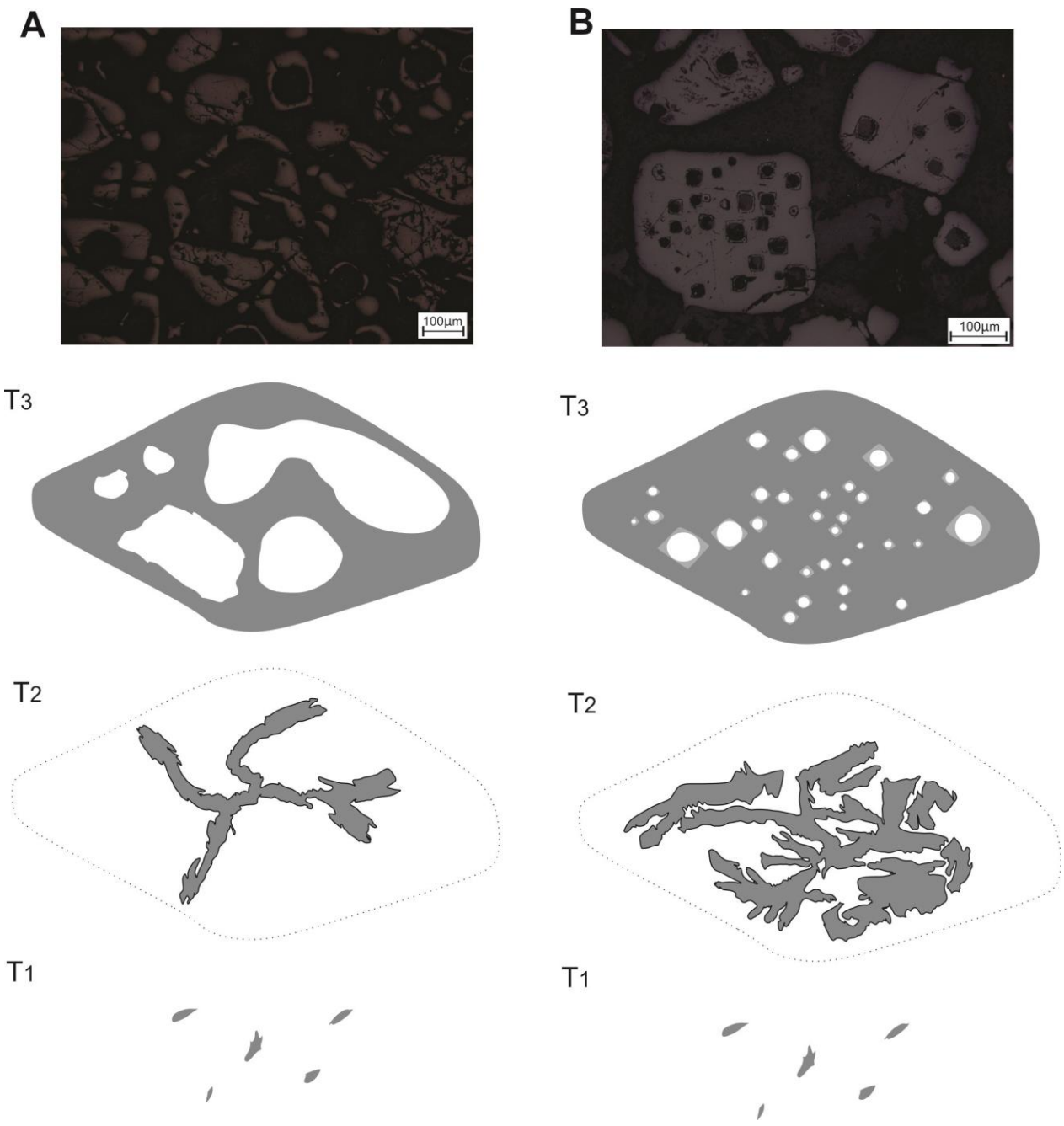

Fig. 2.14: Schematic model and phtomicrographs illustrating the crystallization of different inclusion-bearing chromite grains. T1, T2 and T3 represent the progressive evolution of the crystallization. A) Crystallization of inclusion-bearing chromite crystals from chromitite of the Transition Zone (Lower Group). B) Crystallization of inclusion-bearing chromite crystals from chromitite of the Mafic Zone (Upper Group).

2.8 - Conclusions

The principal conclusions of this study are as follows:

a) Chromitites in the Luanga Complex occur mainly in the upper portions of the Transition Zone, where they are hosted by ultramafic cumulates, and through the immediate contact with the overlying Mafic Zone, where they are hosted by plagioclase-bearing cumulates. This stratigraphic interval consists of several cyclic units interpreted as the result of successive influxes of primitive magma.

b) Chromite crystals in chromitites from the Transition Zone (i.e., Lower Group Chromitites - LGC) have distinctively higher Cr# compared with chromite crystals in chromitites from the Mafic Zone (i.e., Upper Group Chromitites - UGC). The upward decrease of Cr# in chromitites of the Luanga Complex matches the fractionation of the magma from ultramafic cumulates (olivine and/or orthopyroxene cumulates) in the Transition Zone to plagioclase-bearing cumulates in the Mafic Zone.

c) Extensive modification of primary cumulus composition of chromite in chromitite of the Luanga Complex is indicated by rimmed and/or extensively zoned chromite crystal. Zoned chromite indicates an extensive exchange between divalent (Mg, Fe^{2+}) cations and minor to none exchange between trivalent cations (Cr, Al and Fe^{3+}), and should result of subsolidus exchange of Fe^{2+} and Mg between chromite and coexisting silicates during slow cooling of the intrusion.

d) Significant modification of primary cumulus composition of chromite, as indicated in our study for the Luanga Complex, is likely to be common in non-massive chromitites and the rule for disseminated chromites in mafic intrusions. Therefore, the common use of spinel compositions as a petrogenetic indicator for mafic intrusions should be considered with caution.

Acknowledgements

This study was supported by CNPq (Conselho Nacional de Desenvolvimento Científico e Teconológico) and VALE S.A. (Projeto 550398/2010-4). Analytical facilities of the Instituto de Geociências of the University of Brasília (UnB) provided additional support for this research. The authors acknowledge VALE's Exploration Managers for Brazil and Carajás (Mr. Fernando Greco and Mr. Fernando Matos, respectively) for field

support and access to exploration data. Cesar F. Ferreira Filho is a Research Fellow of CNPq and acknowledges the continuous support through research grants and scholarships for the "Metalogenênese de Depósitos Associados ao Magmatismo Máfico-Ultramáfico" Research Group. The authors thank the reviewers (Dr. Iain McDonald and one anonymous) and guest editor (Dr. Sisir Mondal) for their constructive and helpful reviews. Federico Cuadros is thanked for assistance with electron microprobe analysis at the Universidade de Brasília. Eduardo T. Mansur holds a scholarship from Coordenação de Aperfeiçoamento de Pessoal de Nível Superior (CAPES) and this study is part of his M.Sc. thesis developed at the Instituto de Geociências (Universidade de Brasília).

References

Araújo, O.J.B., Maia, R.G.N., João, X.S.J., Costa, J.B.S., 1988. A megaestruturação arqueana da Folha Serra dos Carajás. Congresso Latino Americano de Geologia, Belém-Brazil, Anais, pp. 324-338.

Arndt, N.T., Naldrett, A.J., Pyke, D.R., 1977. Komatiitic and Iron-Rich Tholeiitic Lavas of Munro Township, Northeast Ontario. J. Petrol. 18, 319-369.

Augé, T., 1987. Chromite deposits in the northern Oman ophiolite: Mineralogical constraints. Mineral. Deposita 22, l-10.

Ballhaus, C.G., Stumpfl, E.F., 1986. Sulfide and platinum mineralization in the Merensky reef: evidence from hydrous silicates and fluid inclusions. Contrib. Mineral. Petrol. 94, 193-204.

Barnes, S.J., 1985. The petrography and geochemistry of Komatiite flows from the Abitibi greenstone-belt and a model for their formation. Lithos 18, 241-270.

Barnes, S.J., 1998. Chromite in komatiites, 1. Magmatic controls on crystallization and composition. J. Petrol. 39, 1689–1720.

Barnes, S.J., 2000. Chromite in komatiites, II modification during greenschist to mid – amphibolite facies metamorphism. J. Petrol. 41, 387- 409.

Barnes, S.J., Hill, R.E.T., 1995. Poikilitic chromite in komatiitic cumulates. Mineral. Petrol. 54, 85-92.

Barnes, S.J., Roeder, P.L., 2001. The range of spinel compositions in terrestrial mafic and ultramafic rocks. J. Petrol. 42, 2279-2302.

Borisova, A., Ceuleneer, G., Kamenetsky, V., Arai, S., Bejina, F., Abily, B., Bindeman, I., Polve, M., de Parseval, P., Aigouy, T., Pokrovski, G.S., 2012. A new view on the petrogenesis of the Oman ophiolite chromitites from microanalyses of chromite-hosted inclusions. J. Petrol. 53, 2411-2440.

Danyushevsky, L.V., Della-Pasqua, F.N., Sokolov, S., 2000. Reequilibration of melt inclusions trapped by magnesian olivine phenocrysts from subduction-related magmas: Petrological implications. Contrib. Mineral. Petrol. 138, 68-83.

Dardenne, M.A., Ferreira Filho, C.F., Meirelles, M.R., 1988. The role of shoshonitic and calc-alkaline suites in the tectonic evolution of the Carajás District, Brazil. J. South Am. Earth Sci. 1, 363-372.

Diella, V., Ferrario, A., Girardi, V.A.V., 1995. PGE and PGM in the Luanga mafic-ultramafic intrusion in Serra dos Carajás (Pará State, Brazil). Ore Geol. Rev. 9, 445-453.

Docegeo - Rio Doce Geologia e Mineração, 1988. Revisão Litoestratigráfica da Província Mineral de Carajás. 35º Congresso Brasileiro de Geologia, Belém, Brasil, Anais, Sociedade Brasileira de Geologia, pp. 11-59.

Eales, H.V., Marsh, J.S., 1983. Al/Cr ratios of coexisting pyroxenes and spinelloids in some ultramafic rocks. Chem.Geol. 38, 57–74.

Eales, H.V., Reynolds, I.M., 1986. Cryptic variations within chromitites of the Upper Critical Zone, northwestern Bushveld Complex. Econ. Geol. 81, 1056-1066.

Evans, B.W., Frost, B.R., 1975. Chrome-spinel in progressive metamorphism - a preliminary analysis. Geochim. Cosmochim. Acta 39, 959-972.

Feio, G.R.L., Dall'Agnol, R., Dantas, E.L., Macambira, M.J.B., Santos, J.O.S., Althoff, F.J., Soares, J.E.B., 2013. Archean granitoid magmatism in the Canaã dos Carajás area: Implications for crustal evolution of the Carajás province, Amazonian craton, Brazil. Precamb. Res. 227, 157-185.

Ferreira Filho, C.F., Cançado, F., Correa, C., Macambira, E.M.B., Siepierski, L., Brod, T.C.J., 2007. Mineralizações estratiformes de EGP-Ni associadas a complexos

acamadados em Carajás: os exemplos de Luanga e Serra da Onça. In: Publitec Gráfica & Editora, Contribuições à Geologia da Amazônia, vol. 5, pp. 01-14.

Gibbs, A.K., Wirth, K.R., Hirata, W.K., Olszewski Jr, W.J., 1986. Age and composition of the Grão Pará Group volcanics, Serra dos Carajás. Rev. Bras. Geoc. 16, 201-211.

Godel, B.M., Barnes, S.J., Gurer, D., Austin, P., Fiorentini, M.L., 2013. Chromite in komatiites: 3D morphologies with implications for crystallization mechanisms. Contrib. Mineral. Petrol. 165, 173-189.

Gole, M.J., Hill, R.E.T,. 1990. The refinement of extrusive models for the genesis of nickel deposits: implications from case studies at Honeymoon well and the walter Williams formations. Minerals and Energy Res. Institute of Western Australia Report. 68-93.

Haggerty, S.E., 1976. Opaque mineral oxides in terrestrial igneous rocks, in: Oxide minerals 3, D. Rumble, ed., pp. 101-300, Mineral. Soc. Am.

Henderson, P., 1975. Reaction trends shown by chrome-spinels of the Rhum layered intrusion. Geochim. Cosmochim. Acta 39, 1035-1044.

Henderson, P., Wood, R.J., 1981. Reaction relationships of chrome spinels in igneous rocks.Further evidence from the layered intrusions of Rhum and Mull, Inner Hebrides, Scotland. Contrib. Mineral Petrol. 78, 225-229.

Hulbert, L.J., Von Gruenewaldt, G., 1985. Textural and compositional features of chromite in the lower and critical zones of the bushveld complex South of Potgietersrus. Econ. Geol. 80, 872-895.

Irvine, T.N., 1965. Chromian spinel as a petrogenetic indicator. Part 1. Theory. Can. Journ. Earth Sci. 2, 648-672.

Irvine, T.N., 1977. Origin of chromite layers in the Muskox intrusion and other stratiform intrusions: a new interpretation. Geology 5, 273-277.

Li, C., Ripley, E.M., Sarkar, A., Shin, D., Maier, W.D., 2005. Origin of phlogopite-orthopyroxene inclusions in chromites from the Merensky Reef of the Bushveld Complex, South Africa. Contrib. Mineral. Petrol. 150, 119-130.

Liipo, J.P., Vuollo, J.I., Nykanen, V.M., Piirainen, T.A., 1995. Zoned Zn-rich chromite from the Naataniemi serpentinite massif, Kuhmo greenstone belt, Finland. Canad. Mineral. 33, 537-545.

Lorand, J.P., Ceuleneer, G., 1989. Silicate and base-metal sulfide inclusions in chromites from de Maqsad area (Oman ophiolite): a model for entrapment. Lithos, 22, 173-190.

Lorand, J.P., and Cottin, J.Y., 1987. Na-Ti-Zr-H_2O-rich mineral inclusions indicating postcumulus chrome-spinel dissolution and recrystallization in the Western Iaouni mafic intrusion, Algeria. Contrib. Mineral. Petrol. 97, 251-263.

Macambira, M.J.B., Lancelot, J.R., 1996. Time Constraints for the Formation of the Archean Rio Maria Crust, Southeastern Amazonian Craton, Brazil. Inter. Geol. Review 38, 1134-1142.

Machado, W., Lindenmayer, Z.G., Krogh, T.E., Lindenmayer, D., 1991. U-Pb geochronology of Archean magmatism and basement reactivation in the Carajás area, Amazon shield, Brazil. Precamb. Res. 49, 329-354.

Maier, W.D., Barnes, S.-J., 2008. Platinum-group elements in the UG1 and UG2 chromitites, and the Bastard Reef, at Impala platinum mine, Western Bushveld Complex, South Africa: evidence for late magmatic cumulate instability and reef constitution. S. Afr. J. Geol. 111, 159-176.

Mansur, E.T., Ferreira Filho, C.F., 2016. Magmatic structure and geochemistry of the Luanga Mafic-Ultramafic Complex: further constraints for the PGE-mineralized magmatism in Carajás, Brazil. Lithos 266-267, 28-43.

Marques, J.C., Ferreira Filho, C.F., 2003. The chromite deposits of the Ipueira-Medrado Sill, Bahia, Brazil. Econ. Geol. 98, 87-108.

Mondal, S.K., Mathez, E.A., 2007. Origin of the UG2 chromitite layer, Bushveld Complex. J. Petrol. 48, 495-510.

Mondal, S.K., Ripley, E.M., Li, C., Frei, R., 2006: The genesis of Archaean chromitites from the Nuasahi and Sukinda massifs in the Singhbhum craton, India. Precamb. Res. 148, 45-66.

Mukherjee, R., Mondal, S.K., Rosing, M.T., Frei, R., 2010. Compositional variations in the Mesoarchean chromites of the Nuggihalli schist belt, Western Dharwar craton (India): potential parental melts and implications for tectonic setting. Contrib. Mineral. Petrol. 160, 865-885.

Naldrett, A.J., Kinnaird, J., Wilson, A., Yudovskaya, M., McQuade, S., Chunnett, G., Stanley, C., 2009. Chromite composition and PGE content of Bushveld chromitites: part 1: the lower and middle groups. Appl. Earth Sci. IMM Trans. B. 118(3), 131-161.

Naldrett, A.J., Wilson, A., Kinnaird, J., Yudovskaya, M., Chunnett, G., 2012. The origin of chromitites and related PGE mineralization in the Bushveld Complex: new mineralogical and petrological constraints. Mineral. Deposita 47, 209-232.

O'Driscoll, B., Emeleus, C.H., Donaldson, C.H., Daly, J.S., 2010. Cr-spinel seam petrogenesis in the Rhum layered suite, NW Scotland: cumulate assimilation and in situ crystallization in a deforming crystal mush. J. Petrol. 51, 1171-1201.

Pidgeon, R.T., Macambira, M.J.B., Lafon, J.M., 2000. Th-U-Pb isotopic systems and internal structures of complex zircons from an enderbite from the Pium Complex, Carajás Province, Brazil: evidence for the ages of granulite facies metamorphism and the protolith of the enderbite. Chem. Geol. 166, 159-171.

Power, M.R., Pirrie, D., Andersen, J.C.Ø., Wheeler, P.D, 2000. Testing the validity of chrome spinel chemistry as a provenance and petrogenetic indicator. Geology 28, 1027-1030.

Robin, E., Bonté, P., Froget, L., Jéhanno, C., Rocchia, R., 1992. Formation of spinels in cosmic objects during atmospheric entry: A clue to the Cretaceous-Tertiary boundary event. Earth Planet. Sci. Lett. 108, 181-190.

Roeder, P.L., Campbell, I.H., 1985. The effect of postcumulus reactions of composition of chrome-spinels from the Jimberlana Intrusion. J. Petrol. 26, 763-786.

Roeder, P.L., Poustovetov, A., Oskarsson, N., 2001. Growth forms and composition of chromian spinel in MORB magma: Diffusion-controlled crystallization of chromian spinel. Can. Mineral. 39, 397-416.

Rosa, W.D., 2014. Complexos acamadados da Serra da Onça e Serra do Puma: Geologia e petrologia de duas intrusões Máfico-Ultramáficas com sequência de

cristalização distinta na Província Arqueana de Carajás, Brasil. Unpublished M.Sc. Thesis, Universidade de Brasília, Brazil, 65 pp.

Sack, R.O., Ghiorso, M.S., 1991. An internally consistent model for the thermodynamic properties of Fe-Mg-titanomagnetite-aluminate spinels. Contrib. Mineral. Petrol. 106, 474-505.

Siepierski, L., Ferreira Filho, C.F., 2016. Spinifex-textured komatiites in the south border of the Carajas ridge, Selva Greenstone belt, Carajás Province, Brazil. J. South Am. Earth Sci. 66, 41-55.

Siepierski, L., 2016. Geologia, petrologia e potencial para mineralizações magmáticas dos corpos máfico-ultramáficos da região de Canaã dos Carajás, Província Mineral de Carajás, Brasil. Unpublished Ph.D. Thesis, Universidade de Brasília, Brazil, 156 pp.

Souza, Z.S., Potrel, A., Lafon, J.M., Althoff, F.J., Pimentel, M.M., Dall'Agnol, R., Oliveira, C.G., 2001. Nd, Pb and Sr isotopes in the Identidade Belt, an Archean greenstone belt of Rio Maria region (Carajás Province, Brazil): implications for the geodynamic evolution of the Amazonian Craton. Precam. Res. 109, 293-315.

Spandler, C., Mavrogenes, J., Arculus, R., 2005. Origin of chromitites in layered intrusions: Evidence from chromite-hosted melt inclusions from the Stillwater Complex. Geology 33, 893-896.

Spier, C.B., Ferreira Filho, C.F., 2001. The chromite deposits of the Bacuri mafic-ultramafic layered complex, Guyana shield, Amapá State, Brazil. Econ. Geol. 96, 817-835.

Stowe, C.W., 1994. Compositions and tectonic settings of chromite deposits through time. Econ. Geol. 89, 528–546.

Teixeira, J.B.G., Eggler, D.H., 1994. Petrology, Geochemistry, and Tectonic Setting of Archaean Basaltic and Dioritic Rocks from the N4 Iron Deposit, Serra dos Carajás, Pará, Brazil. Acta Geologica Leopoldensia 17, 71-114.

Teixeira, A.S., Ferreira Filho, C.F., Giustina, M.E.S.D., Araujo, S.M., Silva, H.H.A.B., 2015. Geology, petrology and geochronology of the Lago Grande layered complex: Evidence for a PGE-mineralized magmatic suite in the Carajás Mineral Province, Brazil. J. South Am. Earth Sci. 64, 116-138.

Vasquez, M.L., Carvalho, J.M.A., Sousa, C.S., Ricci, P.S.F., Macambira, E.M.B., Costa, L.T.R., 2008. Mapa Geológico do Pará em SIG. Brazilian Geological Survey - CPRM.

Villas, R.N., Santos, M.D., 2001. Gold deposits of the Carajás Mineral Province: deposit types and metallogenesis. Mineral. Deposita 36, 300-331.

Voordouw, R., Gutzmer, J., Beukes, N.J., 2009. Intrusive origin for Upper Group (UG1, UG2) stratiform chromitite seams in the Dwars River area, Bushveld Complex, South Africa. Mineral. Petrol. 97, 75-94.

CAPÍTULO 3

The Luanga deposit, Carajás Mineral Province, Brazil: different styles of PGE mineralization hosted in a medium-size layered intrusion

The Luanga deposit, Carajás Mineral Province, Brazil: different styles of PGE mineralization hosted in a medium-size layered intrusion

Eduardo T. Mansur[1], Cesar F. Ferreira Filho[1], Denisson P.L. Oliveira[2]

[1] Instituto de Geociências, Universidade de Brasília, Brasília-DF, 70910-900, Brazil.

[2] VALE S/A, Av. Getulio Vargas, 671/13º, 30112-020, Belo Horizonte, MG, Brazil

Abstract

The Luanga Complex, located in the eastern portion of the Carajás Mineral Province, hosts the largest Brazilian PGE deposit. The deposit is hosted by a sequence of layered ultramafic and mafic cumulates and has two distinct styles of PGE mineralization. The first, ascribed as Sulfide Zone, consists of a 10 – 50 m thick interval with disseminated sulfides located along the contact of the Ultramafic and Transition Zones of the intrusion. The mineralogy of the Sulfide Zone consists of base metal sulfides with pentlandite > pyrrhotite > >> chalcopyrite. The other PGE mineralization, ascribed as silicate-related PGE, consists of 2-10 m thick stratabound zones across the Transition Zone. These sulfide- and chromite-free rocks, mainly harzburgite and orthopyroxenite, do not show any distinctive texture or change in modal composition that characterize the PGE enrichment. The Sulfide Zone hosts the bulk of PGE resources of the Luanga Complex (i.e., 142 Mt at 1.24 ppm Pt+Pd+Au and 0.11% Ni). The Sulfide Zone and silicate-related PGE show differences in geochemistry behavior of PGE. The Sulfide Zone has Pt/Pd ratios of 0.55 and a positive correlation between all PGE and S. The silicate-related PGE has Pt/Pd ratios of 1.2-1.3 and a strong depletion in IPGE. A remarkable feature is the occurrence of anomalously Ni-rich olivines (up to 7400 ppm Ni) in harzburgites closely associated with silicate-related PGE mineralization. The geochemical and textural differences between these mineralization styles suggest that they were formed by distinct geological processes. Our results supports that the Sulfide-Zone is formed by typical segregation of a sulfide immiscible liquid during fractional

crystallization. However, silicate-related PGE is formed by direct crystallization of platinum group minerals directly from the magma, in response to PGE saturation of the magma.

Keywords: PGE; nickel; layered intrusion; magmatic sulfide; Carajás

3.1 – Introduction

Most of the platinum-group elements (PGE) deposits are hosted by a small number of layered intrusions (Cawthorn et al., 2005 and references therein). These deposits can be generally subdivided into sulfide- and chromite-related, as exemplified by the well-studied world-class PGE deposits of the Merensky reef and UG2 chromitite, from the Bushveld Complex (e.g., Barnes and Maier, 2002; Cawthorn et al., 2002 and 2005; Naldrett, 2004). The concentration of PGE global resources within just a few intrusions probably reflects the extremely efficient processes involved during the formation of PGE deposits (i.e., PGE enrichment in orders of 10^5; Mungal and Naldrett, 2008). The common processes that lead to PGE concentration within sulfide-related (Naldrett, 2004 and references therein; Mungal and Naldrett, 2008) and chromite-related deposits (Finnigan et al., 2008) are considered sufficiently efficient. Anyways, the discussion about alternative processes that lead to PGE accumulation, apart from chromite- and/or sulfide-bearing rocks, and their implications for the exploration of these elements is still open.

Apart from the processes that lead to PGE accumulation, the existence or not of PGE-fertile suites worldwide is still a debated issue. Some authors proposed that LIP containing Ni-Cu-PGE deposits are formed by magmas with distinctive geochemical compositions (e.g., Maier and Groves, 2011; Griffin et al., 2013), while others indicate that a systematic association of unusual magmas and magmatic deposits are not supported by current data (e.g., Fiorentini et al., 2010; Barnes et al., 2015a). The Luanga Complex is part of a cluster of PGE-mineralized layered intrusions at the eastern part of the Carajás Mineral Province (Mansur and Ferreira Filho, 2016). Hence, a discussion about the existence, or not, of a PGE-fertile suite within this region is supported by our results.

This study provides the first systematic geological and geochemical characterization of the PGE deposit of the Luanga Complex. Our results provide evidence for different styles of PGE mineralization (i.e., sulfide- and silicate-related PGE mineralization) within this layered intrusion. These results support a discussion about efficient processes able to concentrate PGE, apart from the conventional sulfide- and/or chromite-related. Additionally, our data fits into the ongoing discussion of the existence of PGE-fertile suites, especially within the Carajás Mineral Province.

3.2 - Regional Setting

3.2.1 - The Carajás Mineral Province

The Carajás Mineral Province is located in the southeastern portion of the Amazonian Craton (Fig. 3.1A). It has become widely known due to several important mineral deposits, including several IOCG and Ni world-class deposits and the largest iron resources of the world (Dardenne and Schobbenhaus, 2001; Klein and Ladeira, 2002; Lobato et al., 2005; Xavier et al., 2010). The Carajás Mineral Province also hosts the world-class Au-Pd deposit of Serra Pelada (Meireles and Silva, 1988; Berni et al., 2014). The province is subdivided in two Archean tectonic domains, separated by a poorly defined Transition Subdomain (Dall'Agnol et al., 2006; Feio et al., 2013). These domains are defined as the Rio Maria Domain to the South and the Carajás Domain to the north (Fig. 3.1B; Vasquez et al., 2008).

The Rio Maria Domain is a typical granite–greenstone terrain (Vasquez et al., 2008). The Andorinhas Supergroup (Docegeo, 1988) comprises several individual Mesoarchean greenstone belts (2,904 ± 29 Ma; Macambira and Lancelot, 1996) and metasedimentary rocks (Huhn et al., 1986; Souza and Dall'Agnol, 1996; Souza et al, 2001). The recent characterization of spinifex-textured komatiites in a greenstone belt sequence within the Transition Subdomain (Siepierski and Ferreira Filho, 2016), suggests that the Andorinhas Supergroup extends further north than indicated in previous regional maps.

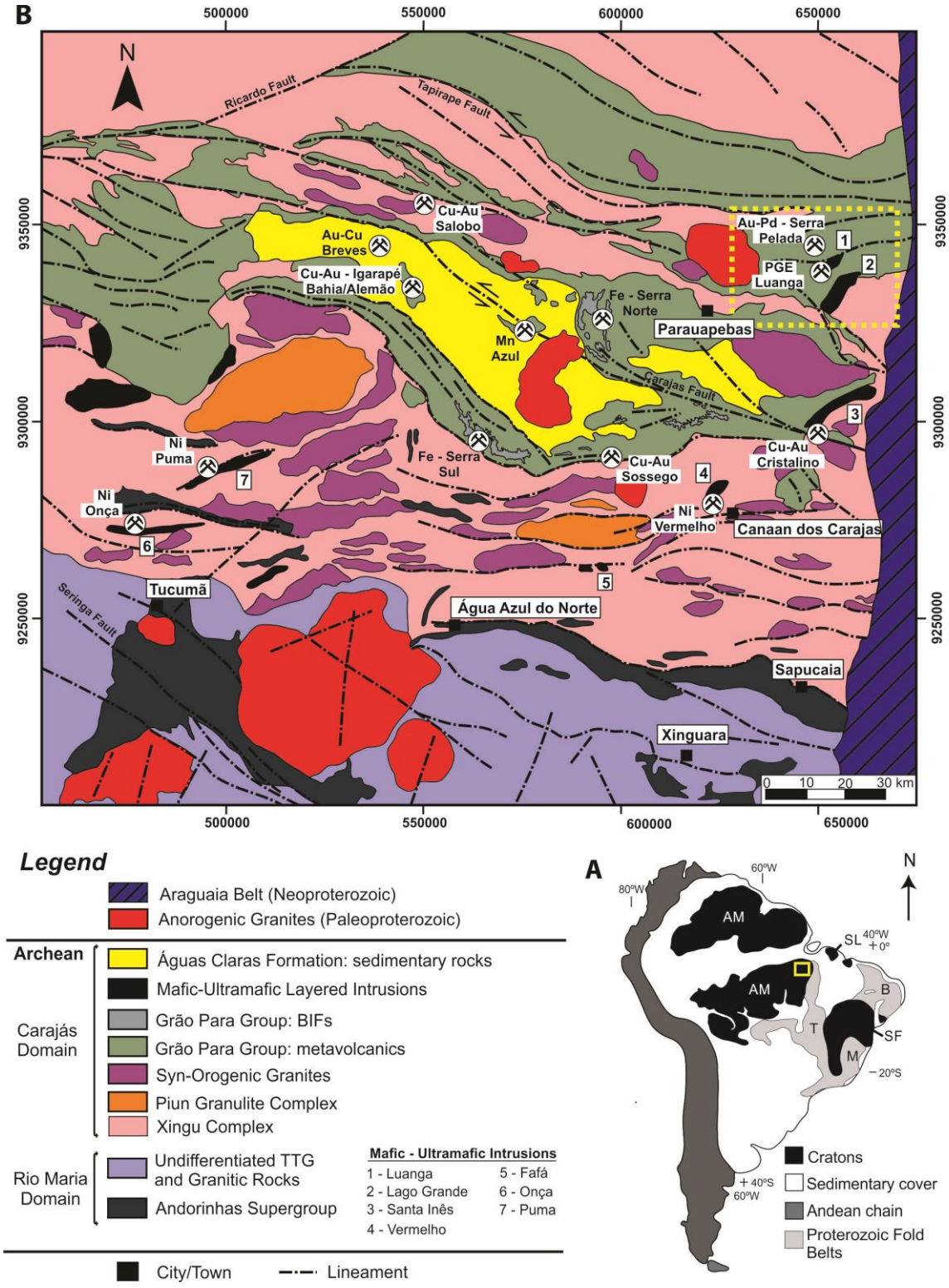

Fig. 3.1: Geological setting. A) Location of the Carajás Mineral Province. AM - Amazonic Craton; B – Borborema Province; M – Mantiqueira Province; SF – São Francisco Craton; T – Tocantins Province. B) Geological map of the Carajás Mineral Province (modified from Vasquez et al., 2008). The dashed rectangle indicates the location of the Serra Leste magmatic suite.

The basement of the Carajás Domain consists mainly of gneiss-migmatite-granulite terrains, generally related to the Xingu Complex (Docegeo, 1988; Machado et al., 1991; Pidgeon et al., 2000). This Domain comprises Archean volcano-sedimentary sequences, which includes the large sequence of metabasalts of the Grão Pará Group (ca. 2.75 Ga; Machado et al., 1991; Vasquez et al., 2008) and several mafic-ultramafic layered intrusions (Docegeo, 1988; Ferreira Filho et al., 2007; Teixeira et al., 2015). Different models have been proposed to explain the origin of these rocks, such as an intra-plate rift model (Gibbs et al., 1986; Villas and Santos, 2001) and also the evolution of a subduction-related environment (Dardenne et al., 1988; Teixeira and Eggler, 1994). These volcano-sedimentary sequences are covered by clastic sedimentary rocks from the Águas Claras Formation (i.e., Rio Fresco Group; Docegeo, 1988; Araújo et al., 1988; Nogueira et al., 1994 and 2000).

3.2.2 - Mafic-ultramafic intrusions and associated mineral deposits of the Carajás Mineral Province

Several mafic-ultramafic layered complexes intrude rocks of the Xingu Complex and Archean volcano-sedimentary sequences (Docegeo, 1988; Ferreira Filho et al., 2007). These intrusions include, among many others, the Serra da Onça and Serra do Puma Complexes (Ferreira Filho et al., 2007; Rosa, 2014) that host large Ni laterite deposits in the western portion of the Carajás Mineral Province, and the Vermelho Complex (Siepierski, 2016) that also host Ni laterite deposit in the Canaan dos Carajás region (Fig. 3.1). The PGE-mineralized layered intrusions of the eastern portion of the Carajás Mineral Province, at the Parauapebas region, include the Luanga and Lago Grande Complexes (Fig. 3.1; Ferreira Filho et al., 2007; Teixeira et al., 2015; Mansur and Ferreira Filho, 2016). Layered intrusions in the Carajás Mineral Province show significant differences in magmatic structures and petrological evolution, thus suggesting that they belong to different Neoarchean magmatic suites (e.g., Ferreira Filho et al., 2007; Rosa, 2014; Teixeira et al., 2015).

The Serra Leste Magmatic Suite (Ferreira Filho et al., 2007) consists of a cluster of small- to medium-size layered mafic-ultramafic intrusions located in the northeastern portion of the Carajás Mineral Province (Fig. 3.1). This suite was originally grouped based on abundant PGE anomalies of the layered intrusions, disregarding any geological, stratigraphic or petrological consideration (Ferreira Filho et al., 2007). Recent studies of the Lago Grande Complex (Teixeira et al., 2015) and Luanga

Complex (Mansur and Ferreira Filho, 2016) are the first systematic stratigraphic and petrological investigations of layered intrusions ascribed to the Serra Leste suite, thus providing data for the composition of their parental magmas and fractionation processes. The Luanga Complex, subject of this study, hosts the bulk of the PGE resources in the Serra Leste region.

3.2.3 – Luanga Complex

The Luanga Complex is a 6 km long and up to 3.5 km wide layered intrusion (Fig. 3.2A) consisting of, from base to top, ultramafic cumulates (Ultramafic Zone), an intercalation of ultramafic and mafic cumulates (Transition Zone) and mafic cumulates (Mafic Zone; Fig. 3.2B; Mansur and Ferreira Filho, 2016). Geological section defined by drilling indicate that the Ultramafic Zone overlies the Transition Zone, which overlies the Mafic Zone, suggesting thus that the layered sequence is tectonically overturned (Fig. 3.2B; Ferreira Filho et al., 2007; Mansur and Ferreira Filho, 2016). The Ultramafic Zone comprises an up to 800 m-thick sequence of serpentinites (i.e., metamorphosed peridotite) with few meters thick orthopyroxenite lenses at the upper portions. The Transition Zone consists of an up to 800 m pile of interlayered ultramafic and mafic cumulate rocks. Interlayering in the Transitin Zone consists of orthopyroxenite, harzburgite and norite in different scale and variable textures. The Mafic Zone consists of an up to 2000 meters-thick monotonous sequence of noritic rocks and minor interlayered orthopyroxenite with subordinated chromitite (Mansur and Ferreira Filho, 2016).

PGE mineralization occurs associated with base metal sulfides between the Ultramafic and Transition Zones (Ferreira Filho et al., 2007) and associated with chromitite layers along the Transition Zone (Diella et al., 1995). A systematic description of different styles of PGE mineralization in the Luanga Complex is presented in this study.

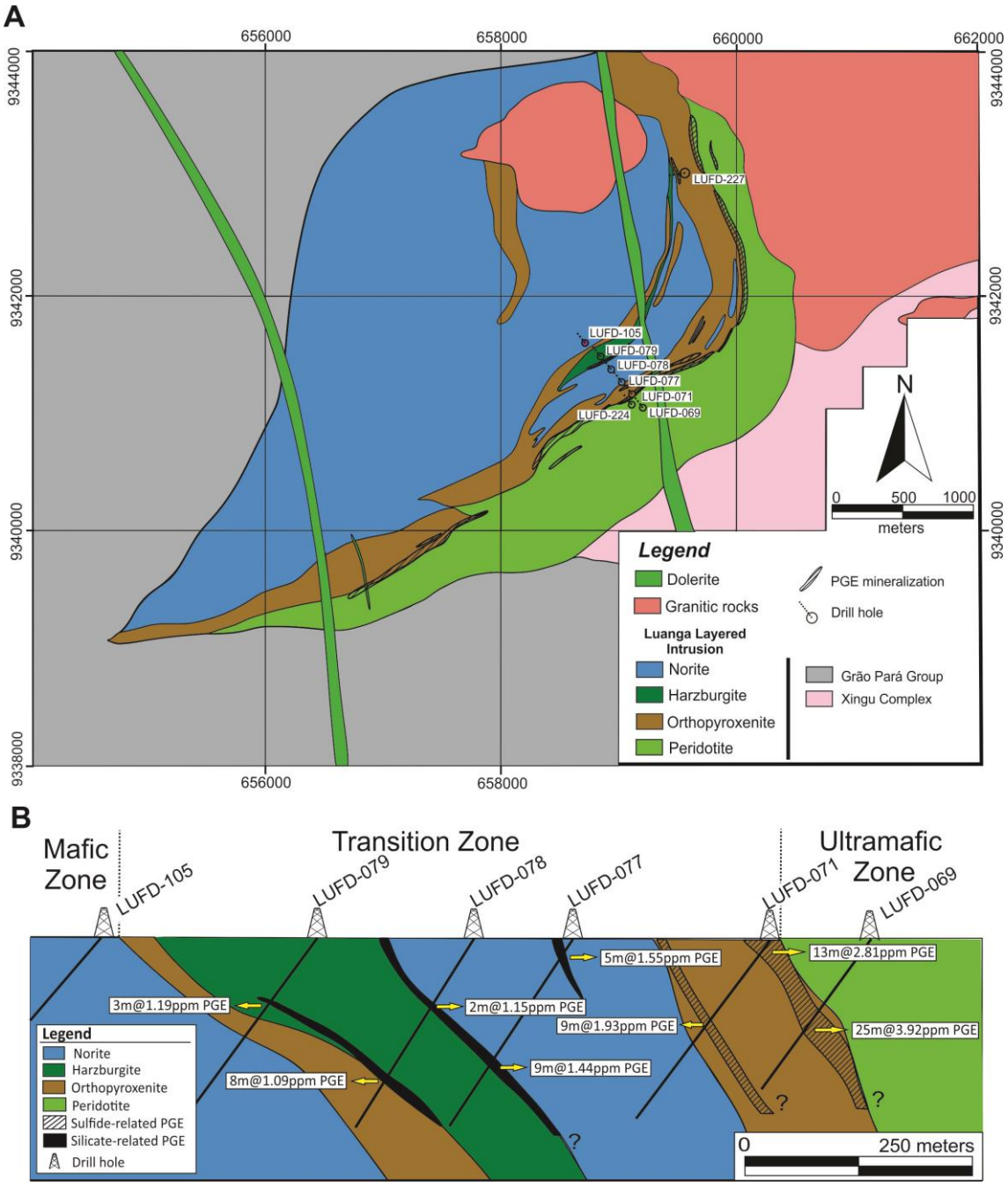

Fig. 3.2: Local geology. A) Geological map of the Luanga Complex (partially modified from unpublished report of VALE). Note the location of drill holes referred to in this study. B) Geological section on the central portion of the layered complex. PGE mineralized intervals are indicated (partially modified from Mansur and Ferreira Filho, 2016).

3.3 – Exploration Review

Mafic-ultramafic rocks and chromitites of the Luanga Complex were identified in 1983 during regional exploration developed by DOCEGEO (now VALE S.A.) in the Serra Leste region. Following the discovery of up to 2-m thick chromitites, DOCEGEO

carried out geological mapping, soil geochemistry survey (400 m x 40 m grid) and ground magnetometric survey in the Luanga Complex. Four diamond bore holes were drilled to test the thickness and lateral continuity of outcropping chromitites. The drilling was not positive for chromite mineralization, but intersected anomalous concentrations of Pt and Pd, including 9 meters at 2.57 ppm of Pt+Pd (i.e., drill core LUFD-04). In 1997, a joint-venture DOCEGEO-Barrick Gold carried out a stream sediment campaign over the Luanga Complex area that identified Au anomalies (up to 3,061 ppb). In 2000, Vale S.A., aiming to increase the Au resources of the Serra Leste Au Project (which included VALE's Serra Pelada deposit), carried out a new soil geochemistry survey to test the Au anomalies indicated by Barrick Gold. The sampling grid, covering the southern portion of Luanga Complex, indicated a 1 km long trend of Pt and Pd anomalies. Due to his anomalous trend with up to 1,450 ppb of Pt+Pd, Vale S.A. carried out in 2000 additional soil geochemistry survey in the northern portion of the Luanga Complex (next to chromitite layers). This sampling indicated another 1 km long Pd and Pt anomalous trend with up to 804 ppb of Pt+Pd, The geochemical survey was extended to the central portion of the layered complex and indicated a 2 km extension trend of Pt and Pd anomalies with up to 1,436 ppb of Pt+Pd, providing a continuous Pt-Pd-Cu anomalous trend along the entire layered intrusion. In 2001, Vale S.A. started an exploration program for PGE in the Serra Leste region. Systematic geological and structural mapping using RADARSAT and TM5 integrated data, along with airborne geophysical survey, led to the discovery of several layered intrusions (e.g., Formiga, Lago Grande, Luanga Norte, Pegasus, Órion, Afrodite). From 2001 to 2007 Vale S.A performed 79,335 meters of diamond drilling and several ore technology characterization tests in layered intrusions of the Serra Leste region. The resource drilling program in the Luanga Complex reached 45,174 meters of diamond drilling. The systematic evaluation indicated that the Luanga Complex hosts a PGE deposit with resources of 142 Mt@ 1.24g/t PGE+Au and 0.11% Ni, for a given cut-off grade of 0.5 g/t PGE+Au. These resources were evaluated for a shallow (i.e., aproximatelly 250 meters deep) open pit.

3.4 - Sampling and Analytical Procedures

For this study, drill holes from the central and northern portions of the Luanga Complex (Figs. 3.2A and 3.2B) were systematically sampled in order to select unweathered rocks. The sampling was supported by litogeochemical data of VALE's

exploration database. Thin polished sections of the selected samples were studied in detail at the microscopy laboratory at University of Brasília. The analytical procedures are described as follows.

3.4.1 - Bulk Rock analyses

For litogeochemical analyses, two representative drill holes that intersect different styles of mineralization (LUFD-224 and LUFD-226; Fig. 3.2B) were selected. Sample preparation and lithogeochemical analyses were performed at ALS Chemex (Canada). Analytical procedures include the whole-rock package plus LOI (ALS Chemex codes: ME-XRF06 and OA-GRA06), total S (ALS Chemex codes: S-IR08), PGE nickel sulfide collection plus Pt, Pd, Au 30g fire assay ICP (ALS Chemex codes: PGM-MS26 and PGM-ICP23) and the 48 elements four acid ICP-MS package (ALS Chemex code: ME-MS61). A complete description of analytical methods is available in the ALS Chemex Home Page (www.alsglobal.com).

3.4.2 - Sm-Nd isotopes

Sm-Nd isotopic analyses followed the method described by Gioia and Pimentel (2000) and were carried out at the Geochronology Laboratory of the University of Brasília (UnB). Whole-rock powders (~3000 mg) were mixed with ^{149}Sm-^{150}Nd spike solution and dissolved in Savillex bombs. Sm and Nd extraction of whole-rock samples followed conventional cation exchange techniques. The isotopic measurements were carried out on a multi-collector Finnigan MAT 262 mass spectrometer in static mode. The $^{143}Nd/^{144}Nd$ ratios were normalized to $^{146}Nd/^{144}Nd$ of 0.7219 and the decay constant used was $6.54 \times 10\text{-}12^{-1}$. The TDM values were calculated using the model of DePaolo (1981). Nd procedure blanks were better than 100 pg. Sm-Nd results for 9 samples of the Luanga Complex are shown in Table 3.1.

3.4.3 – Sulfur isotopes

Sulfur isotopic analyses were carried out at the Geochronology Laboratory of the University of Brasília (UnB) and followed an internal methodology. Approximately 2000µg of sulfide grain powders were enclosed within tin capsules by the automatic sampler Thermo Scientific MAS 200R and introduced at the Thermo Scientific Flash 2000 element analyzer. The sample is heated up to 1800ºC by an automatic addition of oxygen and the combustion products are carried out by helium gas. The SO_2 is separated by a chromatographic column and then sent to the ion fount of the Thermo

Scientific MAT253 IRMS mass spectrometer. After the ionization and acceleration of the sample, gas species with different masses are separated and analysed by faraday cup collectors. The spectrometer is monitored and the obtained results are treated using the software Isodat 3.0.

3.5 - Geology of the Transition Zone and PGE Mineralizations

The Transition Zone of the Luanga Complex (Figs. 3.2 and 3.3) hosts several PGE mineralized intervals (Fig. 3.2B). The following description of the Transition Zone, based on Mansur and Ferreira Filho (2016), aims to provide the stratigraphic setting of the mineralized intervals.

The Transition Zone, about 5 km long and up to 1 km wide, represents the central part of the Luanga Complex (Fig. 3.2A) and comprises a pile of interlayered ultramafic and mafic cumulate rocks (Fig. 3.3). Interlayering of different rocks types occurs in different scales (from few centimeters to dozens of meters), and is a distinctive feature of the Transition Zone. Cumulate rocks have variable textures, from adcumulate to orthocumulate, and variable assemblages of cumulus and intercumulus minerals, resulting in several different rocks types (Fig. 3.3). The most common rock types are orthopyroxenite (orthopyroxene adcumulate), harzburgite (olivine + chromite cumulate with either cumulus or intercumulus orthopyroxene), norite (orthopyroxene + plagioclase cumulate) and chromitite. The stratigraphic division presented in figure 3 is simplified from a complex rock succession and illustrates the main cumulates from the Transition Zone.

Orthopyroxenite (Figs. 3.3A and 3.3C) is a medium- to coarse-grained rock with tabular crystals of orthopyroxene as cumulus mineral. The texture varies from adcumulate to meso- and orthocumulate with plagioclase as the predominant intercumulus mineral (Fig. 3.3C). Harzburgite (Fig. 3.3C) is a medium- to coarse-grained olivine + chromite cumulate with meso- to orthocumululate textures. The contact between orthopyroxenite and harzburgite in the Transition Zone is commonly abrupt (Fig. 3.3C). Norite is a medium-grained orthopyroxene and plagioclase adcumulate rock (Fig. 3.3B). It occurs as discontinuous layers commonly following a gradational upward fractionation from orthopyroxenite, to plagioclase orthopyroxenite and norite.

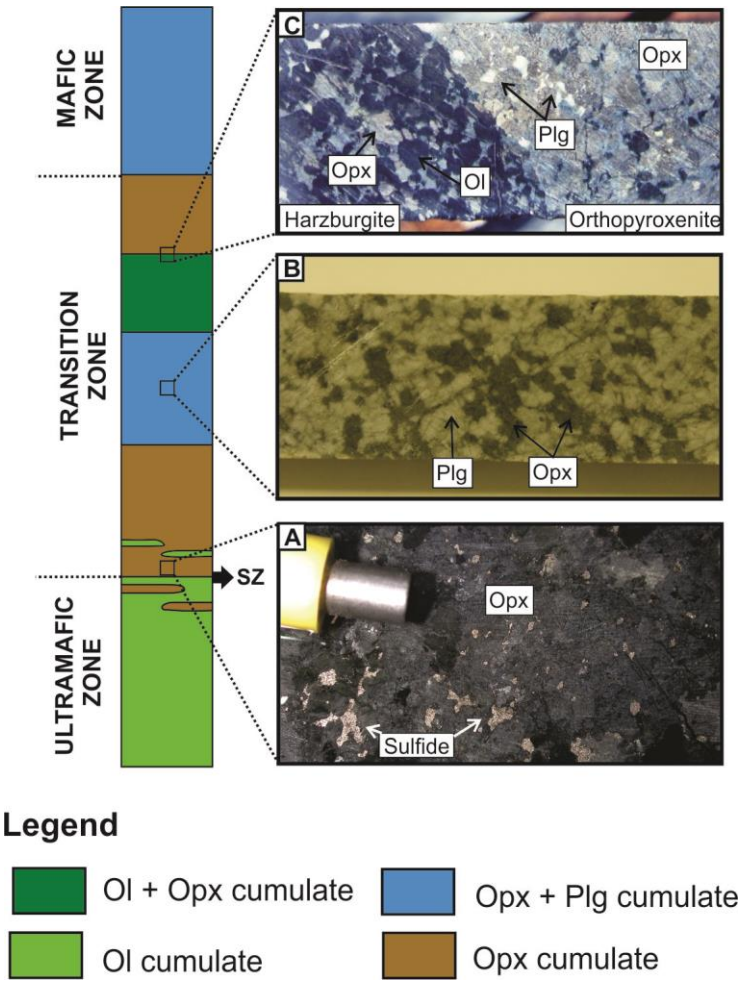

Fig. 3.3: Simplified stratigraphic column for the Luanga Complex. A) Representative core sample of the Sulfide Zone. Medium-grained orthopyroxenite with interstitial base metal sulfides. B) Representative core sample of norite from the Transition Zone. Adcumulate textured norite consisting of orthopyroxene (dark brownish color) and plagioclase (white color). C) Core sample showing a sharp contact of orthopyronenite and harzburgite. Orthopyroxenite consists of cumulus orthopyroxene with minor intercumulus plagioclase, while harzburgite consists of cumulus olivine with intercumulus orthopyroxene. Ol: olivine; Opx: orthopyroxene; Plg: Plagioclase.

Several chromitites occur at the top of the Transition Zone and at the lower part of the Mafic Zone (Diella et al., 1995; Ferreira Filho et al, 2007; Mansur and Ferreira Filho, 2016). These rocks consist of fine-grained euhedral cumulus chromite with variable proportions of interstitial minerals (mainly extensively replaced plagioclase). A systematic description of chromitites throughout the stratigraphy of the Luanga Complex is provided by Mansur and Ferreira Filho (submitted) and they are not addressed in this study.

Apart from PGE mineralization hosted in chromitites (Diella et al., 1995; Ferreira Filho et al., 2007), two distinct styles of PGE mineralization that occur in the Luanga Complex are detailed in this study: i) sulfide-related PGE mineralization and ii) silicate-related PGE mineralization (Fig. 3.2B).

3.5.1 - Sulfide-related PGE

PGE mineralization associated with disseminated sulfides hosts the bulk of PGE resources of the Luanga Complex (i.e., 142 Mt at 1.24 ppm Pt+Pd+Au and 0.11% Ni; VALE internal reports). The stratigraphic section hosting the PGE deposit, referred to as the Sulfide Zone (Mansur and Ferreira Filho, 2016), consists of a 10 – 50 m thick interval with disseminated sulfides located along the contact of the Ultramafic and Transition Zones (Figs. 3.2B and 3.3A). The primary mineralogy of the hosting rocks is commonly replaced by metamorphic assemblages. This metamorphic alteration is heterogeneous and characterized by an extensive hydration that largely preserves primary textures (Fig. 3.3) and the compositional domains of igneous minerals (Ferreira Filho et al., 2007; Mansur and Ferreira Filho, 2016).

The Sulfide Zone is a stratabound PGE mineralization consisting of interstitial sulfides (~ 1-3–vol. %) hosted by variably metamorphically altered orthopyroxenite (Fig. 3.3A) and peridotite (Fig. 3.4A). The location of the Sulfide Zone along the contact zone is variable, such that sulfides may be hosted just by the lowermost orthopyroxenite of the Transition Zone, or encompass both the orthopyroxenite and the underlying peridotite of the Ultramafic Zone (Fig. 3.3A). The mineralogy of the Sulfide Zone does not show major variation through the deposit and consists of base metal sulfides with pentlandite > pyrrhotite > >> chalcopyrite (Fig. 3.4B). Magnetite is commonly developed at the outer border or along fractures in sulfide blebs (Fig. 3.4C). Both magnetite and rare pyrite crystals (Fig. 3.4D) occur in partially altered sulfide aggregates. Chalcopyrite is not abundant (< 10 vol% of the sulfides) and commonly occurs as fine-grained crystals at the borders of larger pentlandite and/or pyrrhotite crystals (Fig. 3.4E). Additionally, thin lamellar chalcopyrite occurs enclosed within pentlandite crystals (Fig. 3.4F). The metamorphic transformation of primary igneous silicates of the hosting rocks (Mansur and Ferreira Filho, 2016) does not seem to significantly modify the sulfide mineralogy.

The occurrence of sulfide minerals is not restricted to the Sulfide Zone. Minor sulfide veinlets occur in thin (up to 8 m thick) discontinuous shear zones located along

the Luanga Complex. Sulfides in these zones have distinct texture and mineralogy described for the Sulfide Zone, showing typically intergrowth with amphibole and predominantly composed by chalcopyrite. These occurrences are ascribed as hydrothermal sulfides.

3.5.2 - Silicate-related PGE

The term silicate-related PGE is used in this study to indicate PGE-mineralized rocks devoid of base metal sulfides and/or chromite. The silicate-related PGE mineralization of the Luanga Complex consists of 2-10 m thick stratabound zones across the Transion Zone. These zones occur above the Sulfide Zone and do not show extensive lateral continuity (Fig. 3.2B). These silicate-related PGE zones commonly occur at the contact between layers of distinct cumulate rocks in the Transition Zone (Figs. 3.2B and 3.3C), but its occurrence within one rock type is also observed (e.g., norite layer intersected by drill hole LUFD-077; Fig. 3.2B). The hosting rocks, mainly harzburgite and orthopyroxenite, do not show any distinctive texture or change in modal composition that characterize the PGE enrichment (Figs. 3.4G and 3.4H). In this way, the PGE enriched intervals were not identified during core logging or routine petrographic studies. These PGE-anomalous intervals were just indicated by their anomalous Pt-Pd contents. A remarkable feature is the occurrence of anomalously Ni-rich olivines (up to 7400 ppm Ni; Mansur and Ferreira Filho, 2016) in harzburgites closely associated with silicate-related PGE mineralization.

3.6 - Litogeochemistry of PGE Mineralizations

Two representative drill holes (LUFD-224 and LUFD-227; Fig. 3.2) were investigated in detail for a systematic characterization of different styles of PGE mineralization of the Luanga Complex.

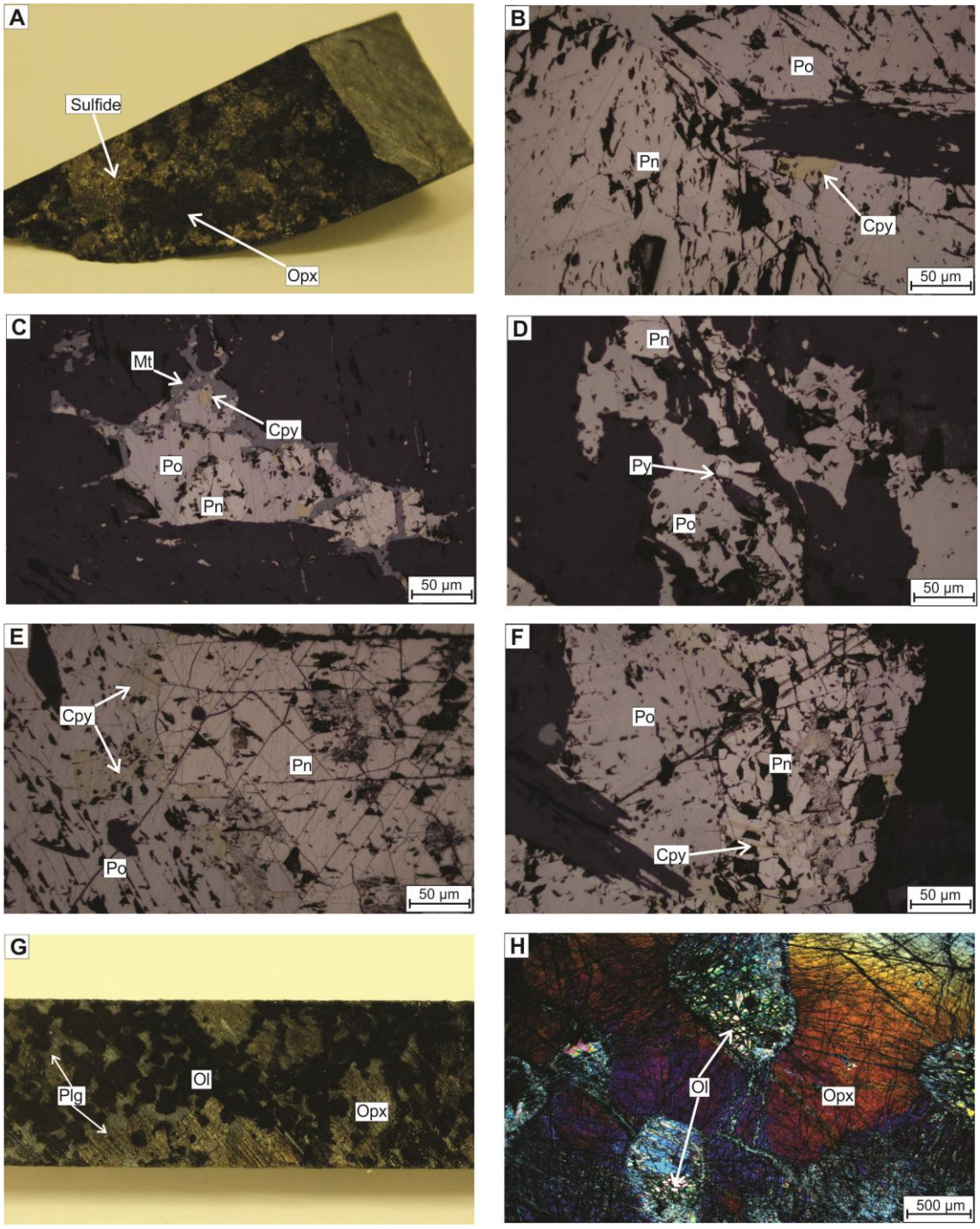

Fig. 3.4: General aspects of the PGE-bearing rocks of the Luanga Complex. A) Core sample of orthopyroxenite from the Sulfide Zone with cumulus orthopyroxene and interstitial base metal sulfides. B) Photomicrograph (reflected light) of typical sulfide assemblage of the Sulfide Zone with pentlandite > pyrrhotite >>> chalcopyrite. C) Photomicrograph (reflected light) of typical intertitial base metal sulfides of the Sulfide Zone. Note that sulfides are partially replaced by magnetite with minor remobilization along fractures to host silicates. D) Photomicrograph (reflected light) of euhedral fine-grained pyrite crystal enclosed within pyrrhotite grains.

Fig. 3.4 (cont.): E) Photomicrograph (reflected light) of chalcopyrite crystals at the contact between pyrrhotite and pentlandite. F) Photomicrograph (reflected light) of intergrowth between thin chalcopyrite lamellae and pentlandite. G) Typical core sample of harzburgite from the Transition Zone. The harzburgite consists of cumulus olivine and intercumulus orthopyroxene and plagioclase. This rock shows high PGE contents (up to 2 ppm) and no sulfide is observed. H) Photomicrograph (crossed polarizers) of the harzburgite core sample shown in G. Note cumulus olivine crystals enclosed in orthopyroxene oikocryst. Cpy: Chalcopyrite; Mt: Magnetite; Ol: olivine; Opx: orthopyroxene; Pn: Pentlandite; Plg: Plagioclase; Py: Pyrite; Po: Pyrrhotite.

The plot of S vs PGE contents for unweathered samples with PGE contents higher than 500 ppb and/or S contents higher than 0.05 wt.% is shown in Figure 3.5. The correlation of these PGE-enriched (> 500 ppb) and/or sulfide-bearing (> 0.05 wt.%) indicates three geochemically distinct groups: i. sulfide-related PGE, ii. silicate-related PGE and iii. hydrothermal sulfides (Fig. 3.5). The sulfide-related PGE group comprises samples with high PGE and S contents (i.e., up to 7000 ppb and 1 wt.%, respectively). These samples correspond to orthopyroxenites and peridotites with interstitial base metal sulfides from the Sulfide Zone (Fig. 3.3A). The silicate-related PGE group comprises samples with high PGE (i.e., up to 2000 ppb) and very low S contents (< 0.1 wt.%). These samples correspond to orthopyroxenites and harzburgites from the Transition Zone (Fig. 3.3C). Finally, the group referred to as hydrothermal sulfides corresponds to samples with high S contents (up to 0.7 wt.%) with low PGE contents (< 300 ppb. A description of these groups is provided as follows.

3.6.1 - Sulfide-related PGE

The groups referred to as sulfide-related PGE and hydrothermal sulfides include samples with S content higher than 0.1 wt.% (Fig. 3.5). The analyses presented in this section are core samples from drill hole LUFD-224 (Fig. 3.2A), which intersected the Sulfide Zone of the Luanga Complex (Fig. 3.6).

The drill hole LUFD-224 intersects the contact between the Ultramafic and Transition Zones, and consequently the Sulfide Zone (Fig. 3.6). A sharp decrease in MgO and Al_2O_3 contents occurs in the transition, from olivine cumulates with interstitial plagioclase below the Sulfide Zone to overlying orthopyroxene cumulates (Fig. 3.6). Two alteration zones located at the bottom of the drill hole LUFD-224 (i.e., the uppermost portion of the stratigraphic column in Fig. 3.6) consists of partially to extensively sheared rocks.

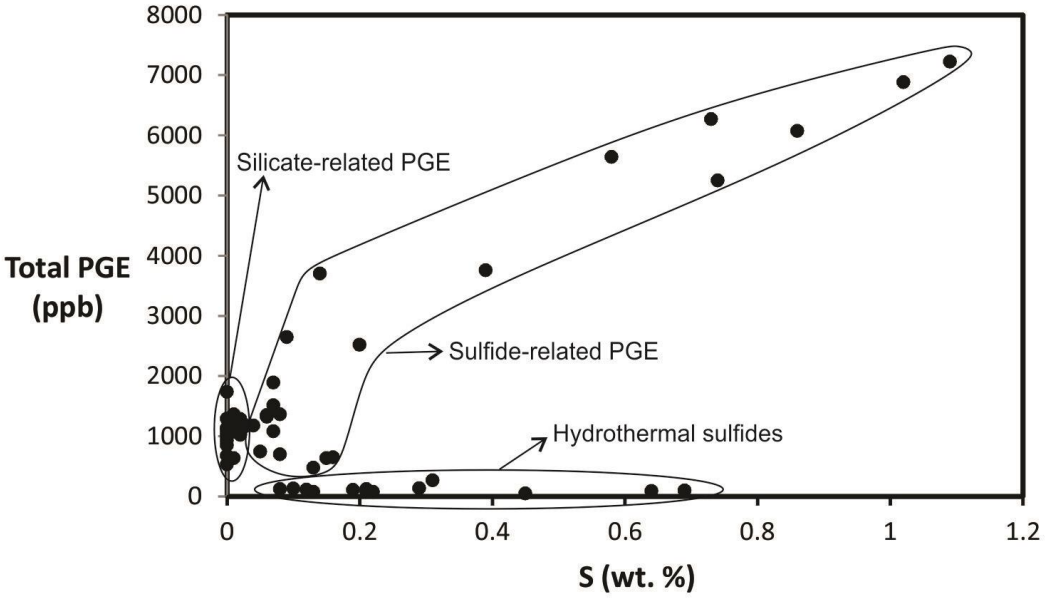

Fig. 3.5: Plot of PGE versus S contents for samples with S and PGE values higher than 500 ppb and 0.01 wt.%, respectively. The samples split into three groups: i. sulfide-related PGE, ii. silicate-related PGE and iii. PGE-depleted sulfides.

These altered intervals (~ 96-112 and 145-162 m in Fig. 3.6) have discrete zones with lower MgO and higher Al_2O_3 and S contents (Fig. 3.6) characterized by abundant amphibole and sulfide veinlets. Except for the weathered rocks, Ni and S show a positive correlation throughout the drill hole LUFD-224, with high Ni contents (> 2500 ppm) limited to the Sulfide Zone (Fig. 3.6). Pt and Pd show positive correlation with S and Ni, but high values are restricted to the Sufide Zone. Hence, samples from the altered intervals above the Sulfide Zone belong to the the hydrothermal sulfides group while samples from the Sulfide Zone belong to the sulfide-related PGE group (Fig. 3.5).

Sulfide-bearing rocks from the Sulfide Zone contain 1-3% of base metal sulfides with pentlandite > pyrrhotite > >> chalcopyrite (Fig. 3.4B). The modal proportion of base metal sulfides in these rocks is consistent with their high Ni tenors (16-18 wt.%; Fig. 3.7A), low Cu tenors (1.3-1.4 wt.%; Fig. 3.7C) and, consequently, high Ni/Cu ratios (10-12; Fig. 3.7B). Samples with meaningful Au contents (i.e. up to 0.25ppm) are restricted to the Sulfide Zone and the Au tenor is around 5 ppm. High PGE contents in drill hole LUFD-224 are restricted to samples from the Sulfide Zone (Fig. 3.6). These samples have strong positive correlation between Pd and S, high Pd tenors (130-140 ppm; Fig. 3.7E), and remarkably consistent Pt/Pd ratios (~ 0.55; Fig. 3.7D). Pt values systematically lower than Pd is a characteristic feature of the Sulfide Zone, with Pt/Pd

consistently lower than 1 along the entire extension of the ore zone. Ru and S also show a positive correlation and Ru tenor is around 2.5 ppm (Fig. 3.7G). These samples show a strong positive correlation between Pd and Ru (Fig. 3.7F), and between Ru and Ir (Fig. 3.7H). The positive correlation between PPGE and IPGE is compatible to the simultaneous segregation of these elements into the immiscible sulfide liquid during magma crystallization.

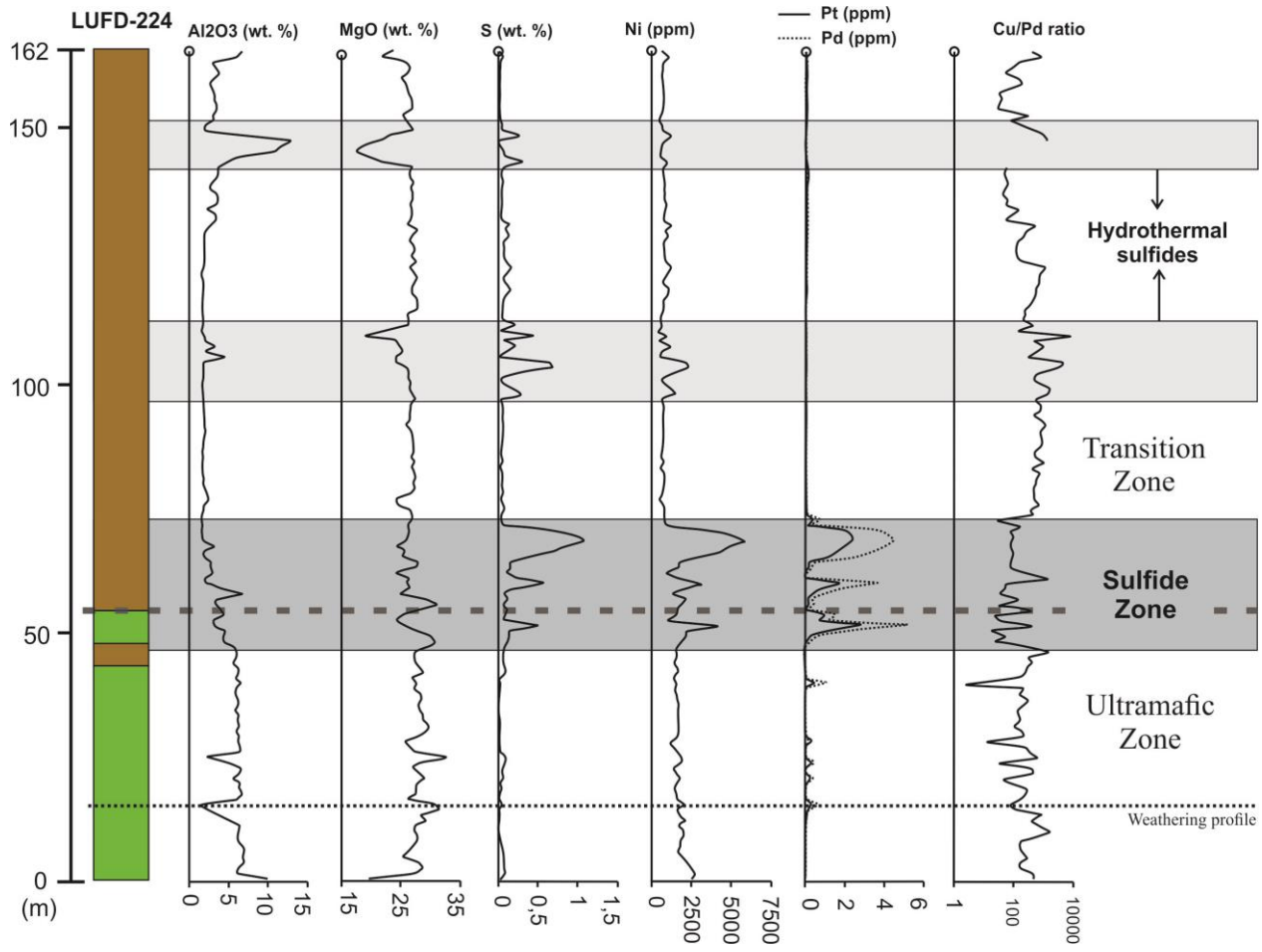

Fig. 3.6: LUFD-224 drill core log and its MgO, Al_2O_3, Ni, Pt, Pd and S assay results and Cu/Pd ratios. The thin dashed black line indicates the lower limit of the weathering profile, while the dashed gray line indicates the contact between the Transition and Mafic Zones. The shadow gray rectangles indicate the Sulfide Zone and hydrothermal sulfides. See Figure 3.2 for the color code of the stratigraphic columnn.

Mantle-normalized patterns (Fig. 3.8) for samples from the Sulfide Zone show high to moderate PGE enrichment (10-1000 times) and minor to moderate Ni, Cu and Co enrichment (2-10 times). The PGE patterns are enriched in Pt, Pd and Rh (i.e., Platinum Group Elements – PPGE) relative to Ir, Ru and Os (i.e., Iridium Group Elements – IPGE). PGE patterns indicate a progressive increase from incompatible

IPGE toward compatible PPGE, as well as a distinctively negative anomaly for Pt and Au (Fig. 3.8).

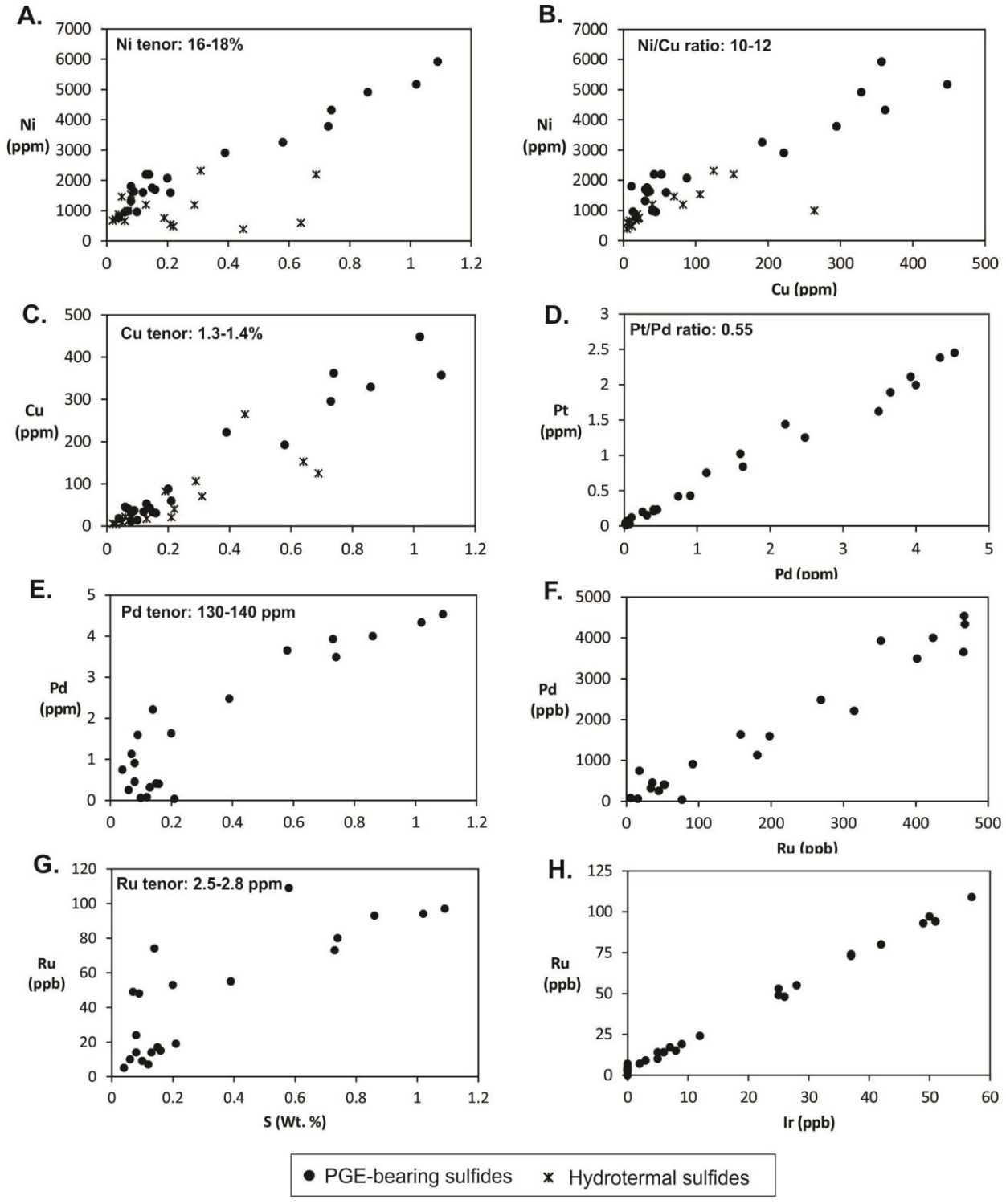

Fig. 3.7: Plots of Ni (a), Cu (c), Pd (e) and Ru (g) vs S, Ni vs Cu (b), Pt vs Pd (d), Pd vs Ru (f) and Ru vs Ir (h) for sulfide-bearing samples from the drill hole LUFD-224. The metal tenors indicated in each plot are calculated based on a linear projection toward 32-35 wt.% total S.

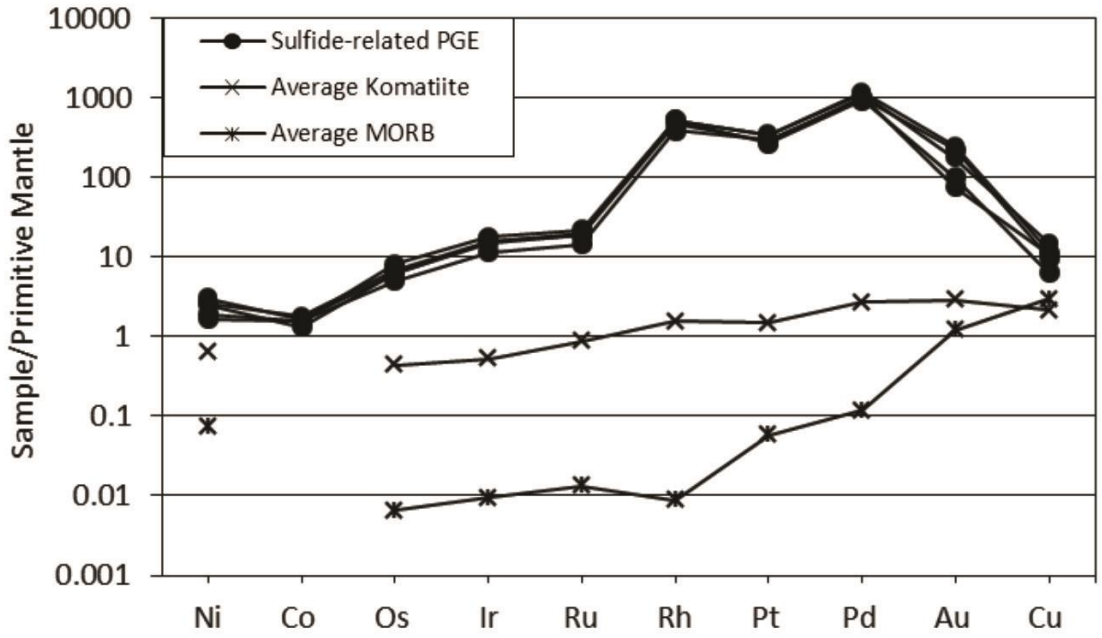

Fig. 3.8: Primitive mantle-normalized chalcophile element profiles for representative samples from the Sulfide Zone. Average komatiite and MORB values are from Crocket (2002). Primitive mantle normalization values are from Sun and McDonough (1989).

3.6.2 - Silicate-related PGE

The group referred to as silicate-related PGE includes samples with PGE contents higher than 500 ppb and very low S contents (Fig. 3.5). The analyses presented in this section are core samples from drill hole LUFD-227 (Fig. 3.2A).

The drill hole LUFD-227 intersected the upper portion of the Transition Zone, comprising mainly orthopyroxenite with minor interlayered harzburgite at the top (Fig. 3.9). The weathering profile is indicated by progressively lower MgO and higher Al_2O_3 contents (Fig. 3.9). The high PGE and S values observed at the top of the drill hole (i.e., the lower portion of the stratigraphic column in Fig. 3.9), partially contained within the weathering profile, consist of samples of the Sulfide Zone at the northern portion of the Luanga Complex (Fig. 3.2A). Samples from the Sulfide Zone in drill hole LUFD-227 are variably weathered and were not considered in the following discussion, aimed to investigate a representative interval of silicate-related PGE mineralization.

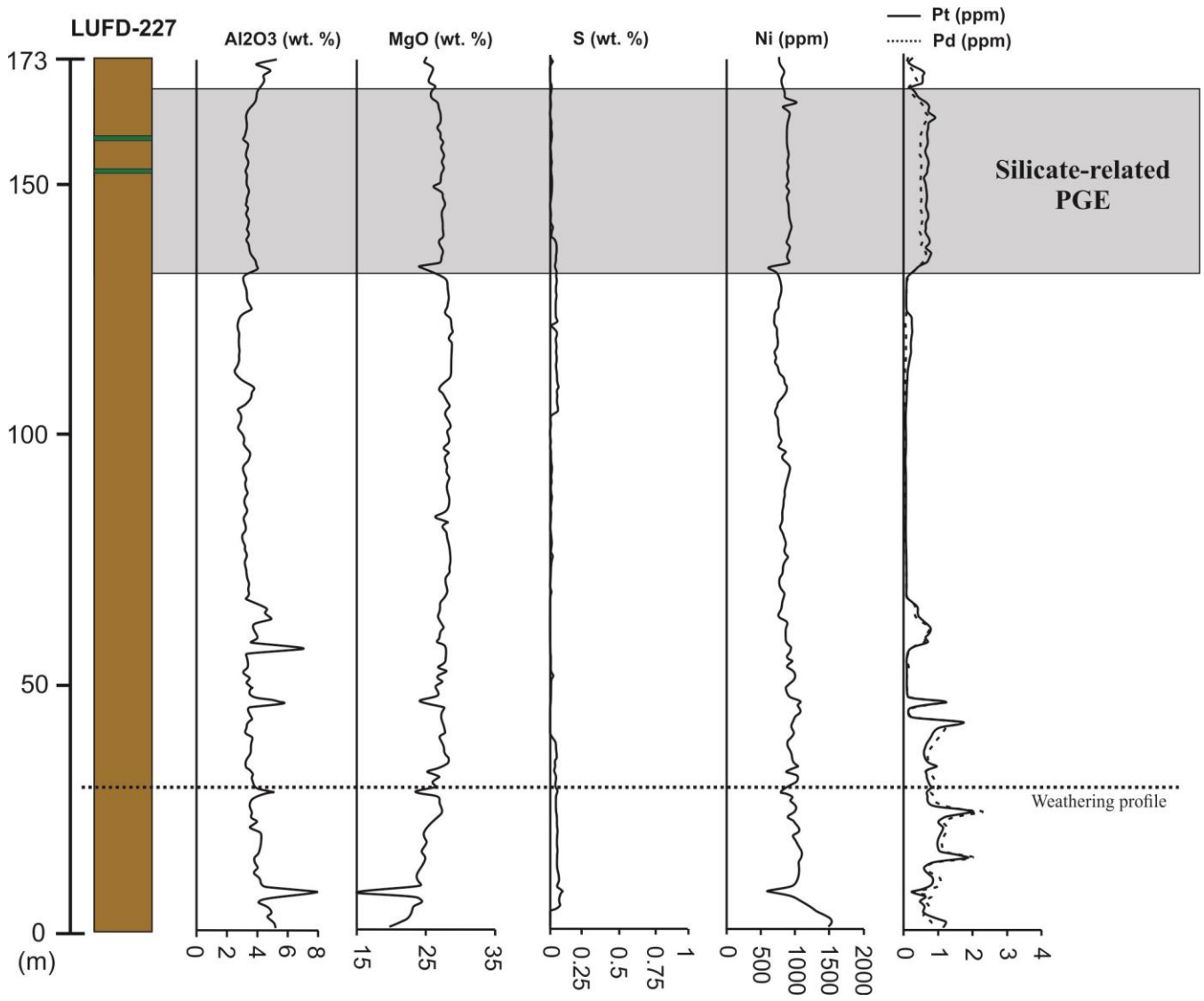

Fig. 3.9: LUFD-227 drill hole log and its MgO, Al_2O_3, Ni, Pt, Pd and S assay results. The thin dashed black line indicates the weathering profile and the shadow gray rectangle indicates the silicate-related PGE mineralized horizon.

Apart from the weathering profile, no significant variation is observed in MgO and Al_2O_3 contents throughout the monotonous sequence of orthopyroxene adcumulates in drill hole LUFD-227 (Fig. 3.9). High Ni values (~ 750-1000 ppm) through the stratigraphy are consistent with Ni contents of 800-1200 ppm in orthopyroxene in the lowermost portion of the Transition Zone reported by Mansur and Ferreira Filho (2016). The reported values for Ni in orthopyroxene of the Transition Zone, together with very low S contents in orthopyroxenite in drill hole LUFD-227 (< 0.1 wt.%), indicate that bulk rock Ni is mainly controlled by silicates. The distribution of Ni also indicates a consistent upward decrease from ~ 1000 ppm above the weathering profile down to ~

750 ppm at the base of the PGE mineralized zone (Fig. 3.9). Following an abrupt increase to ~ 1000 ppm at the base of the PGE mineralized zone, Ni contents remain at values of ~ 1000 ppm in the upper portions of drill hole LUFD-227. High Pt and Pd contents in the silicate-related PGE zone are not correlated with disseminated base metal sulfides and S contents. This PGE-mineralized interval has minor to none sulfides and very low S contents (< 0.1 wt. %). Different from the Sulfide Zone, Pt values are systematically higher than Pd in the silicate-related PGE mineralized interval (Fig. 3.9), with Pt/Pd ratios at 1.2-1.3 values across the entire zone (Fig. 3.10A).

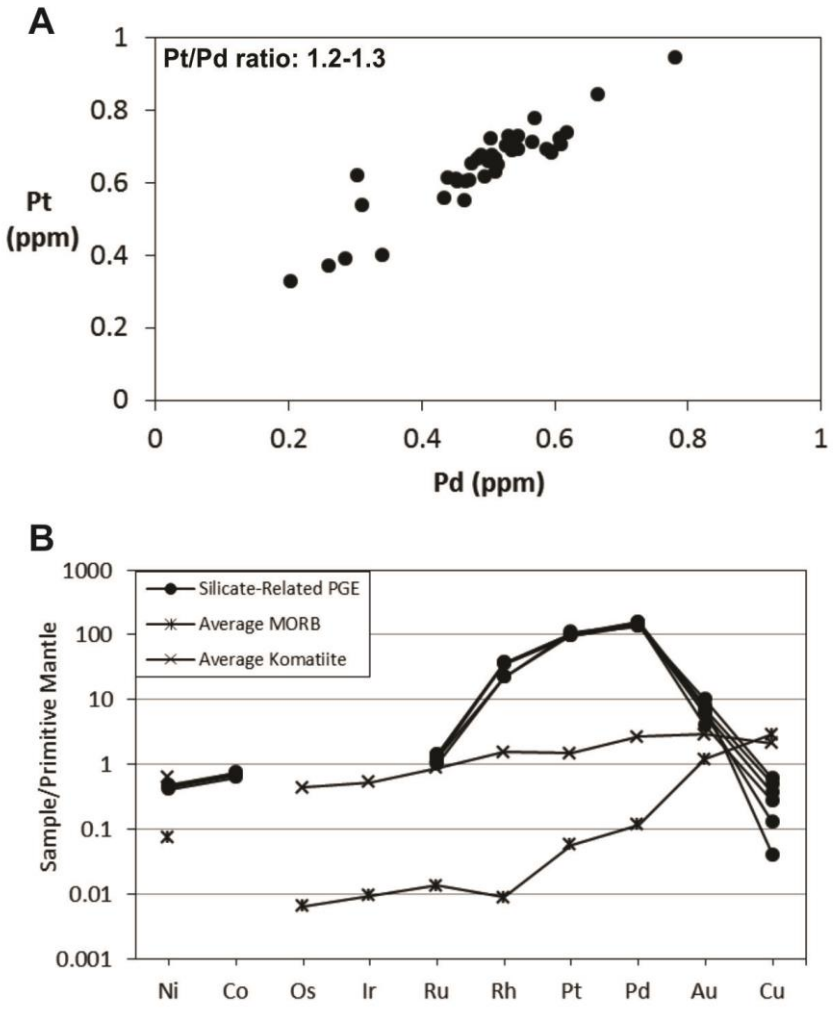

Fig. 3.10: Geochemical analyses of samples from the silicate-related PGE mineralized horizon. A) Plot of Pt vs Pd. B) Primitive mantle-normalized chalcophile element profiles and average Komatiite and MORB values from Crocket (2002). Primitive mantle normalization values are from Sun and McDonough (1989).

Mantle-normalized patterns (Fig. 3.10B) for samples from the silicate-related PGE zone show none to moderate PGE enrichment (1-100 times) and depleted Ni, Cu

and Co contents. The PGE patterns are enriched in PPGE relative to IPGE, with Ir and Os contents below their detection limits, 50 and 30 ppb, respectively. PGE patterns indicate a progressive increase from incompatible IPGE toward compatible PPGE, as well as a distinct negative anomaly for Au (Fig. 3.10B). The low contents of base metals are compatible with the absence of base metal sulfides and low S contents PGE-enriched in this interval.

3.7 - Isotopes

3.7.1 - Neodymium isotopes

The Sm-Nd isotopic data of the Luanga Complex are listed in Table 3.1. Nine representative samples of mafic and ultramafic cumulates were analysed and provide the isotopic variation through the stratigraphy (Fig. 3.11). Nd isotopic data obtained for samples from the Ultramafic and Transition Zones render variably positive εNd (T=2.76Ga) values, bracketed between 0.9 and 11.58. Samples from the Mafic Zone show slightly negative εNd (T=2.76Ga) values, ranging from -0.23 to -0.93. Plotted against the stratigraphy, εNd (T=2.76Ga) values are scattered but show an upward decrease (Fig. 3.11), with negative values restricted to norites of the Mafic Zone.

Table 3.1: Sm–Nd isotopic data of Luanga Complex. UZ: Ultramafic Zone; TZ: Transition Zone; MZ: Mafic Zone.

Sample	Strat. (m)	Zone	Rock type	Sm (ppm)	Nd (ppm)	$^{147}Sm/^{144}Nd$	$^{143}Nd/^{144}Nd$ ± 2SE	$\varepsilon_{Nd\ (0)}$	T_{DM} (0 Ga)	ε_{Nd} (2.76 Ga)
LUFD120B	3000	MZ	Leuconorite PEG	0.598	2.416	0.1498	0.51176+/-10	-17.13	3.09	-0.47
LUFD120A	3000	MZ	Leuconorite	1.014	4.231	0.1448	0.511681+/-6	-18.67	3.04	-0.23
LUFD93-103	1600	MZ	Leuconorite	0.209	0.986	0.1279	0.511338+/-14	-25.36	3.05	-0.92
LUFD79-143	1320	TZ	Norite	0.33	2.073	0.0963	0.510855+/-9	-34.78	2.84	0.90
LUFD78-206	1260	TZ	Plg-Orthopyroxenite	0.157	0.763	0.124	0.511410+/-20	-23.95	2.78	1.89
LUFD78-55	1100	TZ	Norite	0.246	1.79	0.083	0.510845+/-29	-34.98	2.56	5.46
LUFD69-111	815	TZ	Orthopyroxenite (ore)	0.176	0.835	0.1276	0.51152+/-12	-21.8	2.7	2.76
LUFD69-115	810	TZ	Orthopyroxenite (ore)	0.346	1.466	0.1426	0.512242+/-53	-7.72	1.7	11.58
LUFD141-209	150	UZ	Serpentinite	0.67	1.888	0.2145	0.513193+/-16	10.83	-	4.53

3.7.2 - *Sulfur isotopes*

Three sulfide-bearing samples from the Sulfide Zone and one sample from hydrothermal sulfide zone (i.e. sample LUFD-224-102) were analysed in this study (Table 3.2). The $\delta^{34}S$ values for sulfides of these samples are bracketed between -1.69‰ and 0.35‰. The analysed samples, collected from different stratigraphic positions of the Sulfide Zone, show no systematic variation in $\delta^{34}S$ values across the stratigraphy. Additionally, no significant difference in $\delta^{34}S$ values is observed between samples from Sulfide Zone and hydrothermal sulfides.

Table 3.2: Sulfur isotopic data of Luanga Complex.

Sample	$\delta^{34}S$‰
LUFD-224-102	0.35
LUFD-224-62	-0.54
LUFD-69-111	-1.69
LUFD-69-108	-0.25

3.8 – Discussion

3.8.1 - Crustal assimilation and sulfur source

The role of crustal assimilation in the formation of magmatic Ni-Cu-PGE sulfide deposits is widely discussed (e.g., Barnes and Lightfoot, 2005; Mungall and Naldrett, 2008; Naldrett et al., 1999 and 2010). Both Nd and S isotopes are commonly used to evaluate the importance of the assimilation of crustal rocks during ascent and emplacement of mafic-ultramafic intrusions (Maier et al., 2000; Ripley and Li, 2007).

Sm-Nd isotopic data obtained for the Luanga Complex indicates positive εNd (T=2.76Ga) values, except for the slightly negative values of noritic rocks from the Mafic Zone (Fig. 3.11). In terms of crustal assimilation, magmas that assimilated significant amounts of older sialic rocks are expected to show negative εNd values (Maier et al., 2000). Once the cumulates from the Transition and Ultramafic Zones show variably positive εNd values (from 0.9 to 11.58), crustal assimilation of older crustal rocks does not appear to be a significant process during the evolution of their parental magmas. Anyways, noritic rocks from the Mafic Zone show slightly negative εNd values (-0.23 to -0.92), contrasting with the analysed norite sample from the Transition Zone (εNd = 2.56). Noritic rocks from Transition and Mafic Zones of the Luanga Complex have very similar lithogeochemical features (Mansur and Ferreira

Filho, 2016). The distribution of alteration-resistant trace elements of these mafic rocks, characterized by significant Nb and Ta anomalies and LREE enrichment, were interpreted as the product of primitive magmas partially contaminated with older continental crust (Mansur and Ferreira Filho, 2016). This interpretation follows what has been proposed for the magmatic evolution of the Lago Grande Complex (Teixeira et al., 2015). Mafic cumulate rocks from the Luanga and Lago Grande Complexes have very similar distribution of alteration-resistant elements, but the latter has variably negative εNd values (-0.32 to -4.25). Different Nd isotope compositions for the Lago Grande and Luanga Complexes, together with similar fractionation patterns and lithogeochemical compositions of their cumulates, may be interpreted as the result of similar primitive magmas variably contaminated with crustal rocks. This interpretation is consistent with the emplacement of 2.76 Ga layered intrusions within gneisses and migmatites of the Xingu Complex (ca. 3.0 Ga). In this scenario the assimilation of crustal rocks by the primitive magma would be significant for the parental magma of the Lago Grande Complex but minor for the Luanga Complex.

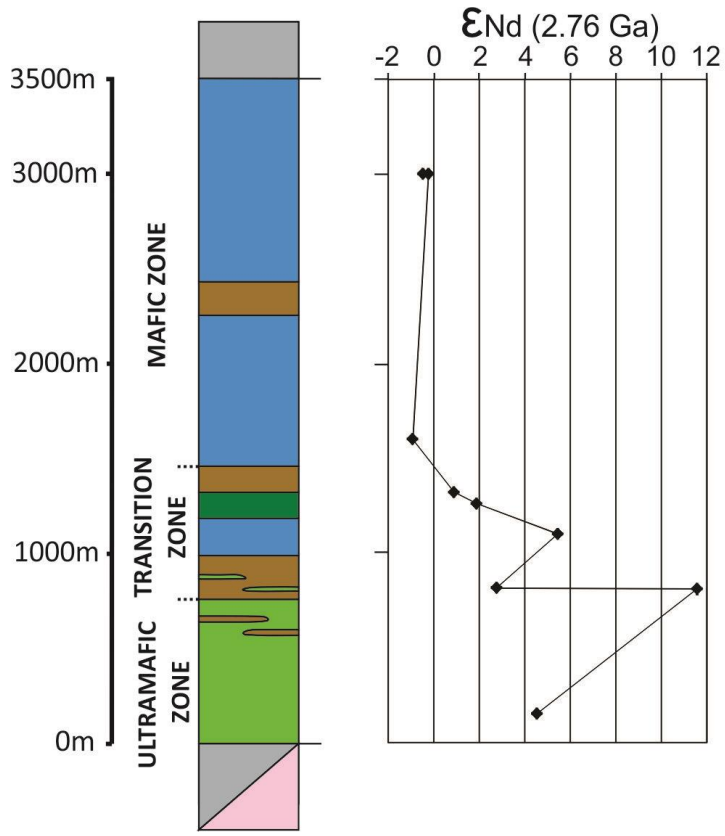

Fig. 3.11: Variations of εNd values throughout the stratigraphy of the Luanga Complex. The εNd values are calculated for an age of 2.76Ga.

The $\delta^{34}S$ values of the mantle are traditionally considered to be 0±2‰, but some studies suggest a larger range around 0‰ (Seal, 2006). The $\delta^{34}S$ values of the analysed samples from the Sulfide Zone of the Luanga Complex fall in the range of 0 ± 2‰, which suggests that the sulfur of these rocks is mantle-derived (Fig. 3.12). However, once the country rocks of the Luanga Complex were not investigated, sulfur isotope results do not provide unequivocal evidence for mantle-derived sulfur, considering that country rocks may also show mantle-like signature for sulfur isotopes. The $\delta^{34}S$ value obtained from a sample of hydrothermal sulfide (i.e. 0.35) is similar to the values obtained for the Sulfide Zone. Hence, is reasonable to propose that these sulfides may be originated by a hydrothermal remobilization of magmatic sulfides of the Sulfide Zone.

The Nd isotopic data for the Ultramafic Zone and Transition Zone, which does not suggest major assimilation of older crustal rocks, is thus compatible with a mantle-derived sulfur signature (Fig. 3.12). Both Nd and S isotope results suggest that sulfur saturation that led to the formation of the Sulfide Zone in the Luanga Complex was not triggered by the addition of external sulfur, as proposed in several studies of Ni-Cu-PGE deposits (Fig. 3.12; Ripley and Li, 2007).

The assimilation of crustal rocks is commonly considered as a key factor for the formation of magmatic sulfide Ni-Cu-PGE deposits in mafic-ultramafic intrusions (e.g., Ripley and Li, 2003; Barnes and Lightfoot, 2005). However, recent studies have also suggested that magmatic deposits were originated from mantle-derived sulfur, as exemplified by the Nebo-Babel Ni–Cu–PGE deposit (Fig. 3.12; Seat et al. 2009), the Platreef PGE–Ni–Cu deposit (Penniston-Dorland et al. 2008) and the Santa Rita deposit (Ferreira Filho et al., 2013). The evidence for another magmatic PGE deposit with mainly mantle-derived sulfur, provided in this study, reinforces the suggestion that an external source of sulfur is not essential for their genesis.

3.8.2 - PGE source

The origin of magmas that lead to the generation of magmatic PGE deposits is controversial. Some authors propose the existence of igneous provinces where PGE-rich magmas were formed (e.g., Maier and Groves, 2011; Griffin et al., 2013). This would explain the spatial concentration of PGE deposits in a few locations worldwide. On the other hand, some authors argument that current data do not indicate the existence of PGE-rich igneous provinces (e.g., Fiorentini et al., 2010; Barnes et al., 2015a). These

authors propose that the generation of PGE deposits result from multiple enrichment factors during evolution of magmas with low PGE contents commonly reported in primitive magmas.

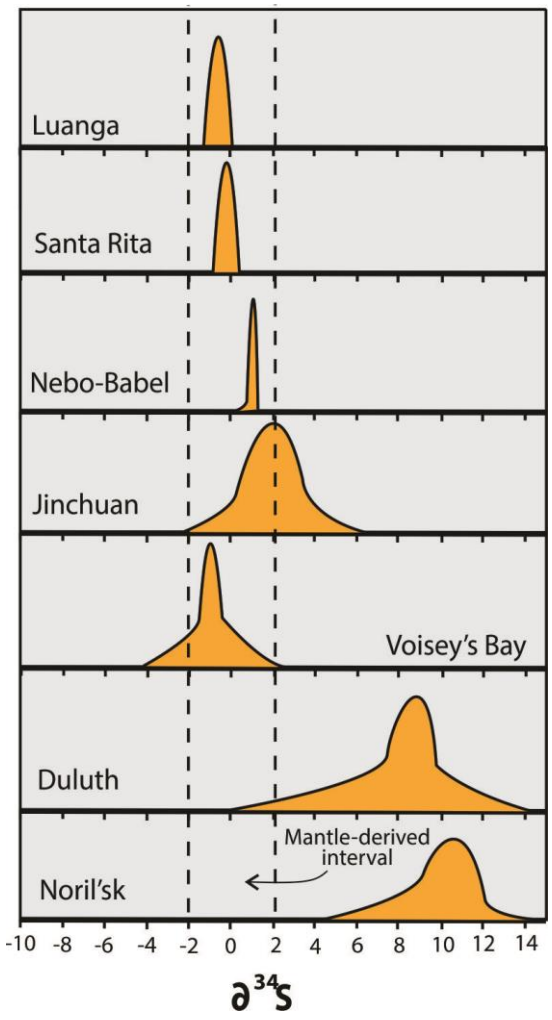

Fig. 3.12: Relation of the $\delta^{34}S$ data for magmatic Ni-Cu-PGE deposits worldwide. The two black dashed lines indicate the mantle-deriver sulfur interval. References - Noril'sk, Duluth, Voisey's Bay, Jinchuan and Nebo-Babel: Seat et al. (2009) and references therein; Santa Rita: Lazarin (2011).

The Luanga Complex is one of the layered intrusions ascribed as part of the Serra Leste suite (Ferreira Filho et al., 2007). This suite was originally grouped based on PGE anomalies and spatial association of the mafic-ultramafic intrusions. Current data, provided by recent studies (Teixeira et al., 2015; Mansur and Ferreira Filho, 2016), support the existence of a PGE-fertile suite within the eastern portion of the Carajás Mineral Province. Whether this magmatic suite originated from anomalous

PGE-rich magmas or by the magmatic evolution of regular mafic magmas is the subject of current studies in the Carajás Mineral Province..

Systematic studies in Lago Grande (Teixeira et al., 2015) and Luanga (Mansur and Ferreira Filho, 2016) Complexes suggest that layered rocks in both intrusions fractionated from moderately primitive basaltic magma. Apart from similar rock types and PGE mineralizations, the magmatic evolution of these layered intrusions resulted in distinct magmatic structure, stratigraphic sequence and Nd isotope composition. Because the composition of the parental magmas of the Luanga and Lago Grande Complexes is not constrained by common features available in several layered intrusions (e.g., chilled margins, volcanic equivalents, feeder dykes), discussions regarding their PGE contents are not straightforward. An unusually PGE-rich parental magma provides a convenient explanation for the abundance of PGE mineralizations in the Serra Leste region, as well as different styles of PGE mineralization in individual intrusions. However, mafic-ultramafic magmas with abnormally enriched PGE contents are uncommon and PGE-mineralized layered intrusions are not usually considered to originate from PGE-rich magmas.

In addition to magmatic PGE deposits hosted in layered intrusions, the Serra Pelada Au-Pd hydrothermal deposit (Meireles and Silva, 1988; Berni et al., 2014) also occurs in the Serra Leste region. The Serra Pelada deposit Au-Pd mineralization is located 10 km northwest from the Luanga Complex (Fig. 3.1B). Berni et al. (2014) propose that the mineralizing fluids of this deposit become enriched in PGE by interacting with mafic-ultramafic rocks of the Serra Leste suite. This assumption contributes for the existence of a PGE-fertile underplate beneath the eastern portion of the Carajás Mineral Province. The existence of a PGE-fertile magmatic province would thus justify the spatial association of several PGE-mineralized layered intrusions and the unusually PGE-enriched Au deposit of Serra Pelada.

3.8.3 - Genetic model for the PGE-deposit

Our results indicate that two highly different styles of magmatic PGE mineralization occur in the Luanga Complex. These are referred to as sulfide- and silicate-related PGE mineralizations (Fig. 3.2B).

The sulfide-related PGE, comprising the Sulfide Zone, consists of PGE associated with interstitial base metal sulfides and resembles typical deposits originated

from sulfide liquids segregated from mafic–ultramafic magmas (e.g., Campbell et al., 1983; Naldrett, 2004). The silicate-related PGE mineralization, on the other hand, occurs in rocks with no base metal sulfides. Host rocks of silicate-related PGE mineralization have no distinctive feature compared to adjacent unmineralized rocks. Sulfide-related and silicate-related PGE mineralization have distinct mantle-normalized PGE profiles (Fig. 3.8 and 3.10A) and Pt/Pd ratios, typically 0.5-06 and 1.2-1.3, respectively. The differences between both mineralization styles, together with its different stratigraphic positions, suggest that they formed by distinct processes. Because these different styles of PGE mineralization are closely associated to the Transition Zone, a genetic model for their origin should be consistent with the magmatic evolution of this stratigraphic interval.

A simplified model for sulfide- and silicate related PGE mineralizations of the Luanga Complex is shown in figure 3.13. The crystallization of olivine cumulates in the Ultramafic Zone without the crystallization of sulfide minerals progressively upgrades the S content of the residual magma (stage 1; Fig. 3.13). The Transition Zone marks an abrupt change in the dynamics of the magmatic chamber, caused by several magma inputs characterized by cyclic units (Mansur and Ferreira Filho, 2016). Hence, these periodic inputs of primitive magma are considered responsible to trigger the S saturation of the magma and consequently the segregation of a sulfide liquid. Due to the high partition coefficients, PGE and base metals segregated into this sulfide liquid (Barnes and Lightfoot, 2005), which originates the Sulfide Zone between the Ultramafic Zone and Transition Zone (stage 2; Fig. 3.13). Sulfur isotopes of the Sulfide Zone have mantle-like signature (Fig. 3.12), which means that sulfur saturation is not likely to be attained by new injections of crustal contaminated magmas.

The silicate-related PGE mineralization occurs above the Sulfide Zone (Fig. 3.2B). The Transition Zone originated from several magmatic pulses, such that the depleted resident magma that followed the segregation of the Sulfide Zone may again become progressively enriched in PGE. Thus, if this magma does not reach the S saturation again, the progressive PGE enrichment would not be accompanied by sulfide segregation. We consider that the development of silicate-related PGE zones indicates PGE saturation in the magma leading to concomitant crystallization of silicates and Platinum Group Minerals (stage 3; Fig. 3.13). The processes that led to PGE accumulation within these horizons are still poorly constrained. The investigation of

platinum group minerals (PGM) is currently being developed to investigate the minerals containing PGE. The accumulation of PGE apart from chromite- and/or sulfide-bearing rocks has been documented in other layered intrusion (Knight et al., 2011; Ferreira Filho et al., 2007). Models suggesting a direct crystallization of PGM from magma have already been proposed (Hiemstra, 1979). Anyways, there is no clear agreement about the processes that originate these chromite- and/or sulfide-free PGE-bearing rocks.

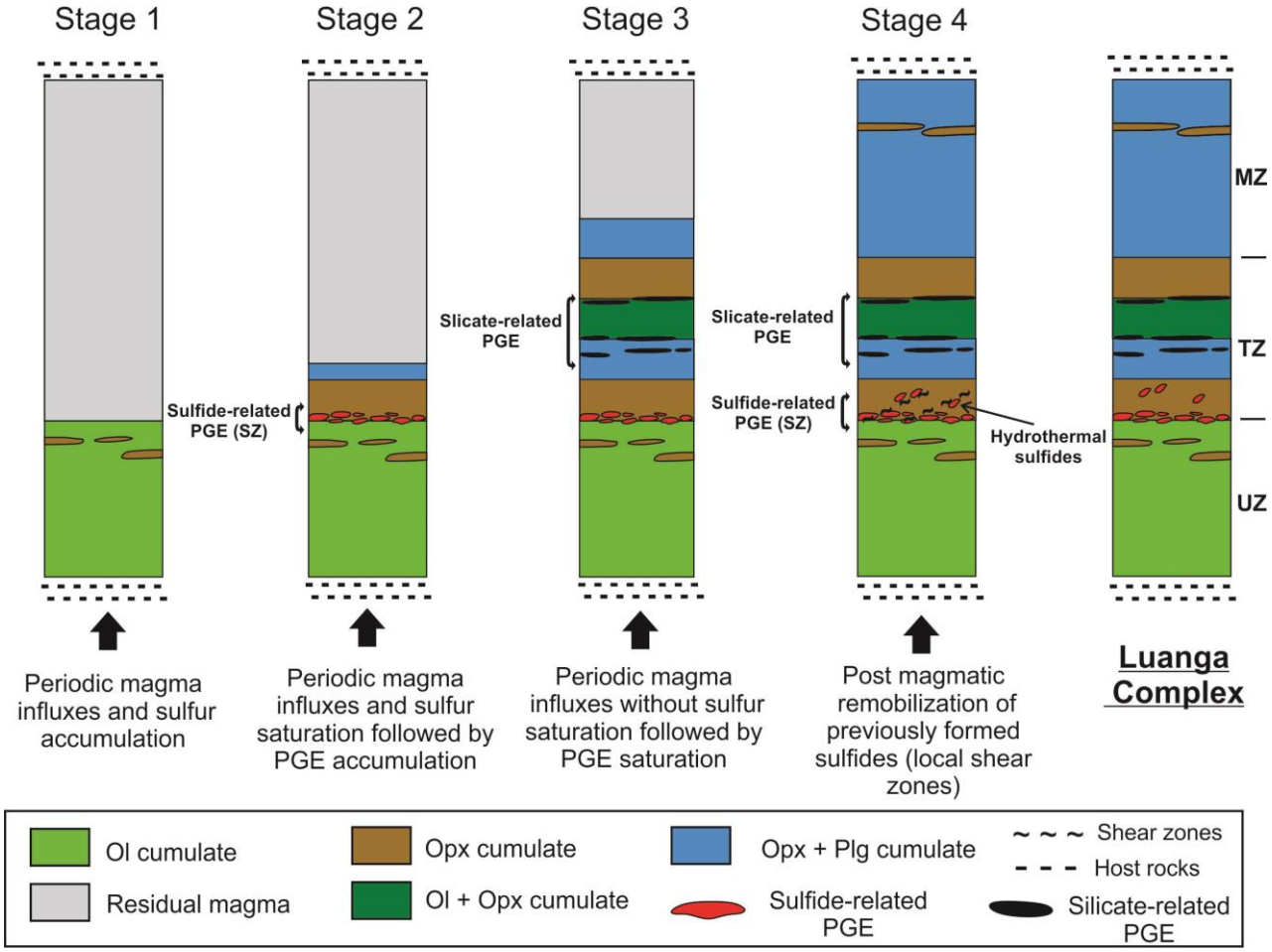

Fig. 3.13: Schematic model illustrating the formation of different styles of PGE mineralization throughout the Luanga Complex. See text for explanation. UZ: Ultramafic Zone; TZ: Transition Zone; MZ: Mafic Zone.

The occurrence of hydrothermal sulfides, with no PGE content and no magmatic characteristics, few meters above the Sulfide Zone (Fig. 3.6), is not genetically related with the magmatic evolution of the complex. These sulfide-bearing rocks are probably formed by post-magmatic hydrothermal processes that remobilizes sulfide minerals but apparently do not concentrate PGE (stage 4; Fig. 3.13). Anyways, it is not the aim of the

present study to discuss the genetic model of these hydrothermal sulfide-bearing rocks, once they do not appear to significantly disturb PGE-bearing rocks.

In summary, the Sulfide Zone marks a moment of S saturation while the silicate-related PGE rich horizons mark the PGE saturation of the magma. The S saturation is triggered by periodic primitive magma influxes at the contact of the Ultramafic Zone and the Transition Zone (Fig. 3.13). The formation of PGE-bearing rocks within stratigraphic horizons that marks dynamic moments in the evolution of a given magmatic chamber is common and also documented in the Bushveld Complex (e.g., Naldrett, 2004). The processes that control the PGE accumulation in sulfide- and chromite-free horizons are still poorly constrained.

3.8.4 - Sulfides with high Ni tenor and its implications

Previous studies, based on extremely high Ni contents in olivine (up to 7500ppm) and orthopyroxene (up to 1600ppm), indicate an anomalously Ni-rich parental magma for the Luanga Complex (Mansur and Ferreira Filho, 2016). The authors considered two possible explanations for the origin Ni-rich magma: i. a parental magma derived from pyroxenitic mantle sources (Sobolev et al., 2007) or ii. Ni upgrading through dissolution of previously formed nickel-rich sulfide melts (Keer and Leitch, 2005). The model proposed by Keer and Leitch (2005) provides an explanation for both the high nickel and PGE contents, as the dissolution of previously formed Ni-Cu-PGE sulfides increases both Ni and PGE of resulting magma. Our results provide additional data to contribute with this discussion and understand the relation between high Ni parental magma and PGE contents of the Luanga Complex.

The study of chalcophile elements in sulfide bearing rocks of the Luanga Complex indicates a positive correlation between Ni and Cu with S (Fig. 3.7). Additionally, these sulfides show remarkably high Ni tenors (up to 18 wt.%) with low Cu tenors (up to 1.4 wt.%). These results are compatible with the sulfide assemblage of pentlandite > pyrrhotite > >> chalcopyrite (Fig. 3.4B) and high Ni contents in olivine and orthopyroxene crystals from the Ultramafic and Transiton Zones (Mansur and Ferreira Filho, 2016). A comparison between Ni, Cu and PGE tenors of different PGE deposits worldwide is given in figure 3.14. The Sulfide Zone of the Luanga Complex stands out among other intrusions due to its high Ni and low Cu tenors, resulting in a very low Ni/Cu ratio. In contrast, PGE tenors are not different, and eventually lower, when compared to other intrusions with much lower Ni/Cu ratios (Fig. 3.14).

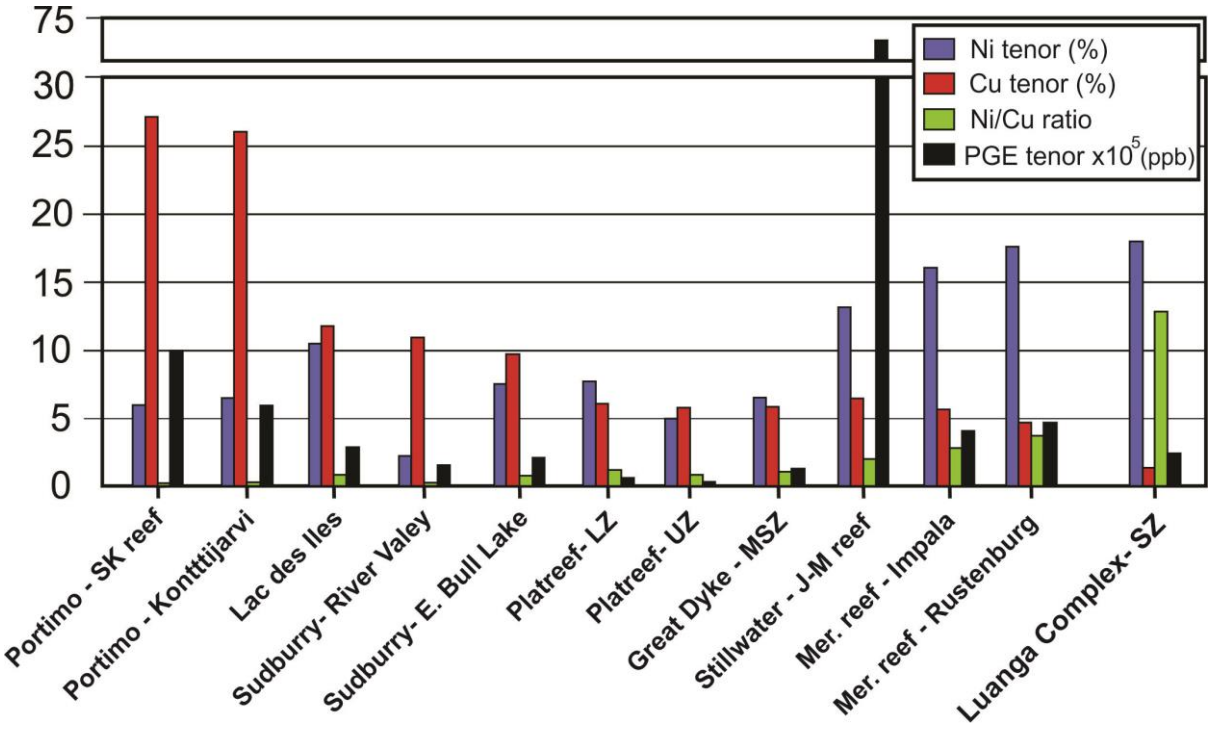

Fig. 3.14: Comparison of Ni, Cu and PGE tenors and Ni/Cu ratios of different PGE deposits worldwide. The data is obtained from Naldrett (2004) and references therein. LZ: Lower Zone; UZ: Upper Zone; MSZ: Main Sulfide Zone; SZ: Sulfide Zone.

Additionally, PGE mineralization is a remarkable characteristic of all the layered intrusions of the Serra Leste suite (Ferreira Filho et al., 2007; Teixeira et al., 2015), while high Ni olivine has so far been documented just in the Luanga Complex (Mansur and Ferreira Filho, 2016). Because systematic studies, including olivine analyses, in layered intrusions of the Serra Leste region is so far restricted to the Lago Grande and Luanga Complexes, the model proposed for PGE mineralization of the Luanga Complex should be considered with discretion for other layered intrusions in the region.

3.8.5 - Constrains for Ni and PGE exploration in the Carajás Mineral Province

The identification of anomalously high-Ni magmatism (Mansur and Ferreira Filho, 2016), as well as the characterization of different styles of PGE mineralization in Luanga Complex in this study, provided additional data to be considered during mineral exploration for magmatic Ni-Cu-PGE in the Carajás Mineral Province. Following the model developed by Kerr and Leitch (2005), Mansur and Ferreira Filho (2016) interpreted these features as the result from the "cannibalization" of previously formed Ni-PGE sulfides. This model, previously proposed to explain the origin of extremely Ni-rich olivines associated with Ni-PGE orebodies in the Kevitsa intrusion in Finland (Yang et al., 2013), implies that the new inputs of Ni-rich fresh magma of the Transition

Zone have partially dissolved early formed sulfides. Exploration for magmatic Ni-Cu-PGE deposits in the Carajás Mineral Province indicated several PGE-mineralized layered intrusions, but typical massive Ni-Cu-PGE deposits were not described in the region. The indirect evidence that such deposits may have formed in the Carajás Mineral Province is very positive for mineral exploration. Massive Ni-Cu-PGE deposits are commonly hosted in small conduit-type mafic-ultramafic intrusions (Barnes et al., 2016), as exemplified by Nebo-Babel (Seat et al., 2009) and Limoeiro (Mota-e-Silva et al., 2013). Fingerprints of conduit-type Ni-Cu sulfide deposits are usually very small, representing thus a challenge to exploration.

Another important feature to be considered during further exploration programs in the Carajás Mineral Province is the occurrence of non-traditional PGE-rich layers in the Luanga Complex. PGE mineralizations that are not related to sulfide- and/or chromite-bearing rocks, characteristic of the silicate-related PGE ore described in this study, do not provide the usual associated geochemical anomalies (e.g., Cu and Cr) expected in PGE deposits. Silicate-related PGE mineralizations are not restricted to the Luanga Complex and also occur in the Serra da Onça Complex (Macambira and Ferreira Filho, 2005; Ferreira Filho et al., 2007) (Fig. 3.1B). These stratabound silicate-related PGE mineralizations are also not identified by any characteristic texture or mineralogical feature during drill core logging. These suggests that they may have been overlooked during previous exploration focused on traditional PGE deposits associated with base metal sulfides or chromitites.

Mafic-ultramafic intrusions in the Carajás Mineral Province have characteristics suggesting a favorable potential to host magmatic Ni-Cu-PGE deposits. The most significant are listed as follows:

i. The Carajás Mineral Province hosts several mafic-ultramafic intrusions within a Neoarchean cratonic terrain;
ii. Many layered intrusions have primitive parental magmas emplaced in dynamic magmatic system (e.g., Vermelho Complex; Luanga Complex);
iii. The cluster of PGE-mineralized intrusions in the Serra Leste region suggests the existence of a PGE-fertile suite in the eastern portion of the Carajás Mineral Province (Ferreira Filho et al., 2007; Teixeira et al., 2015);
iv. New inputs of Ni- and PGE-rich magmas in the Luanga Complex originated from the "cannibalization" of previously formed Ni-PGE sulfides;

3.9 – Conclusions

The main conclusions derived from the present study are listed below.

- Apart from chromitites, two PGE mineralization styles occur in the Luanga Complex. These are referred to as sulfide-related PGE and silicate-related PGE.
- The sulfide-related PGE comprises the Sulfide Zone, a 10-50 m thick stratabound zone of disseminated base metal sulfides (~ 1-3 vol.%) located along the contact of the Ultramafic and Transition Zones.
- The Sulfide Zone has high Ni tenors (16-18 wt.%) and Ni/Cu ratios (10-12), compatible with the high modal percentage of pentlandite in the sulfide assemblage. PGE ore has Pt/Pd ratios lower than 1 (~ 0.55) and PPGE-enriched mantle-normalized patterns.
- The silicate-related PGE mineralization consists of 2-10 meters thick stratabound zones, located stratigraphically above the Sulfide Zone. These PGE-rich zones consist of cumulates (orthopyroxenite and harzburgite) with no distinctive textural and mineralogical features compared to barren rocks.
- Silicate-related PGE is characterized by Pt values systematically higher than Pd with Pt/Pd ratio around 1.2-1.3. Mantle-normalized patterns show high enrichment of Pt, Pd, Rh and Au without significant contents of Ir and Os.
- Nd isotopic data for cumulated from the Ultramafic Transition Zones show positive εNd (T=2.76Ga) values while cumulates from the Mafic Zone show slightly negative values. These positive values suggest that no extensive contamination with older crustal rocks took place during the development of the Luanga Complex.
- Sulfur isotopes show a narrow range of variation for $\delta^{34}S$ values (between -1.69‰ and 0.35‰), which indicates that the sulfur of these rocks are possibly derived from mantelic source.
- Textural and geochemical differences between sulfide- and silicate-related PGE mineralizations support that they formed by different processes. While sulfide-related mineralization results of segregation of immiscible sulfide liquids, silicate-related PGE mineralization formed possibly due to saturation of PGE in the magma and co-precipitation of silicates and PGM.
- The Sulfide Zone shows high Ni tenors and extremely high Ni/Cu ratios when compared to other PGE deposits worldwide.

- Our results provide additional evidences for PGE-fertile magmatism in the eastern portion of the Carajás Mineral Province (Serra Leste suite).

Acknowledgements

This study was supported by CNPq (Conselho Nacional de Desenvolvimento Científico e Teconológico) and VALE S.A. (Projeto 550398/2010-4). Analytical facilities of the Instituto de Geociências of the University of Brasília (UnB) provided additional support for this research. The authors acknowledge VALE's Exploration Managers for Brazil and Carajás (Mr. Fernando Greco and Mr. Fernando Matos, respectively) for field support and access to exploration data. Cesar F. Ferreira Filho is a Research Fellow of CNPq and acknowledges the continuous support through research grants and scholarships for the "Metalogenênese de Depósitos Associados ao Magmatismo Máfico-Ultramáfico" Research Group. Eduardo T. Mansur holds a scholarship from Coordenação de Aperfeiçoamento de Pessoal de Nível Superior (CAPES) and this study is part of his M.Sc. thesis developed at the Instituto de Geociências (Universidade de Brasília).

References

Araújo, O.J.B., Maia, R.G.N., João, X.S.J., and Costa, J.B.S., 1988, A megaestruturação arqueana da Folha Serra dos Carajás, in, Congresso Latino Americano de Geologia, Anais: p. 324-338.

Barnes, S.J., Cruden, A.R., Arndt, N., Saumur, B.R., 2016. The mineral system approach applied to magmatic Ni–Cu–PGE sulphide deposits. Ore Geology Reviews 76, 296–316.

Barnes, S.J., Mungall, J.E., and Maier, W.D., 2015, Platinum group elements in mantle melts and mantle samples: Lithos, v. 232, p. 395-417.

Barnes, S-.J., and Lightfoot, P.C., 2005, Formation of magmatic nickel sulfide deposits and processes affecting their copper and platinum group element contents: Economic Geology 100th Anniversary Volume, p. 179-214.

Barnes, S-J., and Maier, W.D., 2002, Platinum-group element distributions in the Rustenberg Layered Suite of the Bushveld Complex, South Africa, in, Cabri, L.J., ed., The Geology, Geochemistry, Mineralogy and Mineral Beneficiation of Platinum-Group Elements, Canadian Institute of Mining, Metallurgy and Petroleum, Special Volume 54: p. 431-458.

Berni, G.V., Heinrich, C.A., Lobato, L.M., Wall, V.J., Rosière, C.A., and Freitas, M.A., 2014, The Serra Pelada Au-Pd-Pt Deposit, Carajás, Brazil: Geochemistry, Mineralogy, and Zoning of Hydrothermal Alteration: Economic Geology, v. 109, p. 1883-1899.

Campbell, I.H., Naldrett, A.J., and Barnes, S.J., 1983, A model for the origin of the platinum-rich horizons in the Bushveld and Stillwater Complexes: Journal of Petrology, v. 24, p. 133-165.

Carlon, C.J., Molinari, L., Queiroz, R., Felix de Melo, J., 2006, The discovery and exploration of the Jacare ("Alligator") nickel laterite-saprolite deposit, Para State, Brazil: Australian Earth Science Convention, AESC2006, Melbourne, Australia, (http://www.publish.csiro.au/paper/ASEG2006ab023.htm).

Cawthorn, R.G., Merkle, R.K.W., and Viljoen, M.J., 2002, Platinum-group element deposits in the Bushveld Complex, South Africa, in, Cabri, L.J., ed., The Geology, Geochemistry, Mineralogy and Mineral Beneficiation of Platinum-Group Elements, Canadian Institute of Mining, Metallurgy and Petroleum, Special Volume 54: p.389-430.

Cawthorn, R.G., Barnes, S.J., Ballhaus, C., and Malich, K.N., 2005, Platinum group element, chromium and vanadium deposits in mafic and ultramafic rocks: Economic Geology 100th Anniversary Volume, p. 215-249.

Crocket, J.H., 2002, Platinum-group element geochemistry of mafic and ultramafic rocks; in The Geology, Geochemistry, Mineralogy and Mineral Beneficiation of Platinum-Group Elements, in, L.J. Cabri, ed., Canadian Institute of Mining and Metallurgy, Special Volume 54: p. 177–210.

Dall'Agnol, R., Oliveira, M.A., Almeida, J.A.C., Althoff, F.J., Leite, A.A.S., Oliveira, D.C., and Barros, C.E.M., 2006, Archean and Paleoproterozoic granitoids of the Carajás metallogenetic province, eastern Amazonian craton, in, Dall'Agnol, R., Rosa-Costa, L.T., Klein, E.L., ed., Symposium on Magmatism, Crustal Evolution, and

Metallogenesis of the Amazonian Craton, Abstracts Volume and Field Trips Guide: p. 150.

Dardenne, M.A., and Schobbenhaus, C.S., 2001, Metalogênese do Brasil: Brasília, UnB-CNPq, 392 p.

Dardenne, M.A., Ferreira Filho, C.F., and Meirelles, M.R., 1988, The role of shoshonitic and calc-alkaline suites in the tectonic evolution of the Carajás District, Brazil: Journal of South American Earth Sciences, v. 1, p. 363–372.

DePaolo, D.J., 1981, Neodymium isotopes in the Colorado Front Range and implications for crust formation and mantle evolution in the Proterozoic: Nature, v. 291, p. 193-197.

Diella, V., Ferrario, A., and Girardi, V.A.V., 1995, PGE and PGM in the Luanga mafic-ultramafic intrusion in Serra dos Carajás (Pará State, Brazil): Ore Geology Reviews, v. 9, p. 445-453.

Docegeo - Rio Doce Geologia e Mineração, 1988, Revisão Litoestratigráfica da Província Mineral de Carajás, in, SBG-NNO, ed., 35º Congresso Brasileiro Geologia, Belém, Anais: p. 11-59.

Feio, G.R.L., Dall'Agnol, R., Dantas, E.L., Macambira, M.J.B., Santos, J.O.S., Althoff, F.J., and Soares, J.E.B., 2013, Archean granitoid magmatism in the Canaã dos Carajás area: Implications for crustal evolution of the Carajás province, Amazonian craton, Brazil: Precambrian Research, v. 227, p. 157-185.

Ferreira Filho, C.F., Cançado, F., Correa, C., Macambira, E.M.B., Siepierski, L., and Brod, T.C.J., 2007. Mineralizações estratiformes de EGP-Ni associadas a complexos acamadados em Carajás: os exemplos de Luanga e Serra da Onça, in, Contribuições à Geologia da Amazônia, ed., Publitec Gráfica & Editora, volume 5: p. 01-14.

Finnigan, C.S., Brenan, J.M., Mungall, J.E., and McDonough, W.F., 2008, Experiments and models bearing on the role of chromite as a collector of platinum group minerals by local reduction: Journal of Petrology, v. 49, p. 1647-1665.

Fiorentini, M.L., Barnes, S.J., Lesher, C.M., Heggie, G.J., Keays, R.R., and Burnham, O.M., 2010, Platinum-group element geochemistry of mineralized and non-mineralized komatiites and basalts: Economic Geology, v. 105, p. 795-823.

Gibbs, A.K., Wirth, K.R., Hirata, W.K., and Olszewski Jr, W.J., 1986, Age and composition of the Grão Pará Group volcanics, Serra dos Carajás: Revista Brasileira de Geociências, v. 16, p. 201-211.

Gioia, S.M.C.L., and Pimentel, M.M., 2000, The Sm-Nd isotopic method in the geochronology laboratory of University of Brasilia, in, anais da academia brasileira de ciências, volume 72: p. 219-245.

Grainger, C.J., Groves, D.I., Tallarico, F.H.B., and Fletcher, I.R., 2008, Metallogenesis of the Carajás Mineral Province, Southern Amazon Craton, Brazil: Varying styles of Archean through Paleoproterozoic to Neoproterozoic base- and precious-metal mineralisation. Ore Geology Reviews, v. 33, p. 451-489.

Griffin, W., O'Reilly, S.Y., and Begg, G.C., 2013, Continental-root control on the genesis of magmatic ore deposits: Nature Geoscience, v. 6, p. 905-910.

Hiemstra, S. A., 1979, The role of collectors in the formation of the platinum deposits in the Bushveld Complex: Canadian Mineralogist, v. 17, p. 469-482.

Huhn, S.R.B., Santos, A.B.S., Amaral, A.F., Ledsham, E.J., Gouveia, J.L., Martins, L.P.B., Montalvão, R.M.G., and Costa, V.C., 1986, O terreno granito-greenstone da região de Rio Maria-Sul do Pará, In, 35º Congresso Brasileiro de Geologia, ed., Anais, Sociedade Brasileira de Geologia,volume 3: p. 1438-1452.

Kerr, A., and Leitch, A.M., 2005, Self-destructive sulfide segregation systems and the formation of high-grade magmatic ore deposits: Economic Geology, v. 100, p. 311-332.

Klein, C., and Ladeira, E.A., 2002, Petrography and geochemistry of the least altered banded iron-formation of the Archean Carajás Formation, Northern Brazil: Economic Geology, v. 97, p. 643-651.

Knight, R.D., Prichard, H.M., McDonald, I., and Ferreira Filho, C.F., 2011, Platinum group mineralogy of the Fazenda Mirabela intrusion, Brazil: the role of high temperature liquids and sulfur loss: Transactions of The Institution of Mining and Metallurgy Section (applied Earth Science), v. 120(4), p. 211-224.

Lazarin, F.A., 2011, Geologia, petrologia e estudos isotópicos dos depósitos de níquel-cobre sulfetados Santa Rita e Peri-Peri, Nordeste do Brasil: Unpublished M.Sc. thesis, Brasília, Brazil, Universidade de Brasília, 69 p.

Lobato, L.M., Figueiredo e Silva, R.C., Rosière, C.A., Zucchetti, M., Baars, F.J., Seoane, J.C.S., Rios, F.J., and Monteiro, A.M., 2005, Hydrothermal origin for the iron

mineralisation, Carajás Province, Pará State, Brazil, in, Proceedings Iron Ore 2005, The Australian Institute of Mining and Metallurgy, Publication Series, volume 8: p. 99-110.

Macambira, E.M.B., and Ferreira Filho, C.F., 2002, Fracionamento Magmático dos Corpos Máfico-Ultramáficos da Suíte Intrusiva Cateté – Sul do Pará, in, Klein E.L., Vasquez M.L. and Rosa Costa L.T., ed., Contribuições à Geologia da Amazônia, volume 3: p. 105-114.

Macambira, E.M.B., and Ferreira Filho, C.F., 2005, Exploration and origin of stratiform PGE mineralization in the Serra da Onça layered complex, Carajás Mineral Province, Brazil [ext. abs.]: International Platinum Symposium, 10th, Oulu, Finland, 2005, Extended Abstracts, p. 178-181.

Macambira, M.J.B., and Lancelot, J.R., 1996, Time constraints for the formation of the Archean Rio Maria crust, Southeastern Amazonian Craton, Brazil: International Geology Review, v. 38, p. 1134-1142.

Machado, W., Lindenmayer, Z.G., Krogh, T.E., and Lindenmayer, D., 1991, U-Pb geochronology of Archean magmatism and basement reactivation in the Carajás area, Amazon shield, Brazil: Precambrian Research, v. 49, p. 329-354.

Maier, W.D., Arndt, N.T., and Curl, E.A., 2000, Progressive crustal contamination of the Bushveld Complex: evidence from Nd isotopic analyses of the cumulate rocks: Contributions to Mineralogy and Petrology, v. 140, p. 316-327.

Maier, W.D., and Groves, D.I., 2011, Temporal and spatial controls on the formation of magmatic PGE and Ni-Cu deposits: Mineralium Deposita, v. 46, p. 841-857.

Mansur, E.T., Ferreira Filho, C.F., 2016, Magmatic structure and geochemistry of the Luanga Mafic-Ultramafic Complex: further constraints for the PGE-mineralized magmatism in Carajás, Brazil. Lithos, v. 266-267, p. 28-43.

Meireles, E.M., and Silva, A.R.B., 1988, Depósito de ouro de Serra Pelada, Marabá, Pará, In, C. Schobbenhaus, C.E.S. Coelho, ed., Principais Depósitos Minerais do Brasil, DNPM-CVRD, volume 3: p. 547-557.

Mota-e-Silva, J., Ferreira Filho, C.F., Della Giustina, M.E.S., 2013, The Limoeiro deposit: Ni–Cu–PGE sulfidemineralization hostedwithin an ultramafic tubular magma conduit inthe Borborema Province, Northeast Brazil. Economic Geology 108, 1753–

1771.

Mungall, J.E., and Naldrett, A.J., 2008, Ore deposits of the platinum-group elements: Elements, v. 4, p. 253-258.

Naldrett, A.J., 1989, Magmatic sulfide deposits: Clarendon, Oxford University Press, 186 p.

Naldrett, A.J., 2004, Magmatic sulphide deposits: Geology, geochemistry and exploration: Berlin, Springer-Verlag, 728 p.

Naldrett, A.J., 2010, Secular variation of magmatic sulfide deposits and their source magmas: Economic Geology, v. 105, p. 669-688.

Naldrett, A.J., Asif, M., Schandl, E., Searcy, T., Morrison, G.G., Binney, W.P., and Moore, C., 1999, Platinum-group elements in the Sudbury ores: significance with respect to the origin of different ore zones and to the exploration for footwall orebodies: Economic Geology, v. 94, p. 185-210.

Nogueira, A.C.R., Truckenbrod, W., Costa, J.B.S., and Pinheiro, R.V.L., 1994, Análise faciológica e estrutural da Formação Águas Claras, Pré-Cambriano da Serra dos Carajás, in, SBG-NNO, ed., Simpósio de Geologia da Amazônia, extended abstracts: p. 363-364.

Nogueira, A.C.R., Truckenbrod, W., and Pinheiro, R.V.L., 2000, Storm and tide-dominated siliciclastic deposits of the Archean Águas Claras Formation, Serra dos Carajás, Brazil, in, 31th International Geological Congress, ed., extended abstracts: CD-ROM.

Penniston-Dorland, S.C., Wing, B.A., Nex, P.A.M., Kinnaird, J.A., Farquhar, J., Brown, M., and Sharman, E.R., 2008, Multiple sulfur isotopes reveal a primary magmatic origin for the Platreef PGE deposit, Bushveld Complex, South Africa: Geology, v. 36, p. 979-982.

Pidgeon, R.T., Macambira, M.J.B., and Lafon, J.M., 2000, Th-U-Pb isotopic systems and internal structures of complex zircons from enderbite from the Pium Complex, Carajás Province, Brazil: evidence for the ages of granulite facies metamorphism and the protolith of the enderbite: Chemical Geology, v. 166, p. 159-171.

Ripley, E.M., and Li, C., 2003, S isotope exchange and metal enrichment in the formation of magmatic Cu-Ni-(PGE) deposits: Economic Geology, v. 98, p. 635-641.

Ripley, E.M., and Li, C., 2007, Applications of Stable and Radiogenic Isotopes to Magmatic Cu-Ni-PGE Deposits: Examples and Cautions: Earth Science Frontiers, v. 14(5), p. 124–132.

Rosa, W.D., 2014, Complexos acamadados da Serra da Onça e Serra do Puma: Geologia e petrologia de duas intrusões Máfico-Ultramáficas com sequência de cristalização distinta na Província Arqueana de Carajás, Brasil: Unpublished M.Sc. thesis, Brasília, Brazil, Universidade de Brasília, 65 p.

Seal, R.R., 2006, Sulfur isotope geochemistry of sulfide minerals: Reviews in Mineralogy and Geochemistry, v. 61, p. 633-677.

Seat, Z., Beresford, S.W., Grguric, B.A., Gee, M.A.M., and Grassineau, N.V., 2009, Reevaluation of the role of external sulfur addition in the genesis of Ni-Cu-PGE deposits: evidence from the Nebo-Babel Ni–Cu–PGE Deposit, West Musgrave, Western Australia: Economic Geology, v. 104, p. 521-538.

Siepierski, L., 2016, Geologia, petrologia e potencial para mineralizações magmáticas dos corpos máfico-ultramáficos da região de Canaã dos Carajás, Província Mineral de Carajás, Brasil, Unpublished Ph.D. thesis, Brasília, Brazil, Universidade de Brasília, 156 p.

Siepierski, L., and Ferreira Filho, C.F., 2016, Spinifex-textured komatiites in the south border of the Carajás ridge, Selva Greenstone belt, Carajás Province, Brazil: Journal of South American Earth Sciences, v. 66, p. 41-55.

Sobolev, A.V., Hoffman, A., Kuzmin, D., Yaxley, G., Arndt, N., Chung, S.-L., Danyushevsky, L., Elliott, T., Frey, F., Garcia, M., Gurenko, A., Kamenetsky, V., Kerr, A., Krivolutskaya, N., Matvienkov, V., Nikogosian, I., Rocholl, A., Sigurdson, I., Sushchevskaya, N., and Teklay, M., 2007, The amount of recycled crust in sources of mantle-derived melts: Science, v. 316, p. 412-417.

Souza, Z.S., and Dall'Agnol, R., 1996, Caracterização geoquímica e tectônica de rochas meta vulcânicas de "greenstone belts" arqueanos da região de Rio Maria, SE do Pará, in, Boletim IG-USP, ed., special publication, volume 18: p. 97-101.

Souza, Z.S., Potrel, A., Lafon, J.M., Althoff, F.J., Pimentel, M.M., Dall'Agnol, R., and Oliveira, C.G., 2001, Nd, Pb and Sr isotopes in the Identidade Belt, an Archean greenstone belt of Rio Maria region (Carajás Province, Brazil): implications for the geodynamic evolution of the Amazonian Craton: Precambrian Research, v. 109, p. 293-315.

Sun, S.-S., McDonough, W.F., 1989, Chemical and isotopic systematics of oceanic basalts: implications for mantle composition and processes, in, Saunders, A.D., Norry, M.J., ed., Magmatism in the Ocean Basins, Geological Society Special Publication, volume 42: pp. 313–345.

Teixeira, J.B.G., and Eggler, D.H., 1994, Petrology, Geochemistry, and Tectonic Setting of Archaean Basaltic and Dioritic Rocks from the N4 Iron Deposit, Serra dos Carajás, Pará, Brazil; Acta Geologica Leopoldensia, v. 17, p. 71-114.

Teixeira, A.S., Ferreira Filho, C.F., Giustina, M.E.S.D., Araujo, S.M., and Silva, H.H.A.B., 2015, Geology, petrology and geochronology of the Lago Grande layered complex: Evidence for a PGE-mineralized magmatic suite in the Carajás Mineral Province, Brazil; Journal of South American Earth Sciences, v. 64, p. 116-138.

Vasquez, M.L., Carvalho, J.M.A., Sousa, C.S., Ricci, P.S.F., Macambira, E.M.B., and Costa, L.T.R., 2008. Geological map of the Pará state in GIS, Geological Survey of Brazil-CPRM.

Villas, R.N., and Santos, M.D., 2001, Gold deposits of the Carajás Mineral Province: deposit types and metallogenesis: Mineralium Deposita, v. 36, p. 300–331.

Xavier, R., Monteiro, L.V.S., Souza Filho, C.R., Torresi, I., Carvalho, E.R., Dreher, A.M., Wiedenbeck, M., Trumbull, R.B., Pestilho, A.L.S., and Moreto, C. P. N., 2010, The iron oxide copper-gold deposits of the Carajás Mineral Province, Brazil: an updated and critical review, in, Porter, T.M., Org., Hydrothermal Iron Oxide Copper-Gold & Related Deposits: A Global Perspective, vol. 3, Advances in the Understanding of IOCG Deposits, Adelaide, PGC Publishing, volume 3: p. 285-306.

CONCLUSÃO DA DISSERTAÇÃO

As conclusões detalhadas da dissertação estão divididas em três partes, cada uma no final de cada um dos capítulos apresentados. Entretanto, uma versão sintética das conclusões pode ser demostrada desta forma:

1. Sobre a intrusão:

    i. O Complexo Luanga é uma intrusão acamadada de médio porte, subdividido em três porções principais. A evolução do Complexo é dinâmica, marcada pela sucessiva entrada de novos pulsos magmáticos em um sistema magmático aberto.

    ii. Os conteúdos de Ni nas olivinas da Zona de Transição do Complexo Luanga encontram-se entre os maiores valores registrados no mundo. A formação de um magma anômalo em níquel pela dissolução de sulfetos previamente formados é considerada adequada para explicar estes resultados.

2. Sobre a mineralização

    i. Dois estilos diferentes de mineralização de EGP são observados no Complexo Luanga. Estes são indicados como *Sulfide Zone* e *silicate-related PGE* e possuem características distintas.

    ii. A *Sulfide Zone* é um horizonte de 10-50 metros de espessura, localizado na passagem entre as Zonas Ultramáfica e de Transição, com uma disseminação de sulfetos (i.e. 3% vol.). A *silicate-related PGE* é representada por horizontes de 2-10 metros de espessura, estratigraficamente acima da *Sulfide Zone*, que apresentam concentrações anômalas de EGP e nenhuma associação com sulfetos e/ou cromita.

    iii. Diferenças texturais e geoquímicas entre os dois estilos de mineralização indicam que estes se formaram por processos geológicos distintos. A *Sulfide Zone* é formada pela segregação de um líquido imiscível de sulfeto, ao passo que a *silicate-related PGE* é gerada pela saturação do magma em EGP.

iv. Isótopos de S indicam uma fonte mantélica para os sulfetos da *Sulfide Zone*, de forma que não é necessária uma fonte externa de enxofre para que o magma atinja a saturação nesse elemento.

3. Sobre os cromititos

   i. Cromititos estratiformes, com textura variada e espessura de até 60 centímetros, ocorrem ao longo do Complexo Luanga, hospedados no topo da Zona de Transição e base da Zona Máfica.

   ii. Em função do extensivo processo de metamorfismo que afeta as rochas do Complexo Luanga, as composições dos cristais de cromita são modificadas. A alteração da composição primária é marcada em cristais zonados, com Mg# ($Mg/Mg+Fe^{2+}$) progressivamente menor do núcleo para a borda.

   iii. Alterações da composição primária de cristais de cromita comprometem sua aplicabilidade em estudos petrogenéticos.

4. Sobre o magmatismo na Província Mineral Carajás

   i. Os resultados apresentados suportam a existência de uma província fértil para a formação de depósitos de EGP na porção nordeste da Província Mineral de Carajás.

   ii. Os dados de Ni em olivina, bem como o *tenor* de Ni elevado indicam que magmas anômalos em Ni foram gerados na Província Mineral de Carajás.